



**Technical feasibility of carvone production from limonene or carveol using the  
catalytic system FePcCl<sub>16</sub>-SBA15/TBHP**

By

**Diana Lucía Grajales Lopera**

A Research work Submitted in Partial Fulfillment of the Requirements for the Degree of  
Master in Chemical Engineering

Advisor

Lina María González Rodríguez, PhD

**Universidad de Antioquia  
Engineering Faculty  
Chemical Engineering Graduate Program  
Medellín-Colombia  
2016**

## *Acknowledgements*

I am deeply indebted to my family and friends for their support and understanding during my studies, without them this could not be possible and I thank to the live and God for this personal and professional learning opportunity.

I am grateful to my advisor Professor Lina María Rodríguez González and Professor Aida Luz Villa, as head of the Environmental Catalysis Research Group for their patience and support and for the opportunity to join this Research Group where I could find great coworkers that have helped me with their support, interest and advices.

I want to thank also my classmates; especially to Nataly for her valuable and timely help.

Finally I am grateful to Universidad de Antioquia and Colciencias for the financial support through the “Fund for the first project to newly hired professors 2013 – 247”, and the contract RC-572-2012-UT Bio-Red-CO-CENIVAM.

## ***Abstract***

Carvone is a highly cost ketone (119 USD/kg) used in pharmaceutical, flavor and fragrance industries. Its production at industrial scale has been related to the extraction and purification from the essential oils from caraway, dill or spearmint seeds, or to ecologically improper processes. Hence, the study of alternative carvone production routes is an interesting research field. Limonene has attracted the attention as raw material for carvone production, since it is an affordable (44 USD/kg) and available substrate derived from agro-industrial wastes (orange peel oil) and it can undergo allylic oxidation under mild conditions and with environmentally friendly oxidants like *tert*-butyl hydroperoxide (TBHP), where the formation of carveol as intermediate product for carvone synthesis is reported. Among the catalysts reported, Fe phthalocyanine complexes (FePcs) have been shown good activity for allylic oxidation with non-aggressive oxidants.

In this study, it was analyzed the feasibility of carvone production from limonene or carveol, using hexadecachlorinated iron phthalocyanine catalyst immobilized on mesostructured silica SBA-15 (FePcCl<sub>16</sub>-NH<sub>2</sub>-SBA-15) using TBHP under mild conditions. The catalyst synthesis, activity, and stability, as well as possible pathways of reactions are reported here.

According with the results, the FePcCl<sub>16</sub>-NH<sub>2</sub>-SBA-15 was active for limonene and carveol oxidation with TBHP at ambient pressure and 40 °C using acetone as solvent, with maximum yields to carvone near to 6 % (3 hour reaction) and 29 % (1 hour reaction), respectively. Under the reaction conditions, the catalyst behaved as a truly heterogeneous one in both reactions and showed stability up in at least three uses. Slight decrease in the activity of FePcCl<sub>16</sub>-NH<sub>2</sub>-SBA-15 was observed in the fourth re-use, which could be due to adsorption of reactants and products on the catalyst blocking its active sites.

In the mechanistic analysis, the formation of Oxo metal species (Fe<sup>IV</sup> = O) are involved in carveol oxidation by the homolytic cleavage of the TBHP, while for limonene this oxo metal species are involved in the mechanism together with radical species from TBHP. According with the results, a probably competition between substrate and TBHP to be

adsorbed on active sites is observed during the reactions. Several mechanisms with their respective rate expressions were proposed for the carveol reaction, finding that carveol rate expressions derived from pseudo-homogeneous mechanism better represents the experimental results. However, this expression does not represent completely the reaction mechanism, since it does not consider the parallel heterogeneous behavior due to reactants adsorption and the possible effect of carvone concentration, byproducts and side reactions on the reaction rate. On the other hand the rate expression obtained from pseudo-homogeneous mechanism of limonene shows even better high goodness-of-fit, which could be because the free radicals involvement in reactions, being higher for limonene, due to the free radical participation in allylic hydrogen abstraction and limonene hydroperoxide formation.

Finally, according to the results obtained and some Aspen® simulation, the technical feasibility analysis was carried out, concluding that despite the low cost of limonene and the better performance of catalytic system for carveol, the processes have not higher feasibility with the assumptions and conditions used in this work, due to the following drawbacks found: Limonene process has a low yield, thus it requires high amounts of raw materials and high reactor capacity, carveol process presents problems for product purification and high cost of raw material (carveol) and both process require high oxidant excess and have a raw material total cost higher than total income from carvone sales at the price of this in the market. These results are the base for needed improvements to complete design and technical analysis for a possible scaling up of the process

## ***Table of content***

|  |                   |
|--|-------------------|
| <b><u>Acknowledgements</u></b>   | <b><u>I</u></b>   |
| <b><u>Abstract</u></b>   | <b><u>II</u></b>  |
| <b><u>Table of content</u></b>   | <b><u>IV</u></b>  |
| <b><u>List of figures</u></b>  | <b><u>VII</u></b> |
| <b><u>List of tables</u></b>   | <b><u>IX</u></b>  |
| <b><u>Scope and structure of this work</u></b>   | <b><u>X</u></b>   |
| <b><u>1 Chapter 1: Heterogeneous hexadecachlorinated iron phthalocyanine (FePcCl<sub>16</sub>) catalyst. 1</u></b> |                   |
| 1.1 Introduction   | 1                 |
| 1.2 Experimental procedure   | 6                 |
| 1.2.1 Catalyst synthesis   | 6                 |
| 1.2.2 Catalyst characterization  | 8                 |
| 1.3 Results and discussion   | 12                |
| 1.4 Partial conclusions  | 21                |
| <b><u>2 Chapter 2: Carvone production from limonene and carveol</u></b>  | <b><u>22</u></b>  |
| 2.1 Introduction   | 22                |
| 2.2 Experimental procedure   | 25                |
| 2.2.1 Effect of catalyst and TBHP in reactions   | 27                |
| 2.2.2 Determination of reactions products  | 27                |
| 2.2.3 Selection of reaction conditions under which carvone production is favored                                   | 27                |
| 2.2.4 Behavior of reactions through time   | 29                |
| 2.2.5 Initial elucidation of reactions mechanisms  | 29                |
| 2.2.6 Mechanisms and kinetics models   | 31                |

---

|   |                  |
|---|------------------|
| <b>2.3 Results and discussion</b>                                   | <b>33</b>        |
| 2.3.1 Effect of catalyst and TBHP in reactions                      | 33               |
| 2.3.2 Reactions products  | 36               |
| 2.3.3 Reaction conditions under which carvone production is favored | 38               |
| 2.3.4 Behavior of reactions through time                            | 45               |
| 2.3.5 Initial elucidation of mechanisms                             | 47               |
| 2.3.6 Mechanisms and kinetics models                                | 53               |
| <b>2.4 Partial conclusions</b>                                      | <b>63</b>        |
| <br>  |                  |
| <b><u>3 Chapter 3: Catalyst stability and recyclability</u></b>     | <b><u>65</u></b> |
| <br>  |                  |
| <b>3.1 Introduction</b>   | <b>65</b>        |
| <b>3.2 Experimental procedure</b>                                   | <b>65</b>        |
| 3.2.1 Leaching tests  | 66               |
| 3.2.2 Recycling experiments   | 66               |
| 3.2.3 Used catalyst characterization                                | 66               |
| <b>3.3 Results and discussion</b>                                   | <b>66</b>        |
| 3.3.1 Leaching tests  | 66               |
| 3.3.2 Recycling experiments   | 69               |
| 3.3.3 Used catalyst characterization                                | 70               |
| <b>3.4 Partial conclusions</b>                                      | <b>75</b>        |
| <br>  |                  |
| <b><u>4 Chapter 4: Technical feasibility of the process</u></b>     | <b><u>76</u></b> |
| <br>  |                  |
| <b>4.1 Introduction</b>   | <b>76</b>        |
| <b>4.2 Aspen simulation</b>   | <b>78</b>        |
| <b>4.3 Results and discussion</b>                                   | <b>81</b>        |
| <b>4.4 Partial conclusions</b>                                      | <b>88</b>        |
| <br>  |                  |
| <b><u>General conclusions</u></b>                                   | <b><u>89</u></b> |
| <br>  |                  |
| <b><u>Recommendations</u></b>                                       | <b><u>92</u></b> |
| <br>  |                  |
| <b><u>References</u></b>  | <b><u>93</u></b> |

---

**Appendix A: calculation models** **105**

---

**Appendix B: Matlab ® hybrid algorithm** **106**

---

**Appendix C: Matlab results for mechanism D.** **113**

---

**Appendix D: Matlab results for mechanism J.** **115**

---

**Appendix E: Matlab results for mechanism O.** **117**

---

## List of figures

|   |           |
|---|-----------|
| <i>Figure 1.1.1. Porphyrins (A) and phthalocyanines (B) complexes, isoindole unit (C) and meso-nitrogen bridges (D) .....</i>   | <i>1</i>  |
| <i>Figure 1.1.2. Hexadecachlorinated iron phthalocyanine complex (FePcCl<sub>16</sub>).....</i>   | <i>2</i>  |
| <i>Figure 1.1.3. Monomeric and dimeric anchoring FePcCl<sub>16</sub>.....</i>   | <i>4</i>  |
| <i>Figure 1.1.4 MCM-41 (left) and SBA-15 (right) structures. Figure taken from (15) .....</i>   | <i>5</i>  |
| <i>Figure 1.2.1. SBA-15 activation (A), mixture of support, 3-APTES and m-xylene (B) and heating under argon atmosphere (C).....</i>  | <i>7</i>  |
| <i>Figure 1.2.2. Dispersion of FePcCl<sub>16</sub> in pyridine (A), suspension of SBA-15 in pyridine (B) and dropwise addition of complex-pyridine mixture to the support-pyridine suspension (C).....</i>                  | <i>8</i>  |
| <i>Figure 1.3.1. SEM images (x1,000 and x20,000) of synthesized SBA-15 (A), amino modified NH<sub>2</sub>-SBA-15 (B) and supported catalyst FePcCl<sub>16</sub>-NH<sub>2</sub>-SBA-15 (C).....</i>                          | <i>13</i> |
| <i>Figure 1.3.2. TEM images of SBA-15 (A) and FePcCl<sub>16</sub>-NH<sub>2</sub>-SBA-15 (B).....</i>  | <i>14</i> |
| <i>Figure 1.3.3. N<sub>2</sub> adsorption/desorption isotherms of SBA-15, NH<sub>2</sub>-SBA-15 and FePcCl<sub>16</sub>-NH<sub>2</sub>-SBA-15.....</i>  | <i>15</i> |
| <i>Figure 1.3.4. Pore size distribution of SBA-15, NH<sub>2</sub>-SBA-15 and FePcCl<sub>16</sub>-NH<sub>2</sub>-SBA-15 .....</i>  | <i>16</i> |
| <i>Figure 1.3.5. XRD pattern for SBA-15, NH<sub>2</sub>-SBA-15 and FePcCl<sub>16</sub>-NH<sub>2</sub>-SBA-15.....</i>   | <i>17</i> |
| <i>Figure 1.3.6: UV-vis analysis of NH<sub>2</sub>-SBA-15 and FePcCl<sub>16</sub>-NH<sub>2</sub>-SBA-15.....</i>  | <i>19</i> |
| <i>Figure 1.3.7. Raman analysis of NH<sub>2</sub>-SBA-15, FePcCl<sub>16</sub>, and FePcCl<sub>16</sub>-NH<sub>2</sub>-SBA-15 .....</i>  | <i>20</i> |
| <i>Figure 2.1.1:(4S)-(+)-carvone or d-carvone (A) and (4R)-(-)-carvone or L-carvone (B).....</i>  | <i>22</i> |
| <i>Figure 2.1.2: Hydroxylation of carvoxime .....</i>   | <i>23</i> |
| <i>Figure 2.1.3: Allylic oxidation of limonene .....</i>  | <i>23</i> |
| <i>Figure 2.1.4: R (+) limonene or D-Limonene (A) and S (-) Limonene or L-limonene (B).....</i>   | <i>24</i> |
| <i>Figure 2.1.5: Dehydrogenation of carveol .....</i>   | <i>25</i> |
| <i>Figure 2.2.1: Reaction system.....</i>   | <i>26</i> |
| <i>Figure 2.2.2: Experimental set for reactions under inert atmosphere.....</i>   | <i>30</i> |
| <i>Figure 2.3.1: Performance of TBH with FePcCl<sub>16</sub>-NH<sub>2</sub>-SBA-15 catalyst system in limonene reaction. ....</i>   | <i>33</i> |
| <i>Figure 2.3.2: Support effect of the limonene conversion (A) and the epoxide selectivity (B) and carvone (C) at the allylic oxidation of limonene with FePcCl<sub>16</sub> / TBHP system. ....</i>                        | <i>34</i> |
| <i>Figure 2.3.3: Performance of TBH/ FePcCl<sub>16</sub>-NH<sub>2</sub>-SBA-15 catalytic system in carveol reaction.....</i>  | <i>35</i> |
| <i>Figure 2.3.4: Variation of reaction rates of limonene epoxide (A), carvone (B) and limonene (C) with variation of TBHP/limonene molar ratio with an active site(Fe) concentration of 0.16 mol % (Fe /limonene). ....</i> | <i>41</i> |
| <i>Figure 2.3.5: Limonene and carveol conversion through time. ....</i>   | <i>45</i> |
| <i>Figure 2.3.6: Carvone and limonene epoxide yield versus limonene conversion.....</i>   | <i>46</i> |
| <i>Figure 2.3.7: Carvone yield and selectivity versus carveol conversion. ....</i>  | <i>46</i> |
| <i>Figure 2.3.8: Iron phthalocyanine peroxide complexes formation. Taken from (5).....</i>  | <i>48</i> |
| <i>Figure 2.3.9: Homolytic and heterolytic cleavage. Taken from (2) .....</i>   | <i>48</i> |
| <i>Figure 2.3.10: Effect of the scavenger (2,4-DBP) in the conversion of limonene and TBHP.....</i>   | <i>49</i> |
| <i>Figure 2.3.11: Effect of the catalyst in the TBHP decomposition.....</i>   | <i>50</i> |
| <i>Figure 2.3.12: Limonene allylic oxidation under air and inert atmosphere.....</i>  | <i>52</i> |



---

|   |           |
|---|-----------|
| <i>Figure 2.3.13: Effect of active sites (Fe) concentration (L) on limonene (Figure A) and carveol (Figure B) consumption initial rates (change of substrate concentration in the time unit). .....</i> | <i>53</i> |
| <i>Figure 2.3.14: Effect of substrates concentration on limonene (Figure A) and Carveol (Figure B) initial reaction rate. ....</i>  | <i>54</i> |
| <i>Figure 2.3.15: Effect of TBHP concentration (C<sub>B</sub>) on limonene (Figure A) and carveol (Figure B) initial reaction rate. ....</i>  | <i>55</i> |
| <i>Figure 3.3.1: FePcCl<sub>16</sub>-NH<sub>2</sub>-SBA-15 leaching test in carveol reaction. ....</i>  | <i>67</i> |
| <i>Figure 3.3.2: FePcCl<sub>16</sub>-NH<sub>2</sub>-SBA-15 leaching test in limonene reaction. ....</i>   | <i>67</i> |
| <i>Figure 3.3.3: Conversion of carveol and limonene after catalyst removal and addition of free radical scavenger (2, 4-DPB) at 0.5 and 1 hours respectively. ....</i>                                  | <i>68</i> |
| <i>Figure 3.3.4: Uv-vis analysis for FePcCl<sub>16</sub> (black line) and liquid reaction mixture after 24 hour carveol reaction at best conditions. ....</i>   | <i>69</i> |
| <i>Figure 3.3.5: SEM images (x1,000 and x20,000) of recovered catalysts used 3 times in 24 hours Limonene (Figure A) and carveol (Figure B) reactions. ....</i>   | <i>71</i> |
| <i>Figure 3.3.6: TEM images of recovered catalysts used 3 times in 24 hours Limonene (Figure A) and carveol (Figure B) reactions. ....</i>  | <i>71</i> |
| <i>Figure 3.3.7: N<sub>2</sub> adsorption/desorption isotherms of the catalyst used 3 times in 24 h limonene reactions. ....</i>  | <i>72</i> |
| <i>Figure 3.3.8: Pore size distribution of the catalyst used 3 times in 24 h limonene reactions. ....</i>   | <i>73</i> |
| <i>Figure 3.3.9: UV-vis analysis of fresh catalyst (black line) and catalyst used 3 times in 24 h limonene reactions (gray line). ....</i>  | <i>73</i> |
| <i>Figure 3.3.10: Raman analysis of fresh catalyst and catalyst used 3 times in 24 h limonene reactions. ....</i>   | <i>74</i> |
| <i>Figure 4.1.1: specific features of fine chemicals .....</i>  | <i>76</i> |
| <i>Figure 4.3.1: RBatch reactor. ....</i>   | <i>81</i> |
| <i>Figure 4.3.2: Specification for carveol reaction in RBatch. ....</i>   | <i>82</i> |
| <i>Figure 4.3.3: Comparison between carveol mole fractions predicted with ASPEN and the experimental data. ....</i>   | <i>82</i> |
| <i>Figure 4.3.4: Comparison between carveone mole fractions predicted with ASPEN and the experimental data. ....</i>  | <i>83</i> |
| <i>Figure 4.3.5: Definition of yield for Limonene (Figure A) and Carveol (Figure B) RYield reactors. ....</i>   | <i>84</i> |
| <i>Figure 4.3.6: General flowsheet for both processes. ....</i>   | <i>84</i> |

## List of tables

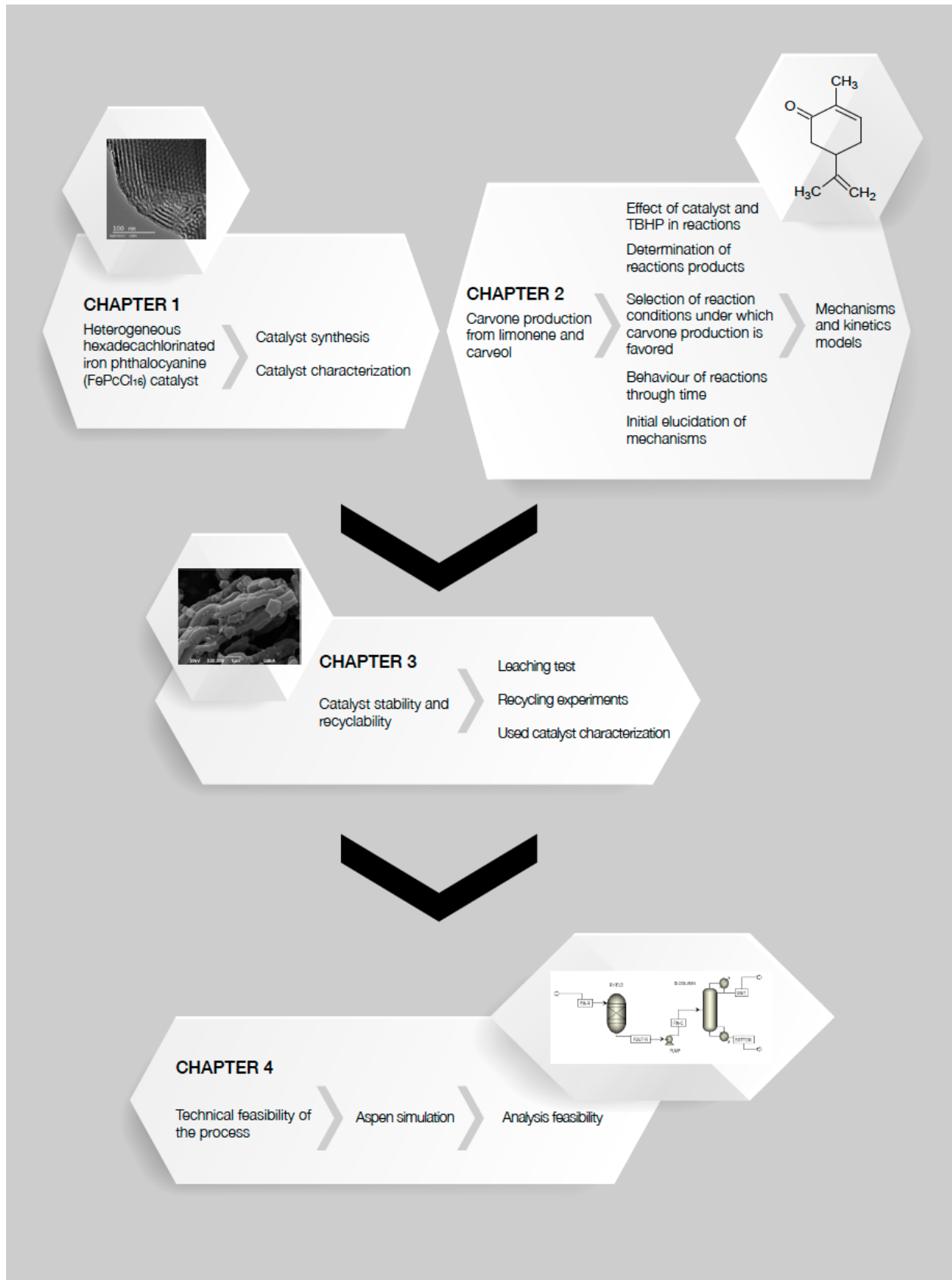
|   |    |
|---|----|
| <i>Table 1.2.1. Characterization techniques</i> .....   | 9  |
| <i>Table 1.3.1. Iron content in finished catalysts</i> .....  | 13 |
| <i>Table 1.3.2. Surface area, pore volume and average pore size of support, modified support and catalyst</i> .....   | 14 |
| <i>Table 1.3.3: Structural parameters of SAB-15, NH<sub>2</sub>- SBA-15 and FePcCl<sub>16</sub>-NH<sub>2</sub>-SBA-15.</i> .....  | 18 |
| <i>Table 1.3.4: TGA analysis of SAB-15, NH<sub>2</sub>- SBA-15 and FePcCl<sub>16</sub>-NH<sub>2</sub>-SBA-15.</i> .....   | 21 |
| <i>Table 2.2.1. Chromatographic analysis parameters</i> .....   | 26 |
| <i>Table 2.2.2: Variables ranges</i> .....  | 28 |
| <i>Table 2.2.3: Limonene complementary experiments</i> .....  | 29 |
| <i>Table 2.2.4: Carveol complementary experiments</i> .....   | 29 |
| <i>Table 2.2.5. Statistics used for model comparison (66)</i> .....   | 32 |
| <i>Table 2.3.1: Limonene reaction byproducts</i> .....  | 37 |
| <i>Table 2.3.2: Carveol reaction byproducts</i> .....   | 38 |
| <i>Table 2.3.3 Limonene reaction rate, <math>-r_{\text{limonene}}</math> (mmol<sub>limonene</sub> / g<sub>Fe</sub> · min) at different stirring speeds</i> .....          | 39 |
| <i>Table 2.3.4 Limonene reaction rate, <math>-r_{\text{limonene}}</math> (mmol<sub>limonene</sub> /g<sub>Fe</sub> · min) with different catalyst particle sizes</i> ..... | 39 |
| <i>Table 2.3.5: Effect of active sites catalyst concentration on reactions rates with a constant TBHP/limonene molar ratio of 2.6</i> .....                               | 40 |
| <i>Table 2.3.6: Effect of TBHP/Fe molar ratio (1600-1706.7) on the initial reaction rates with a constant limonene concentration of 0.08 M</i> .....                      | 42 |
| <i>Table 2.3.7: Results limonene reactions at 30 minutes, 313 K and 875 rpm.</i> .....  | 43 |
| <i>Table 2.3.8: Results carveol reactions at 30 minutes, 313 K and 875 rpm</i> .....  | 44 |
| <i>Table 2.3.9. Rate expressions for carveol proposed mechanism</i> .....   | 58 |
| <i>Table 2.3.10. Parameter estimated for rate expressions with the best fitting</i> .....   | 61 |
| <i>Table 2.3.11.Pseudohomogeneous mechanism for limonene and estimated parameter</i> .....  | 63 |
| <i>Table 3.3.1: Recycling experiments for limonene reaction</i> .....   | 69 |
| <i>Table 3.3.2: Recycling experiments for carveol reaction</i> .....  | 70 |
| <i>Table 4.2.1. Definition of reactor capacity</i> .....  | 80 |
| <i>Table 4.2.2. Composition of reactors input stream</i> .....  | 81 |
| <i>Table 4.3.1. Operating conditions for RADFRAC model in limonene (A) and Carveol process (B)</i> .....  | 85 |
| <i>Table 4.3.2. Aspen simulation results for limonene process</i> .....   | 86 |
| <i>Table 4.3.3. Aspen simulation results for carveol process</i> .....  | 87 |
| <i>Table 4.3.4. Cost of raw material and product for each process.</i> .....  | 88 |

## *Scope and structure of this work*

Carvone is a fine chemical product in rising demand, widely used in medical field and in flavor and fragrance industries (to enhance taste and odor). A carvone production process with high yields and low generation of waste, is still a challenge. In this sense, iron phthalocyanine complexes have attracted the attention as biomimetic catalyst with suitable application in oxidation reactions with non-aggressive oxidants like *tert*-butyl hydroperoxide (TBHP). Hence, this research project aimed to evaluate the performance of the hexadecachlorinated iron phthalocyanine catalyst immobilized on mesostructured silica (SBA-15), in the production of carvone from limonene and carveol using TBHP.

This research work gives an approach to the mechanisms of carvone production from limonene and carveol with this catalytic system and it provides a preliminary analysis about the aspects that affect technical feasibility of these processes. The results in this work are the base for improvements needed to complete design and technical analysis, and suggest that improvements in the catalytic systems should be made, before the application of the process at larger scale.

The results are presented in 4 chapters as depicted in the following page. Each chapter includes an introduction with the general aspect of the specific topic, descriptions of the procedures carried out, the results obtained with their analysis and partial conclusions.



Chapter 1 presents the synthesis and characterization of hexadecachlorinated iron phthalocyanine catalyst ( $\text{FePcCl}_{16}\text{-NH}_2\text{-SBA-15}$ ), explaining the main features in its preparation steps. Additionally this chapter displays the results of some characterization techniques that validate its successful synthesis.

Chapter 2 exposes the catalytic activity of  $\text{FePcCl}_{16}\text{-NH}_2\text{-SBA-15}$  catalyst for limonene and carveol reactions with TBHP and the experimental results that gives an approach to their mechanisms and active species involved, which is very important for the development of efficient catalysts.

Chapter 3 speaks about the stability and recyclability of the catalyst, with the objective of providing evidence related to the effect of the reactions processes over the heterogeneous catalyst and the possible variations occurred on this during the reactions.

With the results obtained from the previous chapters and some Aspen® simulation, Chapter 4 shows a preliminary analysis about the feasibility of carvone production using the catalytic systems here studied, limonene/TBHP/ $\text{FePcCl}_{16}\text{-NH}_2\text{-SBA-15}$  and carveol/TBHP/ $\text{FePcCl}_{16}\text{-NH}_2\text{-SBA-15}$ .

Finally, general conclusions and recommendations for future work are presented with the idea to give a summarized overview of the main results of this work.

# 1 Chapter 1: Heterogeneous hexadecachlorinated iron phthalocyanine ( $FePcCl_{16}$ ) catalyst.

## 1.1 Introduction

Enzymes like Cytochrome P-450 are capable of performing difficult oxidation reactions under mild conditions, for this reason in latest years many studies have been focused on chemically mimic, the enzymes behavior with the objective of reproduces their catalytic activity under mild and clean conditions (1,2).

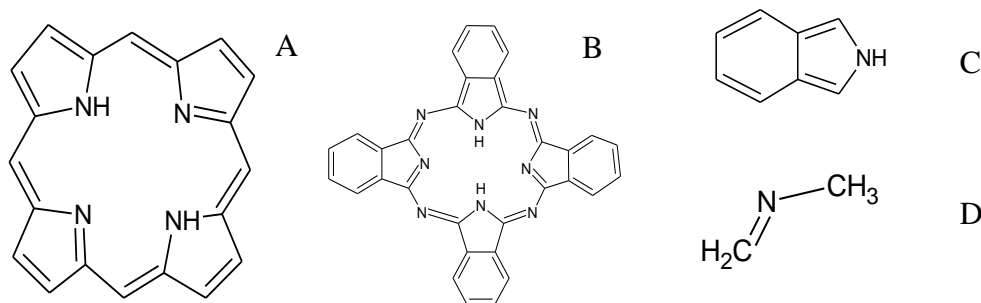


**Figure 1.1.1.** Porphyrins (A) and phthalocyanines (B) complexes, isoindole unit (C) and meso-nitrogen bridges (D)

Porphyrins (**Figure 1.1.1 A**) and phthalocyanines (**Pcs, Figure 1.1.1 B**) are examples of bio-inspired catalyst of the cytochrome P-450 enzymes and have been used for variety of catalytic reactions (2). As it was mentioned in a recent review about the topic (2), porphyrins are widely used by nature in the active sites of enzymes responsible for catalytic aerobic oxidations, reduction and transport of dioxygen, and destruction of peroxides and their use in catalytic chemistry is well-documented. However, the attention has been centered in metallic phthalocyanine complexes (MPc), since, despite their insolubility in common organic solvents, they are, in contrast with porphyrins, more available, stable (thermal and chemically) and can be prepared simply and cheaply for industrial applications (3–6). This fact is consistent with the current challenge of developing efficient bio-inspired catalyst readily accessible on a large scale (2).

Pcs are 18  $\pi$ -electron molecules which can accommodate a wide range of atoms in their central cavity to form MPc (7), they consist of four isoindole units (**Figure 1.1.1 C**), which are linked angularly by four meso-nitrogen bridges (**Figure 1.1.1 D**), leading to a macrocyclic aromatic molecule (8). MPc worldwide production has been higher than 80,000 ton/year (6); these complexes are widely used in different fields such dyes and pigments, semiconductors and non-linear optical devices, information storage systems, liquid crystal applications, among other large-scale industrial processes. Additionally, since MPc are perspective compounds for photodynamic therapy of cancer, their toxicological properties have been intensively studied (6,7).

The review written by B. Sorokin (2), states that, despite the limited number of reviews about MPc, many new catalytic applications of MPcs has been recently published, with special interest in cobalt complexes for reduction and iron complexes ( $FePcs$ ) for oxidation with non-aggressive oxidants such as hydrogen peroxide, tert-butyl hydroperoxide (TBHP) or molecular oxygen. Phthalocyanine complexes have been and will be playing an increasing role in the development of sustainable and clean catalytic oxidations as well as for other reactions and they keep a great promise for the future (2).

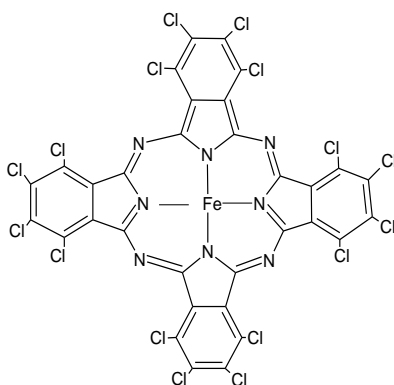


**Figure 1.1.2. Hexadecachlorinated iron phthalocyanine complex ( $FePcCl_{16}$ )**

One of the interesting application of MPc as catalyst is in fine chemistry, where it is expected to make the preparation of elaborated products more efficient, resulting in the less expensive and cleaner processes. For example, it has been previously reported that iron

## ***Chapter 1: Heterogeneous hexadecachlorinated iron phthalocyanine (FePcCl<sub>16</sub>) catalyst.***

---

phthalocyanine with chlorinated substituents (**Figure 1.1.2**), FePcCl<sub>16</sub>-NH<sub>2</sub>-S immobilized on amorphous silica is a suitable stable catalyst for limonene allylic oxidation, giving selectivity to carvone formation of 16% under mild conditions (9,10), nonetheless selectivity improvement are required.

Usually, catalysts can be anchored on a support with the intention to provide recyclability, and influencing its stability and activity. Some liquid phase oxidation similar to that of this project scope, with hydrogen peroxide or t-butyl hydroperoxide (TBHP) as oxidant, can be successfully improved in the presence of heterogeneous catalysts, due to advantages connected with the catalyst stability, the possibility of separation and regeneration of heterogeneous catalyst and even connected to increasing of desired product selectivity (2,11).

Homogeneous MPc has been successfully employed in catalytic reactions, but immobilization of MePc on solid supports is highly desirable for synthesizing easier separable heterogeneous catalysts that, in some cases, can be re-used (6). That is the case of d-FePcS complex supported on SiO<sub>2</sub>, which heterogenization influence the pathway of allylic oxidation of cyclohexene to be predominant rather than epoxidation (2).

One of the available methods to immobilize the MPc complex on a support is the covalent anchoring. It has been reported that the immobilized catalysts obtained by this method are more stable and leaching proof, since covalent bonds are formed between the solid support and the metal complex. Furthermore, the anchoring method, usually provided a more uniform distribution of the complex on support surface, which could led to a higher catalytic performance compared with those of neat catalysts and materials prepared by other methods (2,6). Catalyst can be anchored as monomeric or dimeric species (**Figure 1.1.3 A and B, respectively**), influencing the properties of the catalyst (activity and selectivity) (6).



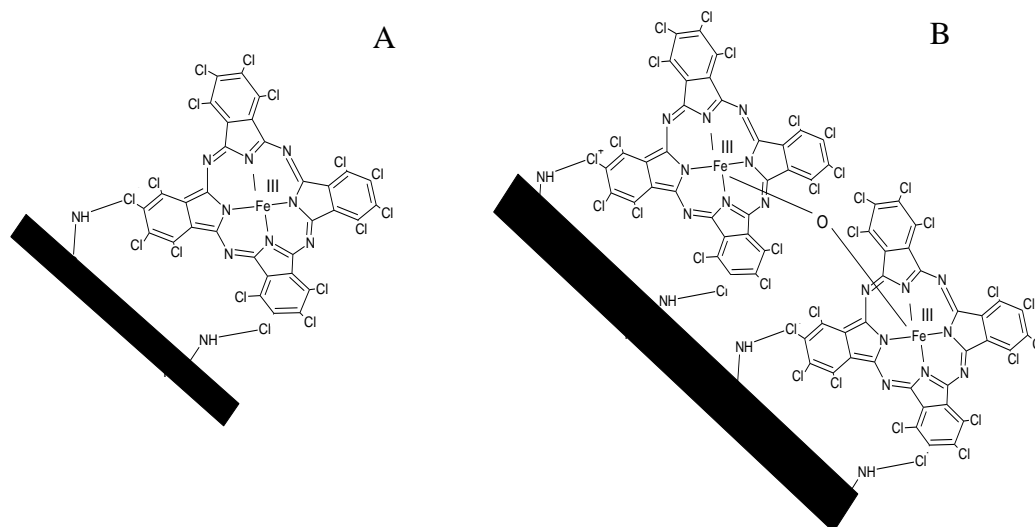


Figure 1.1.3. Monomeric and dimeric anchoring  $FePcCl_{16}$

In order to evaluate the effect of the support on the yield of oxidation with MPC, other supports like mesostructured silica, have been researched. Alexander B. and coworkers obtained higher activities of iron tetrasulfophthalocyanine grafted over mesostructured silica in the oxidation of 2,3,6-trimethylphenol, suggesting a diffusion limitation of the large organic molecules within the porous system of the mesostructured containing catalyst (5). The catalytic studies of Joseph T. and coworkers revealed that anchoring of VO (Salten) on functionalized SBA-15 enhances the stability of VO (Salten) complexes during the oxidation reaction of limonene in presence of urea hydroperoxide (UHP) by suppressing the formation of inactive  $\mu$ -oxovanadium species. This covalently anchored complex proved to be efficient catalyst for the oxidation of limonene (12).

In this way, mesostructured silica could be used to anchor FePc in order to influence its stability, activity and products distribution in oxidation of sterically demanding substrates as limonene and carveol. This kind of supports could influence the products formation and distribution, due to the presence of the SiOH groups, the possible immobilization of catalyst inside the channels through strong covalent bonds and the pore size that can induce shape selectivity, pore transport limitations of the large organic molecules within the

porous system and suppression of inactive  $\mu$ -oxo species formation impacting the reaction behavior and catalyst stability (12–14).

Mesostructured supports are materials with well-ordered mesopores, namely pore sizes within 20 Å and 500 Å (15). Within the known mesostructured supports they are:

- MCM-41 (*Figure 1.1.4*): it is a solid with a regular arrangement of cylindrical mesopores, independently adjustable pore diameter, between 2 and 5 nm, a sharp pore distribution, a large surface, a large pore volume and a smaller wall thickness (around 1 nm) (16).

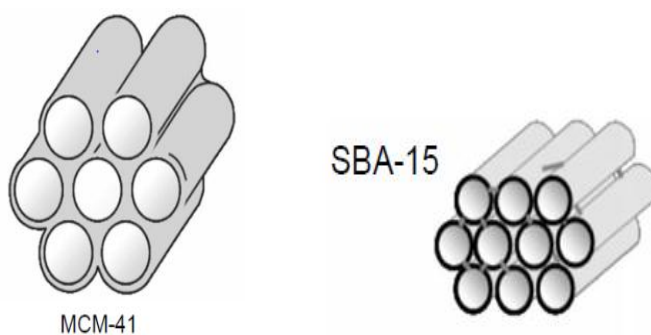


*Figure 1.1.4 MCM-41 (left) and SBA-15 (right) structures. Figure taken from (15)*

- SBA-15 (*Figure 1.1.4*): mesoporous silica based on uniform hexagonal pores with a narrow pore size distribution and a tunable pore diameter of between 5 and 15 nm. The thickness of the framework walls is about 3.1 to 6.4 nm, which, between other factors, gives the material a higher hydrothermal and mechanical stability. The high internal surface area of typically 400–900 m<sup>2</sup>/g makes SBA-15 a well suited material for various applications (catalysis, separations, and advanced optical materials) (17).

Application of high surface area materials like MCM-41 and SBA-15, help with the spatial separation of catalytic species that behave very similarly to the active centers in true molecular catalysis (18). Previous reports showed that Ti-SBA-15 was more stable under the reaction conditions during the phenol epoxidation than the Ti-MCM-41 catalyst (11).

Since SBA-15 larger pores seem to be more preferable for covalent bonding of big molecules like MPcs (18); so based on the promising future of iron phthalocyanines combining with the stability of SBA-15, the selected catalyst for the current work was the

hexadecachlorinated iron phthalocyanine complex (FePcCl<sub>16</sub>) covalently anchored onto an amino modified SBA-15 (NH<sub>2</sub>-SBA-15).

This chapter presents the synthesis and characterization of the selected catalyst FePcCl<sub>16</sub>-NH<sub>2</sub>-SBA-15, aiming to explain the main features in the preparation steps, in order to prove its successful synthesis. This information will be used in future chapters in order to analyze the catalyst role in the reactions and its stability.

## ***1.2 Experimental procedure***

### ***1.2.1 Catalyst synthesis***

The iron phthalocyanine complex (FePcCl<sub>16</sub>) immobilized onto amino modified SBA-15 (NH<sub>2</sub>-SBA-15), was used in this work as heterogeneous catalyst in the carvone production. It was synthesized and characterized according to methods reported in literature (10,19).

#### **Complex synthesis**

The FePcCl<sub>16</sub> complex used, was previously synthesized in the Environmental Catalyst Research Group, according to the procedure reported in literature by González (10).

#### **SBA-15 synthesis**

An amphiphilic triblock co-polymer (EO)<sub>20</sub>(PO)<sub>70</sub>(EO)<sub>20</sub> with the tradename P-123 (average molecular weight 5800, Sigma-Aldrich) and tetraethyl orthosilicate (TEOS, Sigma-Aldrich) were used to synthesize SBA-15 according to the method described by Shah et al (20).

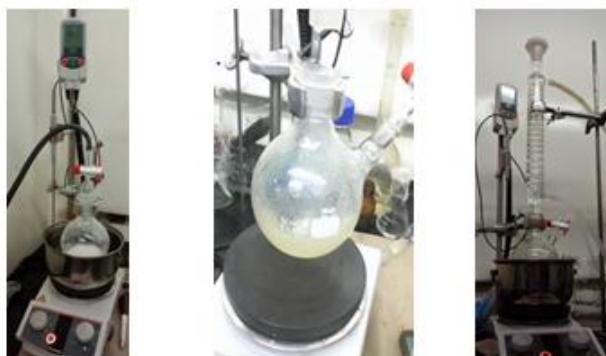
Firstly 6 g of (P-123) were dispersed in 45 mL of water at low stirring speed in order to avoid foam generation, followed by the addition of 180 g of 2 M HCl solution. When the solution was homogeneous, 12.75 g of tetraethyl orthosilicate were added dropwise. The resulting turbid suspension was continuously stirred at 313 K for 24 h, and finally crystallized under static conditions at 373 K for 2 days, in a Teflon-lined autoclave. After crystallization, the solid was filtered, washed with deionized water and dried in air at room temperature, before being calcined in static air at 823 K for 24 h to decompose the P-123 and to obtain a white powder (SBA-15). The calcination was carried out with the following

heating rate: 5 K/min up to 823 K during 24 h, then 10 K/min until 353 K and during 1 hour and finally 10 K/min until 323 K.

Note: before the crystallization the Teflon device was previously washed with hydrofluoric acid (around 3 – 5 % vol).

### **Support modification**

SBA-15 was amino modified to allow the covalent anchoring of the metal complex onto the solid support, in order to obtain a catalyst more stable, leaching free and with a good preserved mesostructure (21,22). The support modification was made with 3-aminopropyltriethoxysilane (3-APTES, Sigma-Aldrich) according with the procedure previously reported by González (10), and summarized below.



(A) (B) (C)  
**Figure 1.2.1. SBA-15 activation (A), mixture of support, 3-APTES and m-xylene (B) and heating under argon atmosphere (C)**

Prior to the modification, SBA-15 was activated degassing it at 150°C and vacuum during 24 h (**Figure 1.2.1 A**). 3-APTES (2 mmol) was added to a suspension of activated support (5 g) in at least 50 mL of m-xylene from Mallinckrodt Chemicals (**Figure 1.2.1 B**). The final mixture was heated at 150° C, under argon atmosphere, until boiling point is reached (**Figure 1.2.1 .C**). At that point, the argon flux is closed and the mixture was refluxed during 15 h. The material (named as NH<sub>2</sub>-SBA-15) was separated by filtration, washed with acetone and dried, first at room temperature and finally at 80 °C under vacuum overnight.

***Immobilization of FePcCl<sub>16</sub>***

The catalyst (FePcCl<sub>16</sub>-NH<sub>2</sub>-SBA-15) was prepared according to the reported procedure (10), as follows: 0.18 g FePcCl<sub>16</sub> complex were dispersed in pyridine (Merck) (0.003 g complex/mL pyridine) and stirred during 7 h at room temperature (**Figure 1.2.2.A**).

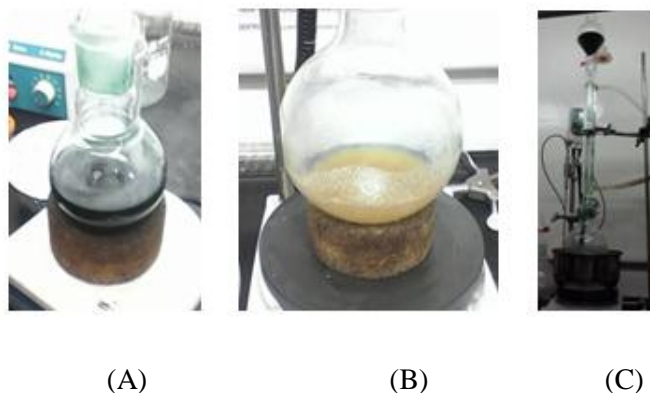


***Figure 1.2.2. Dispersion of FePcCl<sub>16</sub> in pyridine (A), suspension of SBA-15 in pyridine (B) and dropwise addition of complex-pyridine mixture to the support-pyridine suspension (C)***

Simultaneously, a suspension of 3 g SBA-15 in pyridine (0.1 SBA-15 g/mL pyridine) was stirred during 5 min in a round bottom flask (**Figure 1.2.2.B**); then the complex-pyridine mixture was added to the suspension dropwise (**Figure 1.2.2.C**). After the addition of the complex, the new suspension was stirred at room temperature for 1 h and then at reflux (120°C) for 24 h. The *green solid* obtained after cooling was washed with acetone until an odorless solid was obtained. The solid was dried at room temperature, and finally at 100°C during 15 h.

***1.2.2 Catalyst characterization***

The catalyst was characterized using different physico-chemical techniques, in order to determine the composition, structure and properties of the catalyst, as explained below:

Table 1.2.1. Characterization techniques

| Analysis                                    | Objective   | Technique information  |
|---|---|--|
| <b>Atomic Absorption Spectrometry (AAS)</b> | Determination of catalyst iron content            | This technique is based on the use of the wavelengths of light specifically absorbed by an element. They correspond to the energies needed to promote electrons from one energy level to another, higher energy level (23,24). In this work, data were obtained using a flame atomic absorption Model S4 spectrometer from Thermo Electron Corporation. The sample was subjected to total dissolution by digestion with hydrofluoric, hydrochloric and nitric acids in hot and in the final solution the content of each metal is measured. Calibration curves were obtained with solutions prepared from 1000 ppm certified standards for iron.   |
| <b>Small angle X-Ray Diffraction (XRD)</b>  | Confirmation of SBA-15 hexagonal mesoscopic order | XRD is a powerful tool used for the determination of the crystal structure of materials. Through this technique it is possible to determine the crystal structure, its lattice parameters and spacing between lattice planes. The XRD powder patterns can be used like a fingerprint to see if it matches the powder pattern of an already known compound; nevertheless, in this case XRD technique is used to confirm the mesoscopic order and the characteristic hexagonal features of SBA-15, before and after catalyst anchoring, and the conservation of SBA-15 structure after the use of the catalyst (20,25,26). The analysis was carried out in a powder BRUKER diffractometer, model D8 ADVANCE with DaVinci Geometry using $CuK\alpha$ radiation, through a measuring range of $0.5$ to $5^\circ 2\theta$ ; samples were pulverized in a mortar and put into a size of $38 \mu m$ (400 mesh). The sample was settled on a polymethyl methacrylate (PMMA) holder by the filling front technique. |

| Analysis   | Objective   | Technique information   |
|--|---|---|
| <p><b>Scanning Electron Microscopy (SEM)</b></p>     | <p>Evaluation of external morphology of the support and catalyst</p>                  | <p>This technique uses a focused beam of high-energy electrons to generate a variety of signals at the surface of solid specimens. The signals that derive from electron-sample interactions reveal information about the sample including external morphology (texture), and crystalline structure and orientation of materials making up the sample (27,28). Images of fresh and used samples were collected in a JEOL model JSM-6490 (20kV x1.000, x10.000 and x20.000).</p>   |
| <p><b>Transmission Electron Microscopy (TEM)</b></p> | <p>Confirmation of the well-ordered hexagonal arrays and uniform mesopores sizes.</p> | <p>With the transmission Electron Microscope (TEM), the most widely used, electron beams are irradiated on the sample, and transmitted electrons through the sample are focused and imaged under the sample. Since the image can be enlarged several times, microstructures can be directly observed (29). TEM images were collected in a Transmission Electron Microscope Tecnai F20 Super Twin TMP with an emission source, resolution of 0.1 nm at 200 Kv, 1.0 maximum magnification TEM MX camera GATAN US 1000XP-P. For TEM observations, a small amount of sample was dispersed in ethanol and sonicated for 30 min in probe, and then a drop of the sample was taken and placed on a copper grid covered with a Holey Carbon film.</p> |

| Analysis                            | Objective  | Technique information   |
|-------------------------------------|--|---|
| <b>BET analysis</b>                 | Measurement of surface area, pore volume and pore size.  | <p>This technique involves exposing solid materials to gases or vapors at a variety of conditions and evaluating either the weight uptake or the sample volume. The Brunauer, Emmett and Teller (BET) technique is the most common method for determining the surface area, pore volume and pore size of powders and porous materials. Nitrogen gas is generally employed as the probe molecule and is exposed to a solid under investigation at liquid nitrogen conditions (i.e. 77 K). The surface area of the solid is evaluated from the measured monolayer capacity and knowledge of the cross-sectional area of the molecule being used as a probe (30).</p> <p>In this work, a complete analysis (adsorption and desorption) was made in an ASAP 2020 V4.00 (V4.00 J) equipment from Micromeritics. The samples were degassed at 393 K for 480 min, and then the N<sub>2</sub> adsorption was conducted at 76 K.</p> |
| <b>UV-Vis spectroscopy (UV-Vis)</b> | Identification of iron phthalocyanine species (monomeric and $\mu$ -oxo dimeric) anchored onto the support | <p>This techniques is used to quantify the light that is absorbed and scattered by a sample (31). The analyses were carried out using a UV/VIS spectrophotometer (200-900 nm), model EVOLUTION 600, Thermo Scientific, without further sample treatment.</p>  |



| <b>Analysis</b>                           | <b>Objective</b>   | <b>Technique information</b>  |
|---|--|---|
| <b>Raman Spectroscopy (Raman)</b>         | Determination of FePcCl <sub>16</sub> anchoring onto the support                         | Raman spectroscopy is a light scattering technique with the ability to deliver specific chemical identification (32). The Raman spectrometer used was a Nikon model BX41 with plan achromatic objectives 10X, 50X and 100X. Color video camera. Laser He/Ne 633nm 17 MW and laser diode 785 nm of 80 mW. The excitation of the laser at 633 nm, is closer to the resonance with the main Q absorption band of phthalocyanine ligand (Pc). |
| <b>Thermal Gravimetric Analysis (TGA)</b> | Determination of differences between support, modified support, fresh and used catalyst. | Thermal Gravimetric Analysis or Thermogravimetric Analysis is a thermal technique that measures the change in weight of a material as a function of time or temperature in a controlled atmosphere. Measurements help to determine composition or thermal stability (33,34). The analyses were performed between 25 and 800 °C in a TGA Q500 V20. 13 BUILD 39 TA Instrument under nitrogen flow.  |

### **1.3 Results and discussion**

#### **Catalyst characterization**

The characterization results confirm the appropriate synthesis of the catalyst and determine the complex concentration, as described below.

The AAS results for iron content of the finished catalyst batches (% w/w) and their corresponding value in  $\mu\text{mol Fe/g}$  of catalyst are given in **Table 1.3.1**. The difference in the final concentration of the metal is due to experimental error; however, the reproducibility of the catalyst batches performance was successfully tested, using a constant amount of iron complex in a 24 h reaction.

**Table 1.3.1. Iron content in finished catalysts**

| $\text{FePcCl}_{16}$ -SBA15 | Fe % w/w | $\mu\text{mol Fe/ g of catalyst}$ |
|-----------------------------|----------|-----------------------------------|
| <b>Batch 1</b>              | 0.49     | 87.74                             |
| <b>Batch 2</b>              | 0.20     | 35.81                             |

Note: The data showed henceforth corresponds to Batch 2. Batch 1 data were not showed but they are similar.

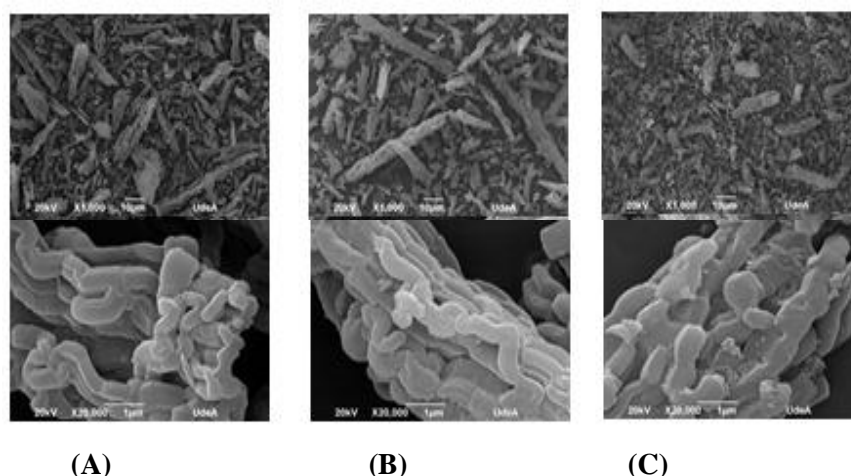


**Figure 1.3.1. SEM images ( $\times 1,000$  and  $\times 20,000$ ) of synthesized SBA-15 (A), amino modified  $\text{NH}_2$ -SBA-15 (B) and supported catalyst  $\text{FePcCl}_{16}$ - $\text{NH}_2$ -SBA-15 (C)**

SEM images of SBA-15 (Figure 1.3.1 A),  $\text{NH}_2$ -SBA-15 (Figure 1.3.1 B) and  $\text{FePcCl}_{16}$ - $\text{NH}_2$ -SBA-15 (Figure 1.3.1. C) show similar particle morphology with many rope-like domains and relatively uniform diameter, that aggregate into a wheat-like microstructure (35). This morphology is characteristic of this kind of material and it remained unchanged through SBA-15 amino modification and  $\text{FePcCl}_{16}$  immobilization (20).

The TEM images in Figure 1.3.2 evidence that both materials (support and supported catalyst) exhibit well-ordered hexagonal mesopores in a 2D array with long 1D channels, agreeing with the characteristic SBA-15 structure, and confirming that the SBA-15 structure remains intact after the complex anchoring (36,37). The iron could not be detected in TEM analysis, probably due to the low concentration of this on the support.

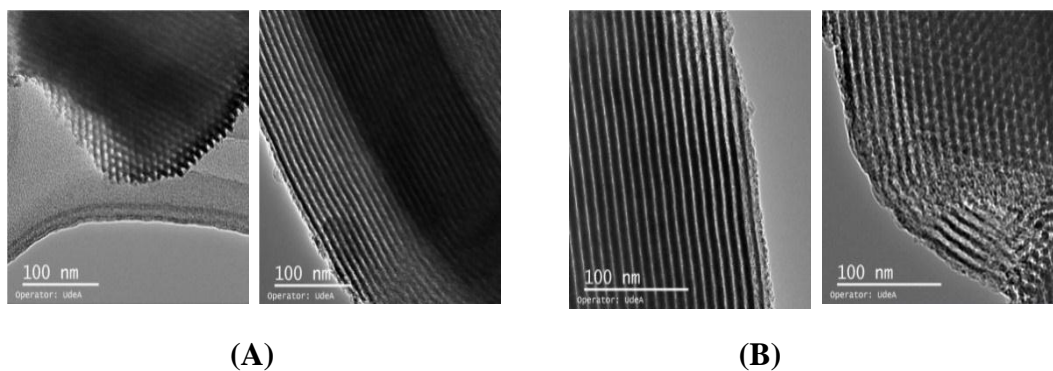


**Figure 1.3.2. TEM images of SBA-15 (A) and  $FePcCl_{16}$ -NH<sub>2</sub>-SBA-15 (B)**

Large surface areas ( $S_{total}$ ) and pore volume ( $V_p$ ) of the materials were evidenced by the BET analysis (**Table 1.3.2**). However, an important decrease in both parameters was observed after the support modification and iron phthalocyanine incorporation.

**Table 1.3.2. Surface area, pore volume and average pore size of support, modified support and catalyst**

| Material                               | $S_{total}$<br>(m <sup>2</sup> /g) | $V_p$<br>(cm <sup>3</sup> /g) | $W_{average}$<br>(Å) |
|--|------------------------------------|-------------------------------|----------------------|
| SBA-15                                 | 655.07                             | 1.13                          | 69.23                |
| NH <sub>2</sub> - SBA-15               | 398.62                             | 0.90                          | 90.59                |
| $FePcCl_{16}$ -NH <sub>2</sub> -SBA-15 | 380.03                             | 0.80                          | 84.63                |

**Figure 1.3.3** presents the N<sub>2</sub> adsorption/desorption isotherms for the three materials SBA-15, NH<sub>2</sub>-SBA-15 and  $FePcCl_{16}$ -NH<sub>2</sub>-SBA-15, a typical irreversible-type IV adsorption isotherm with H1 hysteresis loop is observed, which is characteristic of SBA-15 with typical mesoporous structures of uniform cylindrical pore channels (15,20,25). The inflection was not altered with the SBA-15 amino modification and  $FePcCl_{16}$  incorporation, but the porous volume shows an important decrease with these processes. This fact in concordance with the surface area decrease, could be related with the incorporation of the 3-APTES and the  $FePcCl_{16}$  complex inside the SBA-15 pores, which could partially block them without damaging the SBA-15 mesoporous structure (18).

**Table 1.3.2** also shows a substantial increase in the average pore size ( $w_{\text{average}}$ ) of modified support (NH<sub>2</sub>-SBA-15) and finished catalyst (FePcCl<sub>16</sub>-NH<sub>2</sub>-SBA-15) respect to SBA-15. These results are comprehensible, because the SBA-15 micropores (< 20 Å (15)) could be easily plugged during the amino modification and were not included in the average measurement, which is also confirmed by the profile of pore size distribution (discussed later) and the t-plot analysis (data not shown). On the other hand, after complex is anchored, the average pore size slightly decreases (respect to modified SBA-15), suggesting a possible plugging of mesopores by the complex incorporation inside of them (18,38). However, due to the small size of phthalocyanines, (between 10 and 14 Å (39)), this plugging is probably caused by complex aggregations (18).

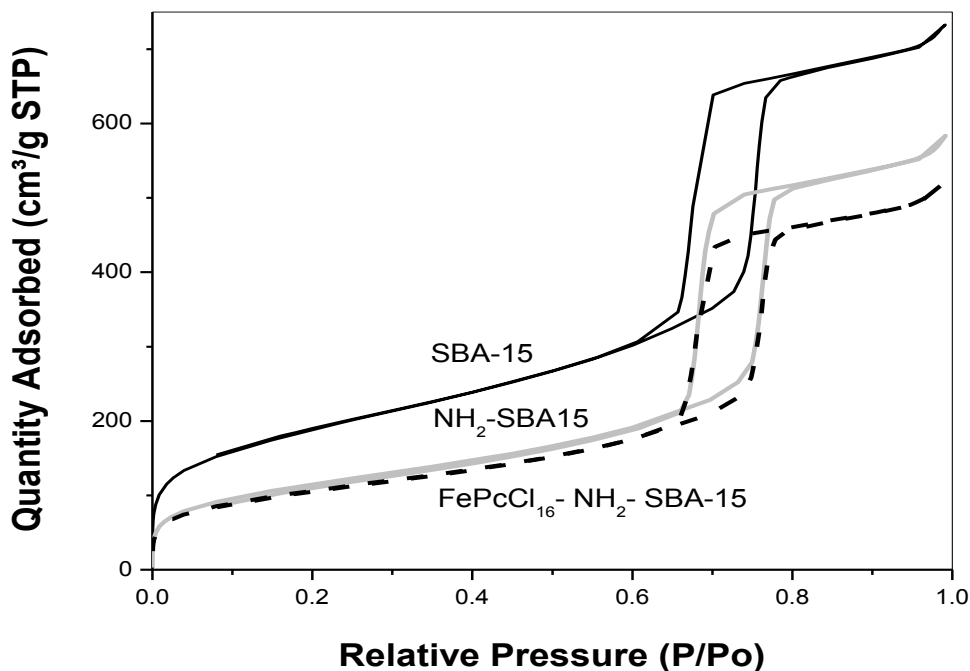


**Figure 1.3.3.** *N<sub>2</sub> adsorption/desorption isotherms of SBA-15, NH<sub>2</sub>-SBA-15 and FePcCl<sub>16</sub>-NH<sub>2</sub>-SBA-15*

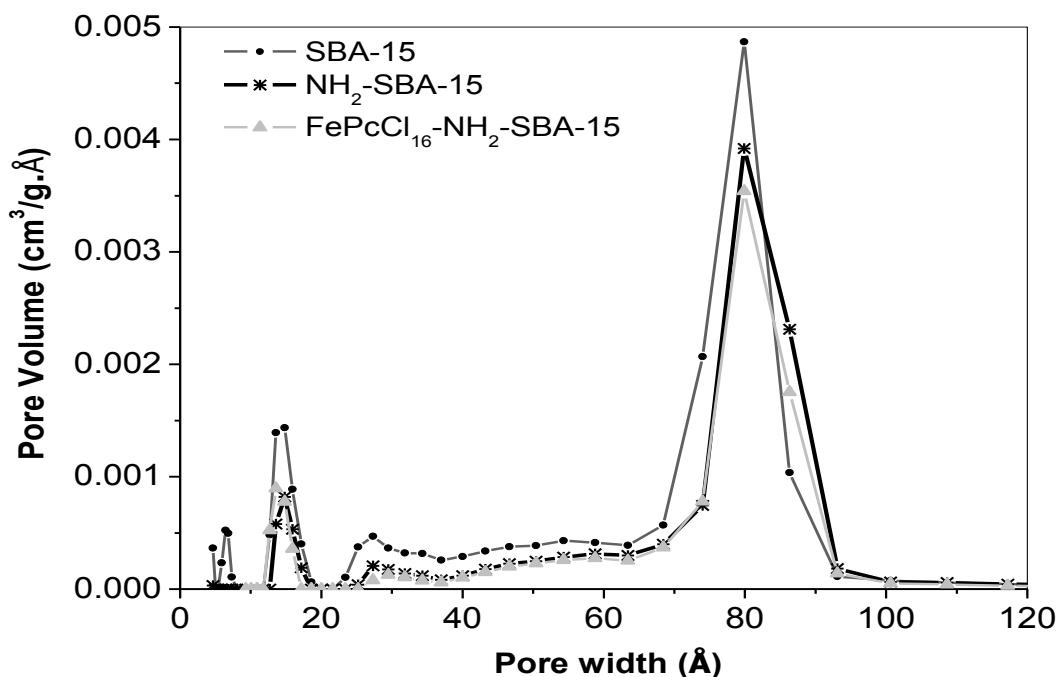
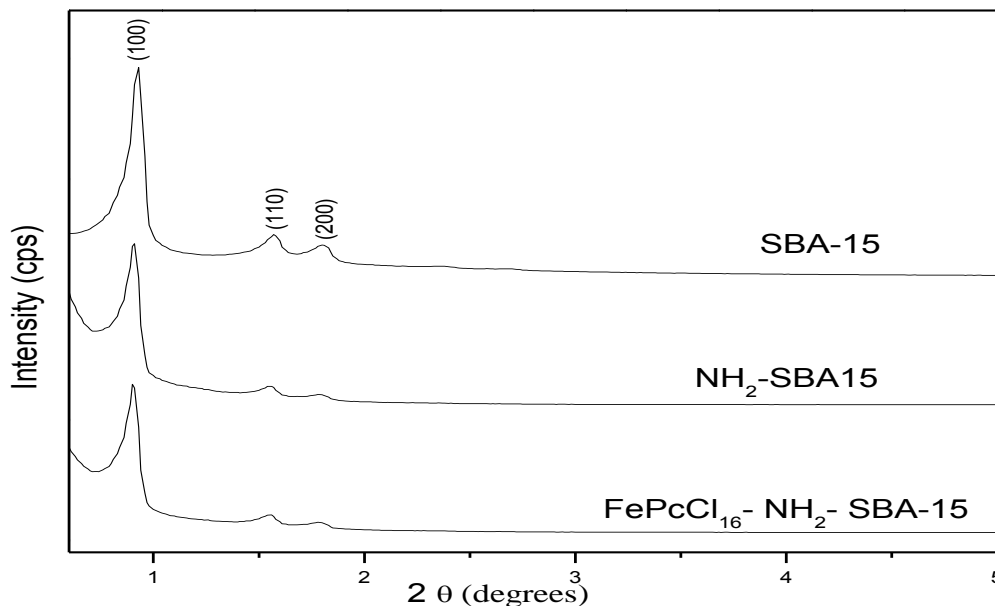


Figure 1.3.4. Pore size distribution of SBA-15,  $NH_2$ -SBA-15 and  $FePcCl_{16}$ - $NH_2$ -SBA-15

Figure 1.3.4 depicts the pore size distributions (PSD) calculated based on the Density Functional Theory (DFT). The three materials show the same primary mesopore width ( $w_{DFT}$ ) of 79.95 Å (higher value than SBA-15 average presented in Table 1.3.2) and a wide range of smaller pores with a broad maximum around 27 Å. In this figure, the presence of micropores (<20 Å) in SBA-15 was also evident, and the volume of micropores decrease significantly with the amino modification and catalyst incorporation, similarly to what has been previously reported for other catalysts like tinc oxides on the same support (20,38). This confirms the easy plugging of micropores mentioned above.

Figure 1.3.5 shows the XRD patterns of SBA-15,  $NH_2$ -SBA-15 and  $FePcCl_{16}$ - $NH_2$ -SBA-15. They exhibit very similar patterns with well-resolved diffraction peaks around  $0.9^\circ$  and two weak peaks at  $1.55^\circ$  and  $1.8^\circ$  due to (1 0 0), (1 1 0) and (2 0 0) Bragg reflections, respectively (20). The presence of the very intense peak (1 0 0) and the two higher order peaks in the tree patterns, indicates that neither the catalyst modification nor the catalyst anchoring affects the structural ordering of SBA-15 (12). Since the peak position is related with the size and shape of the unit cell (40), it could be concluded that the XRD patterns

indicate a good mesoscopic order of the materials and the characteristic hexagonal pore arrays of SBA-15, as it was observed in TEM analysis (**Figure 1.3.2**).



**Figure 1.3.5. XRD pattern for SBA-15,  $NH_2$ -SBA-15 and  $FePcCl_{16}$ - $NH_2$ -SBA-15.**

Figure 1.1.1 also shows a decrease in the intensity of the XDR peaks in the amino modified support ( $NH_2$ -SBA-15) and in the supported catalyst ( $FePcCl_{16}$ - $NH_2$ -SBA-15), this peak intensity is related with the electron density inside the unit cell, and it could confirm that the amino modification and catalyst immobilization has occurred inside the mesopores of SBA-15 (12).

Some XRD analysis were also performed at higher angles, in order to identify the iron phthalocyanine characteristic peaks at  $2\theta$  at  $6.75^\circ$ ,  $15.53^\circ$ , and  $24.68^\circ$  (41). Those peaks were not detected, suggesting a high dispersion of the complex or too small amount of complex to be detected by this analysis (42).

In addition, the pore wall thickness ( $b_{DFT}$ ) can be calculated from XRD data and the primary mesopore width ( $w_{DFT}$ ) defined through BET analysis (25), subtracting  $w_{DFT}$  from the distance between the centers of adjacent pores or XRD unit-cell parameter ( $a$ ). This later parameter was assessed from the (2 0 0) interplanar spacing ( $d_{(200)}$ ) using Equation 1.3-1 (15). The  $d_{(200)}$  was used instead of the  $d_{(100)}$  due to some inconsistencies observed

during the interplanar spacing calculation (Equation 1.3-2), which could suggest low reliability determining the position of lower angles peaks.

$$\text{Equation 1.3-1} \quad a^2 = \frac{4}{3} d^2 [h^2 + hk + k^2]$$

Where:

a= distance between the centers of adjacent pores or XRD unit-cell parameter.

d= interplanar spacing (200) calculated with Equation 1.3-2

h, k and l= Miller index

$$\text{Equation 1.3-2} \quad d_{(200)} = \frac{\lambda}{2 \sin(\theta)}$$

Where:

$\lambda$ = wavelength, (K $\alpha$  of Cu, 1.54060 Å)

$\theta$ = diffraction angle.

**Table 1.3.3: Structural parameters of SAB-15, NH<sub>2</sub>- SBA-15 and FePcCl<sub>16</sub>-NH<sub>2</sub>-SBA-15.**

| <b>Material</b>                                  | <b>d<sub>(200)</sub> (Å)</b> | <b>a (Å)</b> | <b>b<sub>DFT</sub> (Å)</b> |
|--|------------------------------|--------------|----------------------------|
| <b>SBA-15</b>                                    | 48.85                        | 112.82       | 32.92                      |
| <b>NH<sub>2</sub>- SBA-15</b>                    | 49.16                        | 113.54       | 33.63                      |
| <b>FePcCl<sub>16</sub>-NH<sub>2</sub>-SBA-15</b> | 49.39                        | 114.06       | 34.16                      |

The unit-cell parameter obtained for SBA-15 (**Table 1.3.3**) is similar to those reported in literature (25). Additionally, it could be observed in the same table, that the change in these parameters due to the support modification and catalyst incorporation is meaningless (less than 2%). This agrees with the hypothesis of complex incorporation inside the pores, inducing reduction of pore volume and surface area, without affecting the support structure.

**UV-Vis** absorption is one of the most important properties of phthalocyanine derivatives, because the spectral shape of an absorption spectrum is closely related to the molecular and electronic structure of the compound (8). **Figure 1.3.6** shows UV-vis results of amino

modified support and supported catalyst. It could be clearly observed that  $NH_2$ -SBA-15 does not show any characteristic band, while  $FePcCl_{16}$ - $NH_2$ -SBA-15 presents the main UV-vis bands of immobilized iron phthalocyanines on SBA-15. Supported  $FePcCl_{16}$  material showed a green color; this color arise from ligand  $\pi - \pi^*$  transition of C-N bonds associated with monomeric species immobilized on the support, confirmed also by the UV-vis bands around 423 and 682 nm (5). UV-vis band around 626 nm confirms the presence of  $\mu$ -oxo dimeric species in the catalyst (5). Finally, the UV-vis band around 360 nm present in the supported catalyst is associated with  $\pi - \pi^*$  transitions of the  $C = C$  double bonds of the phthalocyanine complex, suggesting that the complex remained intact during the immobilization process(10,43).

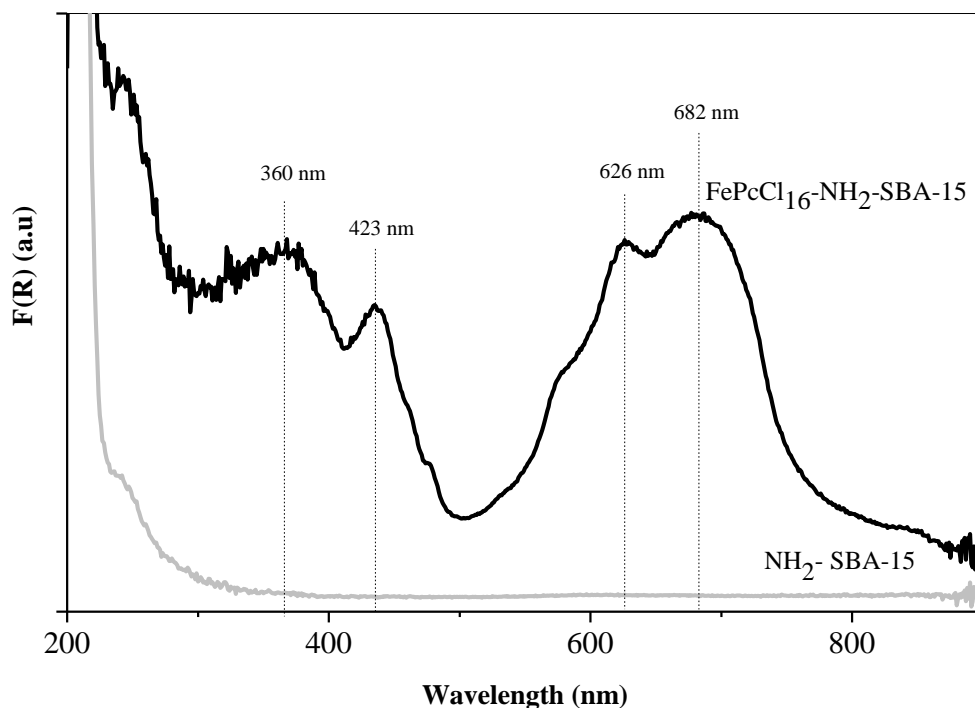


**Figure 1.3.6: UV-vis analysis of  $NH_2$ -SBA-15 and  $FePcCl_{16}$ - $NH_2$ -SBA-15.**

In a previous work (10), the FT-IR spectroscopy analysis was reported as an adequate technique for identifying tertiary N-oxide compounds (*strong bands N-O*  $960\text{ cm}^{-1}$  and  $1350\text{ cm}^{-1}$ ); however, the strong bands of  $SiO_2$  at  $1100\text{ cm}^{-1}$  and  $800\text{ cm}^{-1}$  (Si-O-Si) overlapped the phthalocyanines bands. As SBA-15 material is a siliceous material, FTIR analysis is not suitable for confirming the presence of the  $FePcCl_{16}$  in the support. Using Raman spectroscopy, **Figure 1.3.7** amino modified SBA-15 does not show significant



bands in the analyzed range (200 – 1100 nm), assuring that the bands in the  $\text{FePcCl}_{16}$ - $\text{NH}_2$ -SBA-15 catalyst are due to the  $\text{FePcCl}_{16}$  complex.

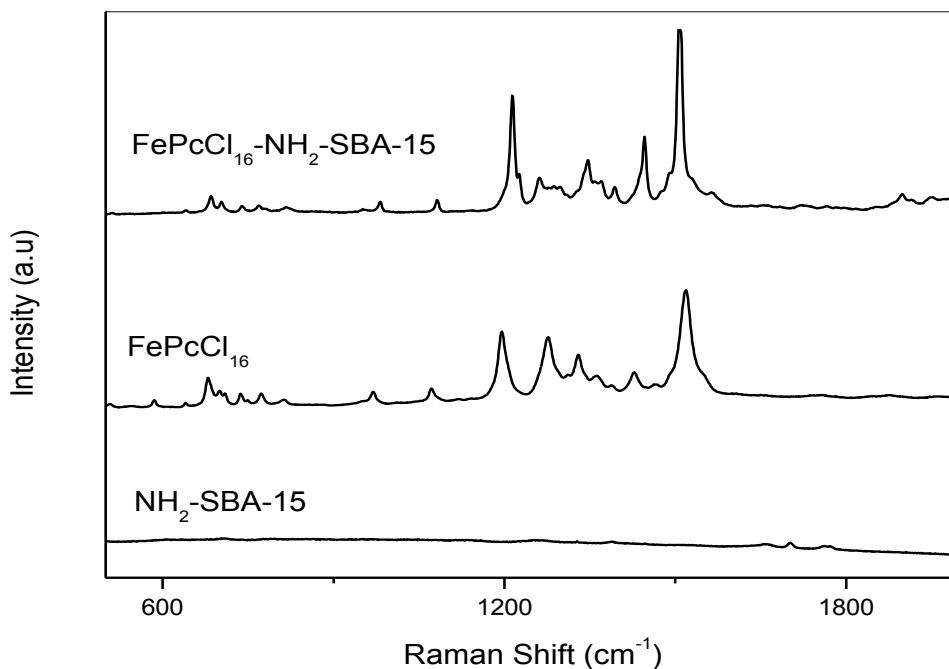


**Figure 1.3.7. Raman analysis of  $\text{NH}_2$ -SBA-15,  $\text{FePcCl}_{16}$ , and  $\text{FePcCl}_{16}$ - $\text{NH}_2$ -SBA-15**

According with **Figure 1.3.7** complex ( $\text{FePcCl}_{16}$ ) and supported catalyst ( $\text{FePcCl}_{16}$ - $\text{NH}_2$ -SBA-15) have similar bands; this similarity could indicate that the complex is not altered during the anchoring process. The bands observed between 680 and 750  $\text{cm}^{-1}$ , could be associated with both, C-Cl stretch (550 – 790  $\text{cm}^{-1}$ ) in the periphery of the phthalocyanine (44) and Pc ring “breathing” around 681 – 686  $\text{cm}^{-1}$  (45–48). In addition, the medium bands around 780 – 787  $\text{cm}^{-1}$  are associated to C=N aza stretching (49), and the strong bands around 1199 – 1205  $\text{cm}^{-1}$  are typically associated to C-H bend (45–48,50). The medium bands between 1299-1322  $\text{cm}^{-1}$  correspond to C=C pyrrole and benzene stretching, while the weak and medium bands around 1335-1457  $\text{cm}^{-1}$  are referred to isoindole stretching. Finally the strong bands around 1501-1525  $\text{cm}^{-1}$  correspond to coupling of pyrrole and aza stretching (45–48). These typical bands were observed in Raman analyses performed at the conditions reported in **Table 1.2.1**.

Finally, total weight loss obtained from TGA analyses are presented in **Table 1.3.4**. Results confirms the support modification and catalyst anchoring, since an increase in weight loss is observed after both processes, which can be attributed to the thermal decomposition of chemically bonded aminopropyl ligands and FePcCl<sub>16</sub> complex, respectively.

**Table 1.3.4: TGA analysis of SBA-15, NH<sub>2</sub>- SBA-15 and FePcCl<sub>16</sub>-NH<sub>2</sub>-SBA-15.**

| <b>Material</b>                                  | <b>Total weight loss, %</b> |
|--|-----------------------------|
| <b>SBA-15</b>                                    | 6.88                        |
| <b>NH<sub>2</sub>- SBA-15</b>                    | 7.96                        |
| <b>FePcCl<sub>16</sub>-NH<sub>2</sub>-SBA-15</b> | 18.39                       |

#### **1.4 Partial conclusions**

- The SBA-15 was successfully synthesized in this work, since different characterization techniques confirm that the material possess the typical rope-like domains with relatively uniform diameter size, and a well-ordered hexagonal mesoporous with uniform cylindrical pore channels with a narrow pore size distribution, as well as high mesoporous surface area and large pore volume with considerable micropores.
- The complex was not altered during the anchoring process, and it was supported as monomeric and  $\mu$ -oxo dimeric species
- The surface area and pore volume decrease after amino modification and complex incorporation; while other structural and morphological characteristics remained unchanged after the supporting processes. This agrees with the complex incorporation inside the SBA-15 pores, which could partially block the pores without damaging the SBA-15 mesoporous structure.
- Due to a high dispersion of the complex or small quantity of immobilized complex, its presence could be detected neither by TEM nor by XRD analysis.
- Raman spectroscopy seems to be a suitable technique to study the effect of the immobilization process onto SBA-15 in the structure of the FePcCl<sub>16</sub>.

## 2 Chapter 2: Carvone production from limonene and carveol

### 2.1 Introduction

Carvone is a molecule containing a keto group, non-conjugated and conjugated C=C double bonds and an asymmetric centre of a definite configuration. This ketone has caraway/dill odour - (4S)-(+)-carvone- or sweet spearmint odour - (4R)-(-)-carvone-, **Figure 2.1.1** A and B, respectively. Carvone is widely used in medical field, in flavor and fragrance industries, as sprouting inhibitor (S(+)-carvone), antimicrobial agent, starting material for other products and biochemical environmental indicator (51,52).

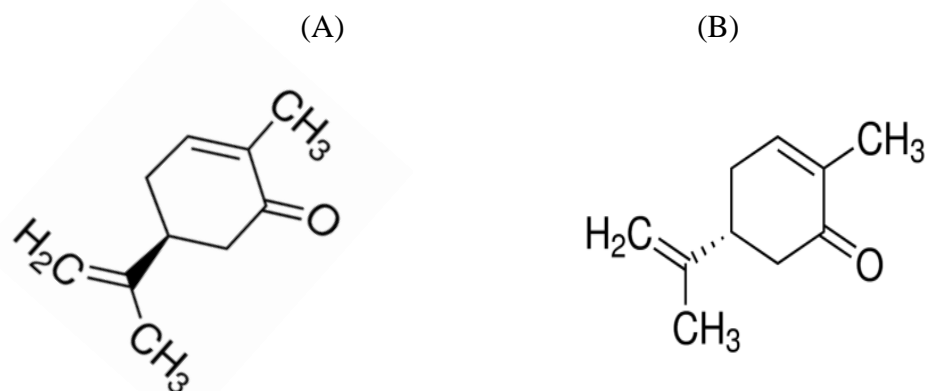


**Figure 2.1.1:** (4S)-(+)-carvone or *d*-carvone (A) and (4R)-(-)-carvone or *L*-carvone (B)

Carvone is in rising demand because its multiple uses, its main production process have been the extraction and purification of essential oils from caraway, dill and spearmint seeds; however, several drawbacks are known to crop production, such as need for large amount of raw material, need for long time, and influence of weather conditions, soil and fertilizer composition; for this reasons, during the last years carvone production has been deeply explored by chemical and biotechnological synthesis in order to satisfy the increased human demand and the environmental awareness of consumers (51,53,54). Studies made by Moll and coworkers (55) indicate that the general preference of agriculturally grown substances over technologically produced substances is unfounded.

There are several methods for the synthesis of carvone; some of them are described below:

**Hydroxylation of carvoxime** (Figure 2.1.2)

This is the classical route, in this process Limonene is treated with nitrosyl chloride to form limonene nitrosyl chloride, which is dehydrohalogenated to carvoxime and finally hydrogenated to carvone (56,57).

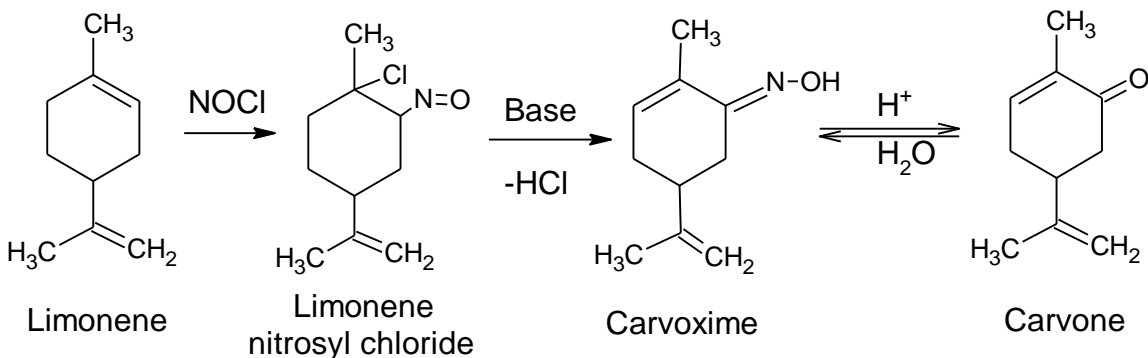


Figure 2.1.2: Hydroxylation of carvoxime

Through this process, yields of 65-70% are obtained, but a highly irritating ( $\alpha$ -terpineol) and a suspected carcinogenic (acetoxime) are formed. Furthermore sulphate is present in the effluent due to its use in product purification and the process has restrictions of security for the use of NOCl or sodium nitrate/concentrated HCl.

**Allylic oxidation of limonene** (Figure 2.1.3)

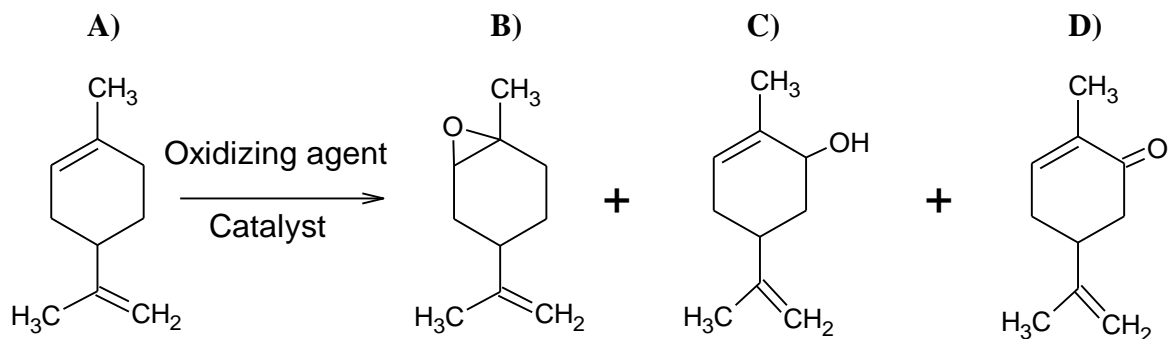
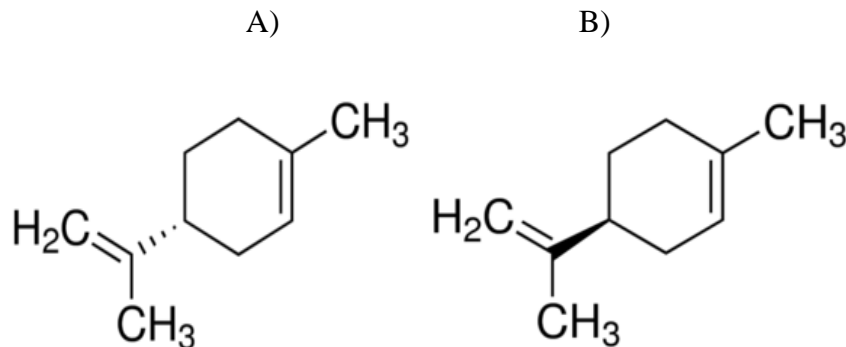


Figure 2.1.3: Allylic oxidation of limonene

Special attention has been given to this route, because limonene is an abundant and low cost raw material and the process could be performed with ecologically acceptable reagents. Limonene is one of the most widely distributed monoterpenes, abundantly present in many essential oils, the isomers *R*(+)limonene and *l*-limonene (**Figure 2.1.4 A and B**) are present in the essential oils of citric fruits and pine trees, respectively (58,59). D-Limonene or *R*(+)limonene is an abundant subproduct (30.000 tons per year worldwide) of the fruit juice industry, which comprises 95% of the orange peel oil that has to be removed to prevent bitterness (10,60). Using this agro-industrial waste as raw material, chemicals like the *R*(-) carvone could be produced, with prices from 5 to 10 times higher than limonene causing additionally a decrease in the pollution generation (3,61).

Allylic oxidation involves free radicals and hydrogen abstraction as dominant reaction and the epoxidation of the double bonds can compete with the allylic oxidation.

Most catalytic systems reported for allylic oxidation of limonene give low product yields (up to 26%) (3); which constitute its main drawback.



**Figure 2.1.4: *R* (+) limonene or D-Limonene (A) and *S* (-) Limonene or L-limonene (B)**

#### Oxidative dehydrogenation of carveol (56)(Figure 2.1.5)

The name of this process - oxidative dehydrogenation - suggests that this is not a true dehydrogenation, as it requires the presence of oxygen for acting either as oxidant or as hydrogen acceptor. Nonetheless, the oxidative dehydrogenation is not common to produce carvone, probably because it proceeds at the temperature above 360°C, which causes decomposition of carveol and carvone and leads to low yields and poor quality (62).

Oxidative dehydrogenation could be performed through Oppenauer oxidation where one hydrogen atom is transferred from carveol to an auxiliary carbonyl compound by a catalytic process. Oppenauer oxidation yield up to 91 % but has disadvantages like the catalyst sensitivity toward hydrolysis, the necessity of an auxiliary and large and labor intensive work-up. With homogeneous catalysis also is reached high yields (up to 93%) but high temperatures and excess of oxidation reagent are required and the use of expensive or toxic catalysts, usually restrict its use (10). Catalysts utilized in this process include metallic copper or silver (62).

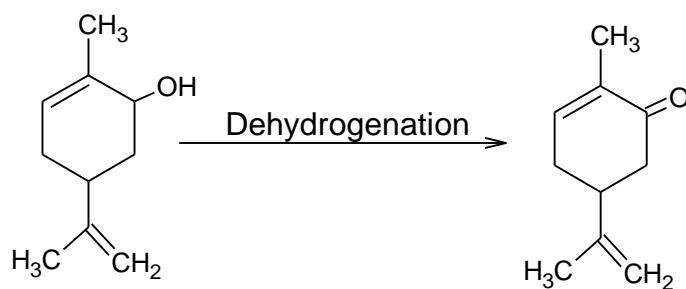


Figure 2.1.5: Dehydrogenation of carveol

FePc complexes have been found as active catalysts for the allylic oxidation of limonene and the oxidative dehydrogenation of carveol, then it becomes important the catalytic system studied in this work (2,10).

This chapter aims to study the behavior of the catalyst FePcCl<sub>16</sub>-NH<sub>2</sub>-SBA-15 for limonene and carveol reactions with TBHP, through an approach to the their mechanisms and active species involved, which is very important for the development of efficient catalysts, and for the understanding of reaction conditions that can help to define the economic feasibility of the process (2,10).

## 2.2 Experimental procedure

Using the catalysts synthesized, it was evaluated the production of carvone from two different substrates, carveol and limonene. In order to study the catalyst performance in these reactions, many experiments were carried out as described in this chapter.

To conduct the experiments a certain amount of catalyst (FePcCl<sub>16</sub>-NH<sub>2</sub>-SBA-15) was added to a 2.0 mL flask with 1.5 mL of substrate (R-(+)-Limonene 97% and L-Carveol, mixture of cis and trans, 95% from Sigma Aldrich) solution in Acetone (99.80%, from J.T. Baker); then a determined amount of commercial TBHP (70 % aqueous, from Sigma Aldrich) was added to the suspension in one step and the reaction mixture was stirred and heated at 313 K in a magnetic stirring hotplate equipped with temperature sensor and a vials heating block (*Figure 2.2.1*).



*Figure 2.2.1: Reaction system*

The reaction products were separated from the catalyst by filtration with a filter syringe and liquid phase reaction products were straightaway analyzed by the FID detector of a GC-MS Agilent 7890A chromatograph and quantified with decane (99%, from Sigma Aldrich) as internal standard. The column and method used were subject to the substrate (*Table 2.2.1*), seeking to achieve better definition of products and reactants peaks and hence, soft the quantification error.

*Table 2.2.1. Chromatographic analysis parameters*

| Parameter                | Substrate | Limonene  | Carveol   |
|--------------------------|-----------|---|---|
| Capillary column (30m)   |           | DB-1  | DB-WAX  |
| Injector temperature, °C |           | 250   | 250   |
| Detector temperature, °C |           | 300   | 270   |
| Oven program             |           | 100°C for 0.5 min, ramp to 160°C at 50°C/min, hold for 12 min, and finally ramp to 175°C at a rate of 50°C/min. | 110°C for 1 min, ramp to 160°C at 10°C/min, hold for 3 min. |
| Run time (min)           |           | 14  | 9   |

### 2.2.1 Effect of catalyst and TBHP in reactions

Reactions without TBHP or catalyst, with  $\text{FePcCl}_{16}$  or supported catalyst were performed, in order to compare their behavior.

### 2.2.2 Determination of reactions products

The peak position of reactants and main products were determined through comparison with commercial samples, except for tert-butanol and TBHP, which presented some experimental problems. The tert-butanol, due to the proximity of its peak to the acetone's peak, and the TBHP due to its thermal decomposition at the temperatures reached in the inlet system of GC (63). Additionally, liquid phase reaction products of some reactions were analyzed with a mass selective detector (MSD Agilent serie 5975) coupled to the GC-MS Agilent 7890A chromatograph, in order to define some probable secondary products.

### 2.2.3 Selection of reaction conditions under which carvone production is favored

For this experimental section, three blocks of experiments were performed in order to determine the best conditions for the reactions, as detailed below. Calculation models are described in Appendix A: calculation models.

#### 2.2.3.1 Mass transfer limitations

For determining a rate law that can represent the chemical reaction, it is required that the expressions are mainly governed by chemicals events and not by mass transfer limitations at the interface (external) or within the catalyst (internal). Usually, the external and internal mass transfer limitations are softened with higher stirring speed and smaller catalyst particle size, respectively (64). The set of reactions in the first block of this section aims to find the conditions at which those limitations decrease and therefore the carvone production is favored; varying the stirring speed (250 – 1400 rpm) and catalyst particle size (between 302 and 49  $\mu\text{m}$ ) to set their optimum values. The set of reactions previously mentioned is referred to three reactions carried out at 313 K, during 5, 15 and 30 minutes, using active sites (Fe) concentration of  $2 \times 10^{-4}$  M, a 0.08 M substrate solution in acetone and 2 (oxidant/substrate) molar ratios. These reactions were carried out in order to calculate their reaction rate, using the initial reaction rate method (64).



### 2.2.3.2 Box-Behnken experimental design

After finding conditions under which carvone production is favored (less mass transfer limitation), some reactions were performed (second block) according to a Box-Behnken experimental design with the range of variable values specified in *Table 2.2.2*. Those results were analyzed in order to determine the effect of those variables on the initial reaction rate of substrate consumption and products formation. For each defined conditions, a set of three reactions was carried out at 313 K, during 5, 15 and 30 minutes, in order to calculate their reaction rate, using the initial reaction rate method (64).

*Table 2.2.2: Variables ranges*

| Variable  | Low value | High value |
|---|-----------|------------|
| Active sites catalyst concentration, % (Fe/limonene)* | 0.06      | 0.25       |
| Oxidant/substrate molar relation                      | 1         | 4.2        |
| Substrate concentration, M                            | 0.03125   | 0.13       |

\* Mol of Fe/100 mol limonene

### 2.2.3.3 Complementary experimentation

In Box-Behnken experimental design, none of the variables were set constants to vary the other; therefore these results were not enough for a complete understanding of the reaction behavior and the mechanism fitting. Further reactions at 30 minutes at 313 K and 875 rpm, were performed to compare the results and to select the best reaction conditions. experimentation was carried out in this section, varying the molar substrate concentration ( $C_A$  for limonene and  $C_D$  for carveol), molar TBHP concentration ( $C_B$ ) and molar active sites (Fe) concentration ( $L$ ) as presented in *Table 2.2.3* and *Table 2.2.4*. For each experiment, it was calculated the substrate conversion ( $X_i$ ), product selectivity ( $S_i$ ) and product yield ( $Y_i$ ), as shown in *Appendix A: calculation models*.

**Table 2.2.3: Limonene complementary experiments**

| Constant variables                               | Changing variable                       |
|--|---|
| C <sub>A</sub> :0.13 M<br>C <sub>B</sub> :0.31 M | L: between 0 and 3 x 10 <sup>-4</sup> M |
| C <sub>A</sub> :0.13 M<br>L:3 x 10 <sup>-4</sup> | C <sub>B</sub> : : between 0 and 1.1 M  |
| L:3 x 10 <sup>-4</sup><br>C <sub>B</sub> :0.31 M | C <sub>A</sub> : between 0 and 0.266    |

**Table 2.2.4: Carveol complementary experiments**

| Constant variables                               | Changing variable                       |
|--|---|
| C <sub>D</sub> :0.13 M<br>C <sub>B</sub> :0.31 M | L: between 0 and 3 x 10 <sup>-4</sup> M |
| C <sub>D</sub> :0.13 M<br>L:3 x 10 <sup>-4</sup> | C <sub>B</sub> : : between 0 and 0.82 M |
| L:3 x 10 <sup>-4</sup><br>C <sub>B</sub> :0.31 M | C <sub>D</sub> : between 0 and 0.219 M  |

#### 2.2.4 Behavior of reactions through time

Some reactions were carried out at different times up to 24 hours, under the best initial conditions defined in this work: 875 rpm, 313 K, substrate concentration of 0.03 M, TBHP concentration of 0.31 M and active sites (Fe) concentration of 3 x 10<sup>-4</sup> M.

#### 2.2.5 Initial elucidation of reactions mechanisms

The experiments described in this section attempt to give ideas about how the studied reactions occur over the heterogeneous catalyst (FePcCl<sub>16</sub>-NH<sub>2</sub>-SBA-15) and their possible pathways.

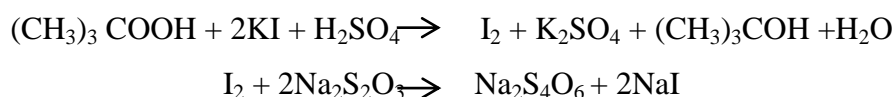
### 2.2.5.1 Evaluation of involvement of free radicals in reactions

Since it has been reported the alkoxy radical formation as the first step in the oxidation over immobilized FePc catalysts with TBHP (2); the formation of radicals throughout the reactions are under discussion and they were evaluated with the experiments described below.

In order to determine the TBHP conversion and radicals formation, samples of the solution were titrated with Na<sub>2</sub>S<sub>2</sub>O<sub>3</sub>, (explained below) (10) before and after oxidation reaction. In some of these reactions, 80 mg of 2, 4-di-tert-butylphenol (2, 4-DBP, 99%, Aldrich) were added for inhibiting the radicals formation.

#### TBHP titration (10)

The iodometric titration was carried out with a standardized 0.1M Na<sub>2</sub>S<sub>2</sub>O<sub>3</sub> solution. 100 μL of solution sample were added to a mixture of 5 mL H<sub>2</sub>SO<sub>4</sub> (30 % wt) and 5 mL KI (30 % wt) obtaining a translucent yellow mixture. Then, Na<sub>2</sub>S<sub>2</sub>O<sub>3</sub> solution was added until a colorless solution was obtained. Following equations represent the reactions that occur during titration.



### 2.2.5.2 O<sub>2</sub> participation and hydroperoxide formation in limonene reaction

It has been found that in the allylic oxidation of cyclohexene with the catalytic system FePcCl<sub>16</sub>-SiO<sub>2</sub>/TBHP, cyclohexenyl hydroperoxide is formed as an intermediate product of a radical pathway with O<sub>2</sub> participation (65). Given the structural similarity of cyclohexene with limonene, the formation of limonene hydroperoxide and the O<sub>2</sub> involvement throughout reaction, were evaluated with the experiments described below.

The hydroperoxides, possibly formed as reaction intermediates cannot be directly detected by GC-MS analysis as they are thermally decomposed at

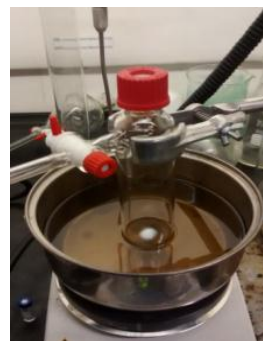


Figure 2.2.2: Experimental set for reactions under inert atmosphere

temperatures above 473 K usually reached in the inlet system of GC (63). Limonene hydroperoxide formation was evaluated by the difference in the concentration of carveol before and after the treatment of a typical reaction sample (0.2 mL) with a solution (0.2 mL) 0.19 M and 0.38 M of triphenylphosphine (PPh<sub>3</sub>) in mixture of 40% dichloromethane (99.8%, Merck) and ethanol (Absolute for analysis, Merck) , during 0.5 and 2 h. PPh<sub>3</sub> readily reduce the hydroperoxide to give quantitative conversion to the corresponding alcohol (63).

To test the O<sub>2</sub> participation in limonene reaction, the catalyst (0.21 mol of Fe per 100 mol of substrate) and 4 mL of 0.13 M substrate solution in acetone were placed in an Ace pressure tube (**Figure 2.2.2**), equipped with bushing and plunger valve. The suspension was frozen with liquid nitrogen and all the air in the reactor was evacuated and replaced by argon; then the suspension was allowed to warm at room temperature. This procedure was carried out three times in order to guarantee complete oxygen evacuation. Then degasified TBHP (2.6 mol TBHP/mol substrate) was added to the solution and the reaction was stirred at 40 °C for 30 minutes. The experiments were repeated without catalyst and without TBHP in order to determine its influence in the reaction and compare results with those obtained in presence of air. The reaction products were separated and analyzed as described before.

### **2.2.6 Mechanisms and kinetics models**

To analyze the effect of reactants and catalyst concentration on initial reactions rates, a set of three reactions was carried out at 313 K and 875 rpm for each experiment condition defined in section 2.2.3.3, during 5, 15 and 30 minutes, in order to calculate their reaction rate, using the initial reaction rate method (64). With this information, several reaction rate expressions were proposed and their validity was determined by correlation with experimental data. The parameters were estimated through non-linear regression with hybrid algorithm Matlab R® (**Appendix B: Matlab ® hybrid algorithm**). The mentioned hybrid algorithm use Matlab Genetic algorithm (GA) to evaluate several initial parameters and find a suitable initial point to use in nonlinear least-squares solver (*lsqnonline*). This hybrid algorithm was defined because the final result with *lsqnonline* is susceptible to changes in the initial parameters. Model comparison was carried out with the goodness-of-fit statistics defined by Matlab (**Table 2.2.5**) (66):

Table 2.2.5. Statistics used for model comparison (66)

| Statistic                                   | Definition   | Equation  |
|---|--|---|
| <b>Sum of squares due to error</b>          | It measures the total deviation of the response values from the fit to the response values. It is called the summed square of residuals (SSE)  | $SSE = \sum_1^N (r_{exp} - r_{cal})^2$ <p>Where:<br/> <math>r_{exp}</math>= experimental reaction rate<br/> <math>r_{cal}</math>=calculated reaction rate with proposed models.<br/>                     N= number of experiments</p>   |
| <b>Mean square error</b>                    | Residual mean square (MSE)   | $MSE = \frac{SSE}{N - p}$ <p>Where:<br/>                     N= number of experiments<br/>                     p= number of fitted coefficients estimated from the response values.</p>   |
| <b>Root mean squared error</b>              | Known as the fit standard error and the standard error of the regression. It is an estimate of the standard deviation of the random component in the data (RMSE)   | $RMSE = \sqrt{MSE}$ <p>Where:<br/>                     MSE= Mean square error</p>   |
| <b>R-Square</b>                             | It measures how successful is the fit for explaining the variation of the data. R-square is the square of the correlation between the response values and the predicted response values. It is also called the square of the multiple correlation coefficients and the coefficient of multiple determinations. | $R - Square = 1 - \frac{SSE}{SST}$ <p>Where:<br/>                     SSE= Sum of squares due to error<br/>                     SST= sum of squares about the mean, <math>\sum_1^N (r_{exp} - \bar{r})^2</math></p>   |
| <b>Degrees of Freedom Adjusted R-Square</b> | It uses the R-square statistic defined above, and adjusts it based on the residual degrees of freedom.   | $Adj. R - Square = 1 - \frac{SSE * (N - 1)}{SST * (N - p)}$ <p>Where:<br/>                     SSE= Sum of squares due to error<br/>                     SST= sum of squares about the mean, <math>\sum_1^N (r_{exp} - \bar{r})^2</math><br/>                     N= number of experiments<br/>                     p= number of fitted coefficients estimated from the response values</p> |

## 2.3 Results and discussion

### 2.3.1 Effect of catalyst and TBHP in reactions

From the *Figure 2.3.1* it could be seen that the presence of the catalyst favors both, the limonene conversion and carvone selectivity at large reaction times (24h). Although, the limonene conversion decreases with the complex immobilization on SBA-15, the carvone selectivity slightly increases (*Figure 2.3.1* and *Figure 2.3.2*). Additionally, it could be concluded that TBHP is essential for carvone production from limonene, due to the very low conversion (<2%) and the null carvone production obtained in the absence of this hydroperoxide (*Figure 2.3.1*).

The presence of monomeric and  $\mu$ -oxo dimeric species in  $\text{FePcCl}_{16}\text{-NH}_2\text{-SBA-15}$  catalysts (previously mentioned), may be responsible for its catalytic activity. However, its activity could be limited due to catalyst pore size (around 80 Å) and the possible immobilization of complex inside the channels (as deduced from catalyst characterization), thus reducing their pore volume and restricting access of the reactants to the active sites. Furthermore, the decrease in limonene conversion caused by catalyst immobilization, could be due to a competition between limonene and TBHP to be adsorbed on the active sites (67).

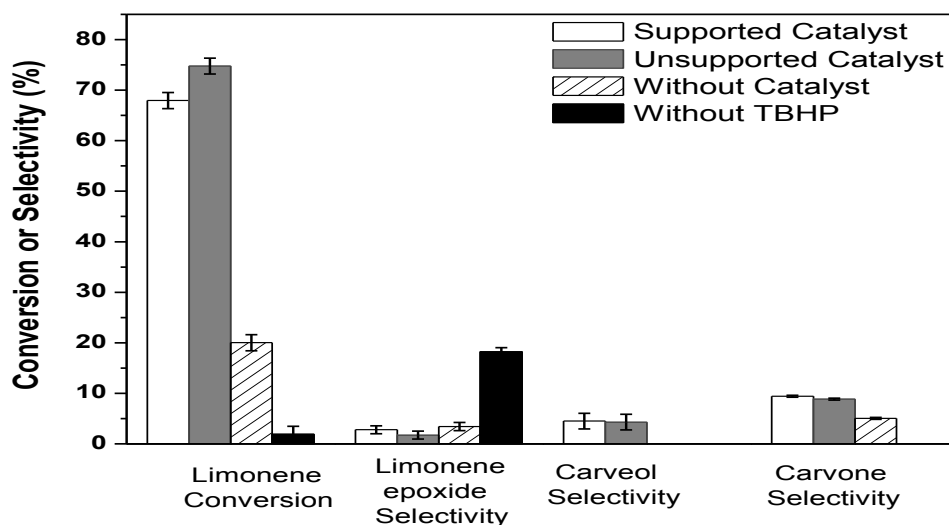


*Figure 2.3.1: Performance of TBH with  $\text{FePcCl}_{16}\text{-NH}_2\text{-SBA-15}$  catalyst system in limonene reaction.*

Reaction conditions: 1.5 mL of 0.13 M limonene in acetone, active sites (Fe) concentration of  $3 \times 10^{-4}$  M, 0.49 mmol of commercial TBHP, 313 K, 24 h.

Moreover, at shorter reaction times, up to 30 minutes (when carveone overoxidation is less probable) it is observed that complex immobilization restricts the epoxide formation (**Figure 2.3.2 B**), and favors carveone formation (**Figure 2.3.2 C**). These results and the high formation of limonene epoxide without catalyst (**Figure 2.3.1**) suggest the existence of two different oxidation pathways. One of these pathways, the allylic oxidation of limonene to carveone is favored by the presence of supported catalyst, probably a one-electron process with radical intermediates (2,68).

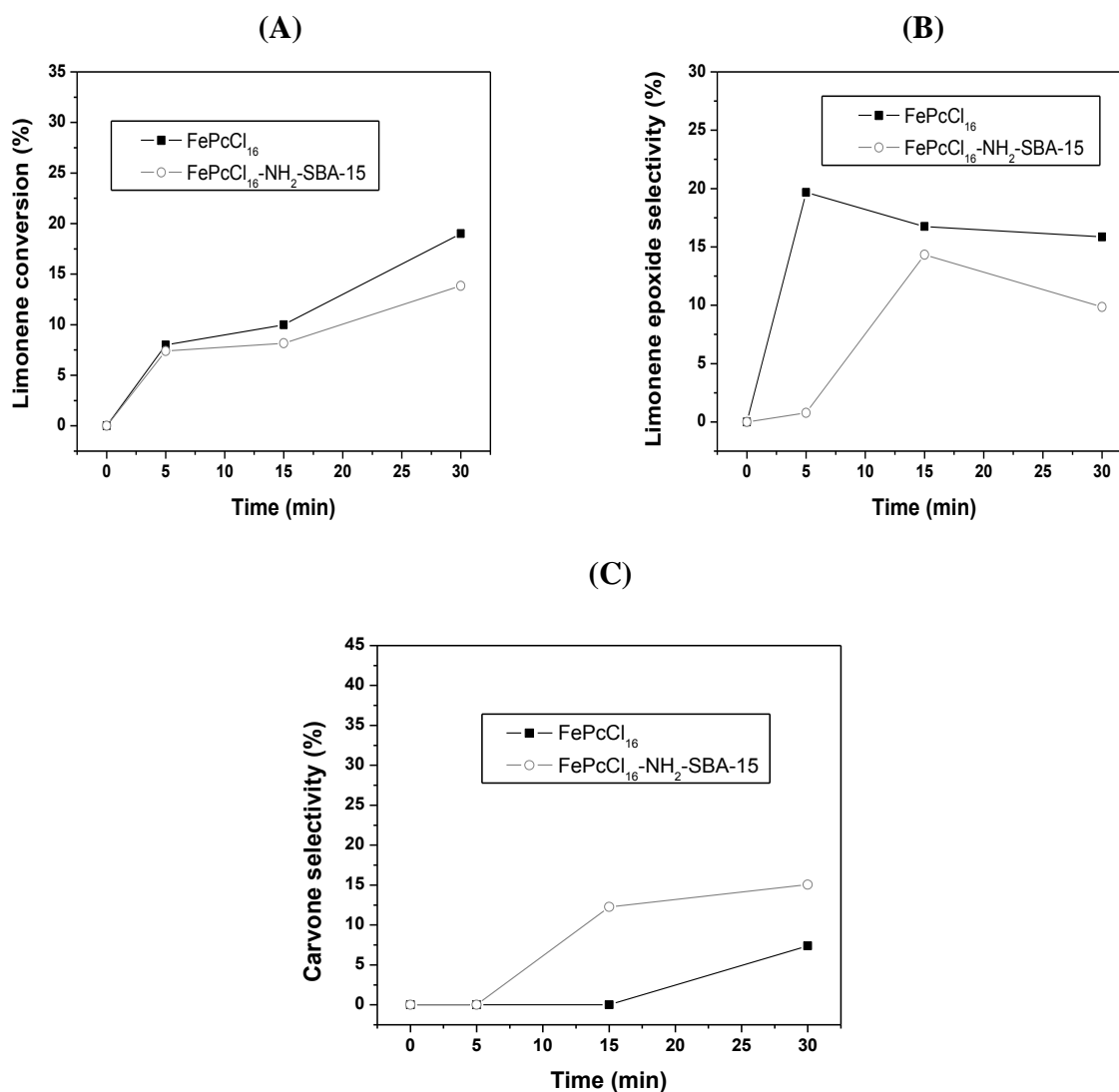


**Figure 2.3.2: Support effect on the limonene conversion (A) and the epoxide selectivity (B) and carveone selectivity (C) at the allylic oxidation of limonene with  $\text{FePcCl}_{16}$  / TBHP system. Reaction conditions: 1.5 mL of 0.13 M solution limonene in acetone, commercial TBHP 0.49 mmol, active sites (Fe) concentration of  $3 \times 10^{-4}$  M.**

Epoxidation of limonene is disadvantaged by supported catalyst; perhaps due to the heterogeneous nature of a metal Oxo species attack to the double bond and the restricted access of the reactants to the active sites due to support characteristics (67).

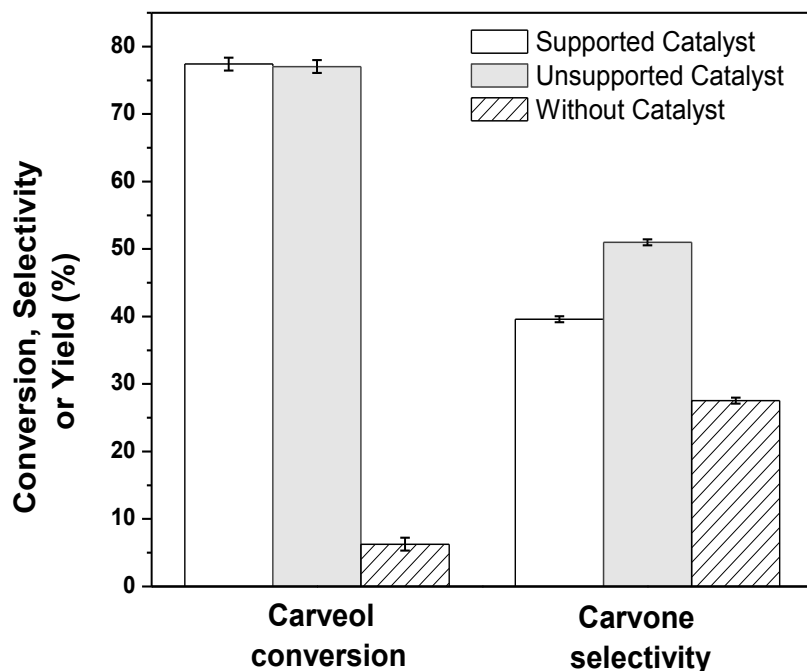


**Figure 2.3.3: Performance of TBH/ FePcCl<sub>16</sub>-NH<sub>2</sub>-SBA-15 catalytic system in carveol reaction**  
 Reaction conditions: 1.5 mL of 0.13 M carveol in acetone, active sites (Fe) concentration of  $3 \times 10^{-4}$  M, 0.49 mmol of commercial TBHP, 313 K, 24 h.

From the **Figure 2.3.3** it could be observed that the presence of the catalyst favors significantly the carveol conversion and carvone selectivity, however the catalyst immobilization on SBA-15 causes a slight reduction in carvone production respect to unsupported catalyst. These results may indicate that carveol dehydrogenation occurs in active sites inside the catalyst pores, and adverse behavior in carvone production might be due to restricted access of the reactants to active sites (69). Finally, it could be concluded that TBHP is essential for carveol reaction, since its conversion without TBHP was not detected (data not shown).

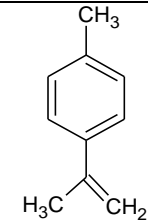
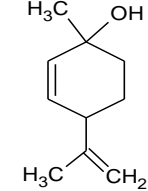
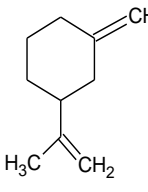
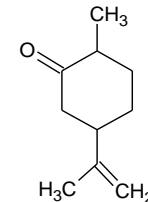
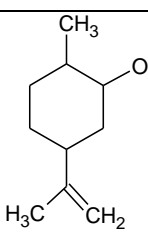
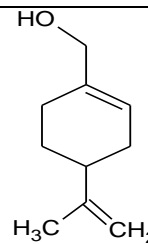


### **2.3.2 Reactions products**

In the catalytic system Limonene/TBHP/FePcCl<sub>16</sub>-NH<sub>2</sub>-SBA-15, the major products detected with the chromatographic analysis were limonene oxide, carvone and carveol in some cases (*Figure 2.1.3 B, D and C*), which are typical in allylic oxidation reactions where there is competition with double bond epoxidation in monoterpenes (10,11). Carveol has been considered as an intermediate product in carvone synthesis (70); therefore, it is not surprising that carvone (*Figure 2.1.3 D*) was detected as the main product of carveol catalytic dehydrogenation with TBHP and FePcCl<sub>16</sub>-NH<sub>2</sub>-SBA-15. On the other hand, since in most of the reaction of limonene oxidation performed in this research, carveol was not detected, it could be inferred that all produced carveol transforms rapidly to carvone, and the reactions step related to carveol production could be the limiting steps of the limonene oxidation with this catalytic system.

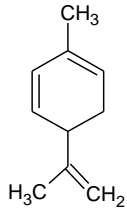
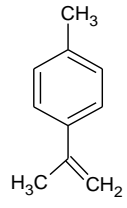
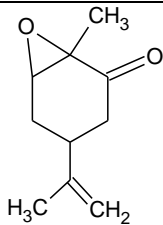
Besides the main products shown in *Figure 2.1.3*, trace amount of several byproducts were detected in both reactions. *Table 2.3.1* and *Table 2.3.2* present the most significant byproducts. The high amount of byproducts (mainly for limonene oxidation), could be explained by the many active sites that substrates possess. However, the proportion in which these byproducts are generated is much smaller than the main products (around half or one third), reason why those byproducts were not considered and quantified in this work. Additionally, tert-butanol was detected as an important byproduct; however it could not be quantified, since its peak in the chromatographic analysis was masked by acetone's peak.

Table 2.3.1: Limonene reaction byproducts

| Entry | Name  | CAS          | Molecule  |
|-------|---|--------------|---|
| 1     | 1-methyl-4-(1-methylethenyl)-Benzene        | 1195-32-0    |    |
| 2     | p-Mentha-2,8-dien-1-ol                      | 0022771-44-4 |    |
| 3     | Cyclohexane,1-methylene-3-(1-methylethenyl) | 13837-95-1   |    |
| 4     | Dihydrocarvone                              | 005948-04-9  |   |
| 5     | 1,6-dihydrocarveol                          | 619-01-2     |  |
| 6     | Perillyl alcohol                            | 000536-59-4  |  |

\*The byproducts presented in this table are defined as the more probable according to the analysis with the mass detector and the literature reports (2,11,54,70–72).

Table 2.3.2: Carveol reaction byproducts

| Entry | Name                                    | CAS         | Molecule  |
|-------|---|-------------|---|
| 1     | 1,3,8-p Menthatriene                    | 021195-59-5 |  |
| 2     | Benzene, 1-methyl-4-(1-methylethen yl)- | 001195-32-0 |  |
| 3     | Carvone oxide                           | 018383-49-8 |  |

\*The byproducts presented in this table are defined as the more probable according to the analysis with the mass detector and the literature reports (11,70,71,73).

The enantiomers d-carvone and l-carvone cannot be separated with standard chromatographic techniques (74). However, according to some sources like Chiral chemistry in flavours & fragrances, (-)-carvone has being manufactured from (+)-limonene since 1960s, by two procedures, one of which includes the (-) carveol production with its subsequently oxidation to (-)-carvone (57,75). Regarding to (-) carveol, its transformation to (-) carvone is also reported by Morriish and Dougulis (73).

### 2.3.3 Reaction conditions under which carvone production is favored

#### 2.3.3.1 Mass transfer limitations

The effect of stirring speed in the limonene reaction for the FePcCl<sub>16</sub>-NH<sub>2</sub>-SBA-15 catalytic system is shown in *Table 2.3.3*.

**Table 2.3.3 Limonene reaction rate,  $-r_{\text{limonene}}$  ( $\text{mmol}_{\text{limonene}} / \text{g}_{\text{Fe}} \cdot \text{min}$ ) at different stirring speeds**

| <b>rpm</b>                               | <b>250</b> | <b>375</b> | <b>500</b> | <b>625</b> | <b>750</b> | <b>875</b> | <b>1000</b> | <b>1100</b> | <b>1250</b> | <b>1400</b> |
|--|------------|------------|------------|------------|------------|------------|-------------|-------------|-------------|-------------|
| <b><math>-r_{\text{limonene}}</math></b> | 23.81      | 21.22      | 21.06      | 26.25      | 25.95      | 26.56      | 24.27       | 26.41       | 24.42       | 24.73       |

Reaction conditions: 1.5 mL of 0.08 M limonene solution in acetone, commercial TBHP 0.24 mmol, active sites (Fe) concentration of  $2 \times 10^{-4}$  M, 313 K, up to 30 min. In this set of reactions *FePcCl<sub>16</sub>-NH<sub>2</sub>-SBA-15* batch 1 was used. SD:  $\pm 2 \text{ mmol}_{\text{limonene}} / \text{g}_{\text{Fe}} \cdot \text{min}$

These results indicate that limonene consumption is relatively constant from 625 rpm, and maximize at 875 rpm, which may be related to growing of external mass transfer caused when the speed of the fluid increases, decreasing the boundary layer through which reactants and products diffuse (64). Although reaction rates variation related with stirring speed is not very significant, it was decided to continue the experiments with a stirring speed of 875 rpm due to its minor external diffusional limitations.

Furthermore, the effect of catalyst particle size in the limonene reaction rate is shown in Table 2.3.4. The small variation observed in this data could be explained by experimental error; hence the mass transfer limitations do not vary significantly with the decrease of particle size and either analyzed sizes could be used henceforth. Due to the availability of catalyst particle size of 49  $\mu\text{m}$ , this size was chosen.

**Table 2.3.4 Limonene reaction rate,  $-r_{\text{limonene}}$  ( $\text{mmol}_{\text{limonene}} / \text{g}_{\text{Fe}} \cdot \text{min}$ ) with different catalyst particle sizes**

| <b><math>\mu\text{m}</math></b>          | <b>302.5</b> | <b>152.5</b> | <b>107.5</b> | <b>76.5</b> | <b>58</b> | <b>49</b> |
|--|--------------|--------------|--------------|-------------|-----------|-----------|
| <b><math>-r_{\text{limonene}}</math></b> | 27.63        | 32.21        | 32.66        | 24.93       | 26.00     | 30.83     |

Reaction conditions: 1.5 mL of 0.08 M limonene solution in acetone, commercial TBHP 0.24 mmol, active sites (Fe) concentration of  $2 \times 10^{-4}$  M, 313 K, up to 30 min. In this set of reactions *FePcCl<sub>16</sub>-NH<sub>2</sub>-SBA-15* batch 1 was used. SD:  $\pm 3.4 \text{ mmol}_{\text{limonene}} / \text{g}_{\text{Fe}} \cdot \text{min}$

As it was mentioned above, the carveol is an intermediate in limonene allylic oxidation; on the other hand the products of both reactions are very similar. Therefore, the stirring speed

and catalyst particle size used for **carveol reactions** were the same determined for limonene.

### 2.3.3.2 Box-Behnken experimental design

#### Analysis of TBHP/limonene and TBHP/Fe molar ratios and active sites concentration variations

The results obtained (*Table 2.3.5*) indicates that for a TBHP/limonene molar ratio of 2.6, the highest limonene reaction rate (131.649 mmol/g<sub>Fe</sub>.min) is obtained with an active sites concentration of 0.19 mol % (Fe/limonene), entry 4. On the other hand, an active sites concentration of 0.25 mol % (Fe/limonene), entry 5, favors formation of carvone over limonene epoxide, being their formation rates 2.979 and 2.803 mmol/g<sub>Fe</sub>.min, respectively.

*Table 2.3.5: Effect of active sites catalyst concentration on reactions rates with a constant TBHP/limonene molar ratio of 2.6*

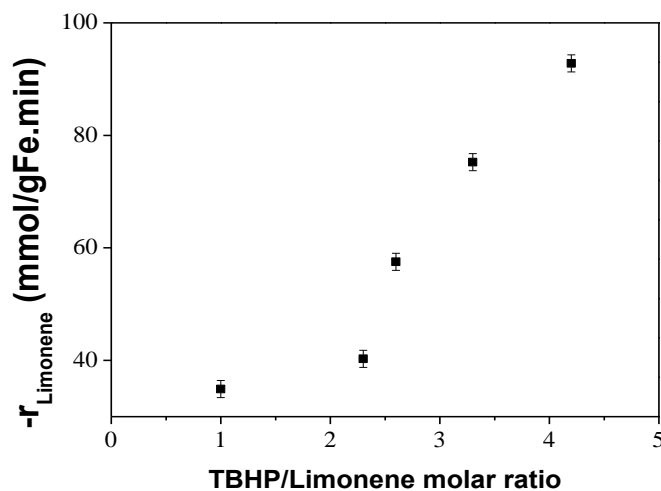
| Entry | Active sites concentration<br>*, %<br>(Fe/limonene) | -r <sub>Limone</sub><br>mmol/g <sub>Fe</sub> .min | r <sub>Carvone</sub><br>mmol/g <sub>Fe</sub> .min | r <sub>Limone epoxide</sub><br>mmol/g <sub>Fe</sub> .min |
|-------|---|---|---|--|
| 1     | 0.06  | 105.780   | 0.000   | 0.000  |
| 2     | 0.13  | 48.494  | 0.000   | 4.621  |
| 3     | 0.16  | 57.533  | 0.000   | 1.434  |
| 4     | 0.19  | 131.649   | 0.000   | 1.138  |
| 5     | 0.25  | 51.929  | 2.979   | 2.803  |

\* Mol of Fe/100 mol limonene

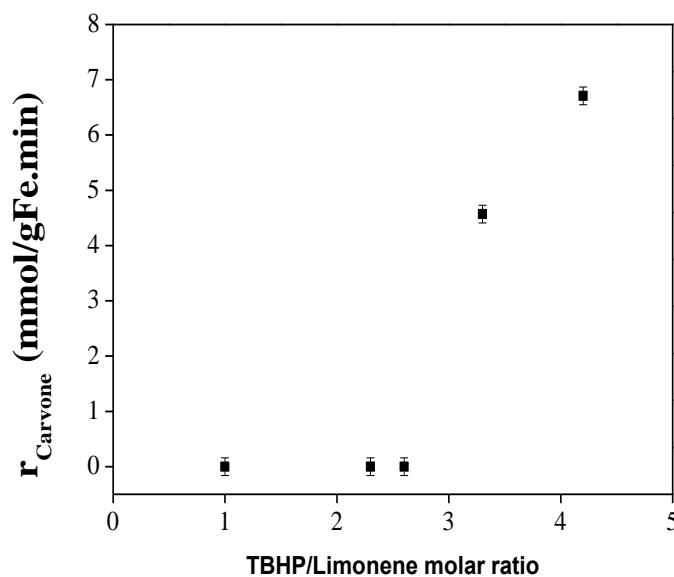
*Reaction conditions: 1.5 mL of limonene solution in acetone, TBHP/limonene molar ratio of 2.6, 313 K, up to 30 min.*

From *Figure 2.3.4* it could be observed that, for an active sites concentration of 0.16 mol % (Fe/limonene), the rise of TBHP/limonene molar ratio causes an increasing trend of limonene consumption (*Figure 2.3.4 A*) and carvone production (*Figure 2.3.4 B*) reaction rates, from 34.90 to 92.79 mmol<sub>limonene</sub>/g<sub>Fe</sub>.min and 0 to 6.7 mmol<sub>carvone</sub>/g<sub>Fe</sub>.min, while the epoxidation reaction rate decreases (*Figure 2.3.4 C*) from 7.30 to 2.14 mmol<sub>limonene epoxide</sub>/g<sub>Fe</sub>.min). These results clearly states, that the oxidant excess favors the limonene consumption and carvone production, this might be due to a competition between substrate and oxidant when their molar relation is short (67)

(A)



(B)



(C)

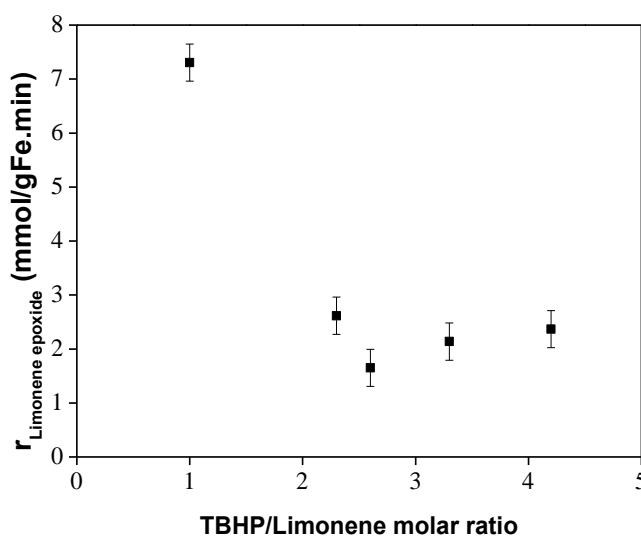


Figure 2.3.4: Variation of reaction rates of limonene epoxide (A), carvone (B) and limonene (C) with variation of TBHP/limonene molar ratio with an active site(Fe) concentration of 0.16 mol % (Fe /limonene).

**Table 2.3.6** shows that at a constant limonene concentration of 0.08 M the highest consumption of limonene (58.544 mmol/g<sub>Fe</sub>.min) and production of carvone (4.596 mmol/g<sub>Fe</sub>.min) were obtained with a TBHP/Fe molar ratio of around 1680 (entry 4); in the case of the limonene epoxide formation rate the maximum value (2.896 mmol/g<sub>Fe</sub>.min) is reached with a TBHP/Fe molar ratio of 1600. A lower ratio of TBHP/Fe implies a greater availability of active sites for TBHP adsorption, thus it would be expected increasing reaction rates by decreasing this ratio; however, the data obtained do not show a distinct trend, suggesting that rates are not only governed by this relationship, but also by other factors as the amount of oxidant and its relation with the limonene concentration.

**Table 2.3.6: Effect of TBHP/Fe molar ratio (1600-1706.7) on the initial reaction rates with a constant limonene concentration of 0.08 M.**

| Entry | TBHP/Fe molar ratio | -r <sub>Limonene</sub> mmol/g <sub>Fe</sub> .min | r <sub>Carvone</sub> mmol/g <sub>Fe</sub> .min | r <sub>Limonene epoxide</sub> mmol/g <sub>Fe</sub> .min |
|-------|---------------------|--|--|---|
| 1     | 1600.0              | 55.150   | 0.000  | 2.896   |
| 2     | 1664.0              | 57.533   | 0.000  | 1.649   |
| 3     | 1672.5              | 55.754   | 0.000  | 1.766   |
| 4     | 1680.0              | 58.544   | 4.596  | 2.036   |
| 5     | 1706.7              | 57.296   | 0.000  | 1.888   |

Reaction conditions: 1.5 mL of 0.08 M limonene solution in acetone, 313 K, up to 30 min.

Due to the limited information obtained from this experimental design and its inadequacy for the mechanism fitting, it was not performed with carveol as substrate, and focus on complementary experiments (section 2.3.3.3)

### 2.3.3.3 Complementary experimentation

**Table 2.3.7** summarizes the results for 30 minutes limonene reactions carried out with Box-Behnken experimental design and complementary experiments. From this table, it could be observed that, despite the short reaction time, there is limonene conversion at all conditions tested, but the carvone production is limited when the reactants concentration is very low (for example entry 1, 2), probably because the amount of carvone produced at short time (30 minutes) could be under the detection limit of chromatograph. From these results, it

could be also observed that limonene conversion as well as carvone yield maximizes in experiment 32. These conditions will be used from now on in this work.

*Table 2.3.7: Results limonene reactions at 30 minutes, 313 K and 875 rpm.*

| Entry     | C <sub>A</sub> , M | C <sub>B</sub> ,M | L, M         | Limonene conversion, X <sub>A</sub> | Carvone selectivity, S <sub>F</sub> | Carvone Yield, Y <sub>F</sub> |
|-----------|--------------------|-------------------|--------------|-------------------------------------|-------------------------------------|-------------------------------|
| 1         | 0.03               | 0.03              | 5E-05        | 9.82                                | 0.00                                | 0.00                          |
| 2         | 0.07               | 0.15              | 1E-04        | 15.03                               | 0.00                                | 0.00                          |
| 3         | 0.13               | 0.49              | 2E-04        | 24.23                               | 6.09                                | 1.47                          |
| 4         | 0.10               | 0.30              | 1E-04        | 20.85                               | 5.44                                | 1.13                          |
| 5         | 0.08               | 0.08              | 5E-05        | 6.22                                | 0.00                                | 0.00                          |
| 6         | 0.08               | 0.17              | 1E-04        | 13.71                               | 0.00                                | 0.00                          |
| 7         | 0.08               | 0.31              | 2E-04        | 25.39                               | 6.25                                | 1.59                          |
| 8         | 0.08               | 0.25              | 1E-04        | 19.62                               | 0.00                                | 0.00                          |
| 9         | 0.03               | 0.08              | 2E-05        | 12.72                               | 0.00                                | 0.00                          |
| 10        | 0.07               | 0.17              | 9E-05        | 15.32                               | 0.00                                | 0.00                          |
| 11        | 0.13               | 0.31              | 3E-04        | 21.43                               | 4.59                                | 0.98                          |
| 12        | 0.10               | 0.24              | 2E-04        | 40.89                               | 0.00                                | 0.00                          |
| 13        | 0.08               | 0.20              | 1E-04        | 15.68                               | 0.00                                | 0.00                          |
| 14        | 0.08               | 0.20              | 1E-04        | 13.95                               | 0.00                                | 0.00                          |
| 15        | 0.08               | 0.20              | 1E-04        | 18.64                               | 0.00                                | 0.00                          |
| 16        | 0.08               | 0.16              | 2E-04        | 13.86                               | 0.00                                | 0.00                          |
| 17        | 0.13               | 0.31              | 7E-05        | 8.08                                | 0.00                                | 0.00                          |
| 18        | 0.13               | 0.31              | 2E-04        | 10.31                               | 0.00                                | 0.00                          |
| 19        | 0.13               | 0.31              | 2E-04        | 10.84                               | 6.62                                | 0.72                          |
| 20        | 0.13               | 0.31              | 2E-04        | 11.31                               | 0.00                                | 0.00                          |
| 21        | 0.13               | 0.31              | 3E-04        | 14.70                               | 4.78                                | 0.70                          |
| 22        | 0.13               | 0.31              | 0E+00        | 2.82                                | 0.00                                | 0.00                          |
| 23        | 0.13               | 0.12              | 3E-04        | 8.29                                | 0.00                                | 0.00                          |
| 24        | 0.13               | 0.27              | 3E-04        | 11.33                               | 0.00                                | 0.00                          |
| 25        | 0.13               | 0.39              | 3E-04        | 15.52                               | 0.00                                | 0.00                          |
| 26        | 0.13               | 0.49              | 3E-04        | 18.81                               | 5.31                                | 1.00                          |
| 27        | 0.13               | 0.00              | 3E-04        | 0.27                                | 0.00                                | 0.00                          |
| 28        | 0.13               | 0.66              | 3E-04        | 21.44                               | 5.23                                | 1.12                          |
| 29        | 0.13               | 0.82              | 3E-04        | 29.69                               | 5.47                                | 1.62                          |
| 30        | 0.13               | 0.97              | 3E-04        | 31.81                               | 3.98                                | 1.27                          |
| 31        | 0.13               | 1.11              | 3E-04        | 33.94                               | 4.00                                | 1.36                          |
| <b>32</b> | <b>0.03</b>        | <b>0.31</b>       | <b>3E-04</b> | <b>41.59</b>                        | <b>6.15</b>                         | <b>2.56</b>                   |
| 33        | 0.07               | 0.31              | 3E-04        | 25.12                               | 5.92                                | 1.49                          |
| 34        | 0.08               | 0.31              | 3E-04        | 21.01                               | 0.00                                | 0.00                          |
| 35        | 0.10               | 0.31              | 3E-04        | 18.65                               | 5.18                                | 0.97                          |



|    |      |      |       |       |      |      |
|----|------|------|-------|-------|------|------|
| 36 | 0.17 | 0.31 | 3E-04 | 10.60 | 0.00 | 0.00 |
| 37 | 0.22 | 0.31 | 3E-04 | 7.69  | 0.00 | 0.00 |
| 38 | 0.27 | 0.31 | 3E-04 | 8.20  | 0.00 | 0.00 |

Results for carveol reactions are presented in **Table 2.3.8**, which shows that despite the short reaction time (30 minutes), there are carveol conversion and carvone production at all conditions tested except in entry 7, this experiment did not show activity because it was performed without TBHP. It could be also concluded that increasing concentrations of active sites and TBHP seems to favor carveol conversion and carvone yield (entry 6 and 13); in contrast, increasing carveol concentration seems to disfavor them (entry 18), maybe due to the lower molar relation TBHP/carveol. From these results, it could be also observed that carveol conversion as well the carvone yield maximizes in experiment 14. These conditions will be used from now on in this work.

**Table 2.3.8: Results carveol reactions at 30 minutes, 313 K and 875 rpm.**

| Entry     | $C_D, M$    | $C_B, M$    | $L, M$         | Carveol conversion, $X_D$ | Carvone selectivity, $S_F$ | Carvone Yield, $Y_F$ |
|-----------|-------------|-------------|----------------|---------------------------|----------------------------|----------------------|
| 1         | 0.13        | 0.31        | 0.0E+00        | 4.15                      | 50.89                      | 1.85                 |
| 2         | 0.13        | 0.31        | 7.5E-05        | 4.04                      | 82.63                      | 3.34                 |
| 3         | 0.13        | 0.31        | 1.6E-04        | 7.20                      | 66.59                      | 4.27                 |
| 4         | 0.13        | 0.31        | 1.9E-04        | 10.44                     | 49.53                      | 4.78                 |
| 5         | 0.13        | 0.31        | 2.3E-04        | 9.87                      | 74.17                      | 7.32                 |
| 6         | 0.13        | 0.31        | 3.0E-04        | 11.30                     | 67.52                      | 7.47                 |
| 7         | 0.13        | 0.00        | 3.0E-04        | 0.00                      | 0.00                       | 0.00                 |
| 8         | 0.13        | 0.12        | 3.0E-04        | 4.26                      | 97.57                      | 4.16                 |
| 9         | 0.13        | 0.27        | 3.0E-04        | 12.76                     | 54.82                      | 6.22                 |
| 10        | 0.13        | 0.39        | 3.0E-04        | 12.77                     | 55.00                      | 6.99                 |
| 11        | 0.13        | 0.49        | 3.0E-04        | 13.36                     | 49.98                      | 6.47                 |
| 12        | 0.13        | 0.66        | 3.0E-04        | 15.18                     | 47.64                      | 7.23                 |
| 13        | 0.13        | 0.82        | 3.0E-04        | 21.66                     | 40.84                      | 8.85                 |
| <b>14</b> | <b>0.03</b> | <b>0.31</b> | <b>3.0E-04</b> | <b>36.37</b>              | <b>60.93</b>               | <b>22.16</b>         |
| 15        | 0.07        | 0.31        | 3.0E-04        | 23.35                     | 63.01                      | 14.71                |
| 16        | 0.08        | 0.31        | 3.0E-04        | 22.40                     | 54.60                      | 12.23                |
| 17        | 0.10        | 0.31        | 3.0E-04        | 17.54                     | 51.92                      | 9.11                 |
| 18        | 0.17        | 0.31        | 3.0E-04        | 13.60                     | 59.64                      | 8.11                 |

At this point, it is also evident that the behavior of the catalytic system with carveol as substrate is much better than with limonene as substrate.

### 2.3.4 Behavior of reactions through time

From *Figure 2.3.5* it could be observed that at the conditions studied, the conversion of both substrates depicts similar behavior. Substrate conversion increase rapidly up to 3 hours, after that it increase only slowly until a conversion around 97%.

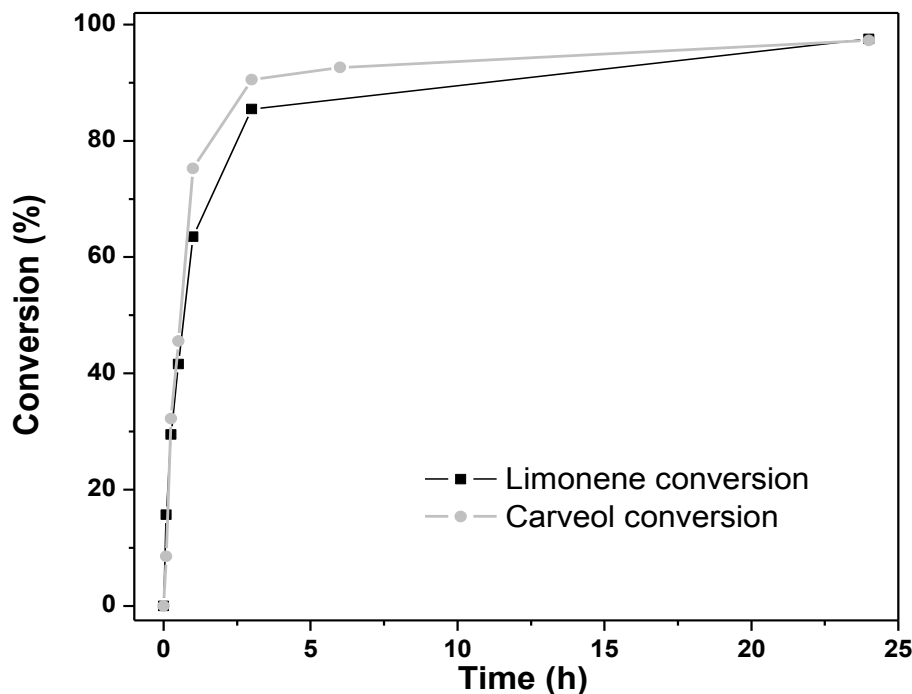


**Figure 2.3.5: Limonene and carveol conversion through time.**

Reaction conditions: 1.5 mL, 875 rpm, 313 K, substrate concentration of 0.03 M, TBHP concentration of 0.31 M and active sites (Fe) concentration of  $3 \times 10^{-4}$  M. Carveol SD:  $\pm 0.96$ .  
Limonene SD:  $\pm 1.19$

*Figure 2.3.6* let see in the limonene reaction, the main product formed initially was limonene epoxide, whereas the selectivity toward carvone only increased when the conversion exceeded 29 %. Then, epoxide could be considered as primary product while carvone as secondary product. Additionally, both carvone and epoxide yields increased only until 85 % conversion was reached, then carvone yield slightly decreased and epoxide yield is stable. This could indicate that after 3 hours (85% limonene conversion) carvone could be overoxidizing and side reactions could be favored. It is also observed that the maximum main products total yield is less than 12%, which is consistent with the high amount of byproducts detected in limonene reaction.

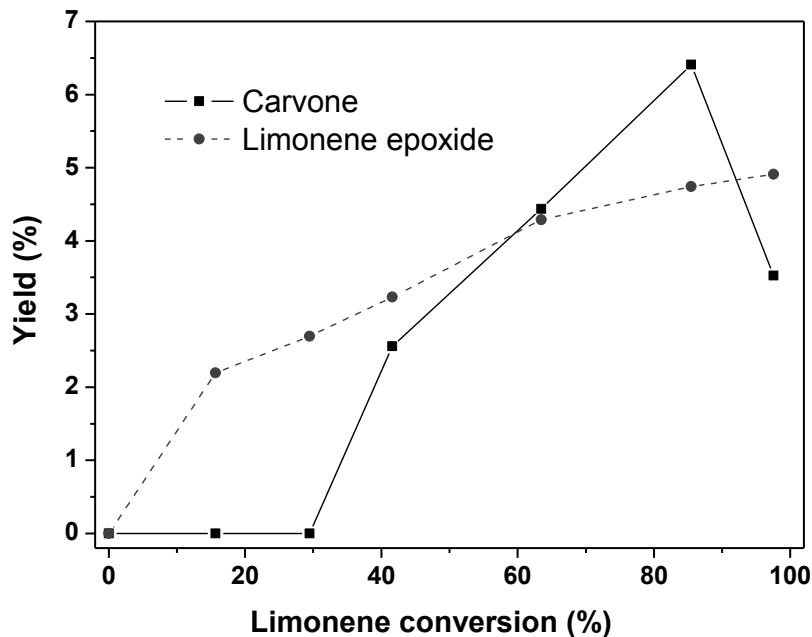


**Figure 2.3.6: Carvone and limonene epoxide yield versus limonene conversion.**  
 Reaction conditions: 1.5 mL, 875 rpm, 313 K, substrate concentration of 0.03 M, TBHP concentration of 0.31 M and active sites (Fe) concentration of  $3 \times 10^{-4}$  M. Carvone SD:  $\pm 1.92$ .  
 Limonene epoxide SD:  $\pm 0.9$

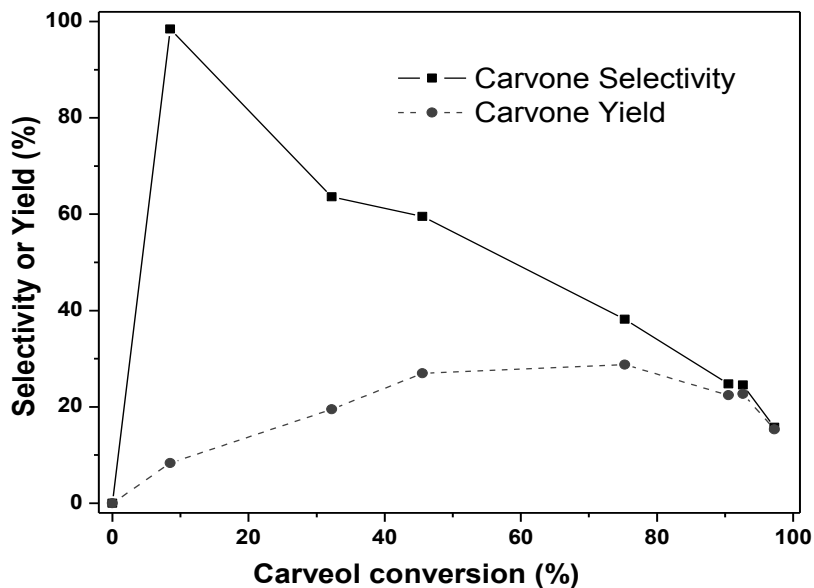


**Figure 2.3.7: Carvone yield and selectivity versus carveol conversion.**  
 Reaction conditions: 1.5 mL, 875 rpm, 313 K, substrate concentration of 0.03 M, TBHP concentration of 0.31 M and active sites (Fe) concentration of  $3 \times 10^{-4}$  M. Carvone yield SD:  $\pm 0.28$ . Carvone selectivity SD:  $\pm 0.44$

Figure 2.3.7 shows that carvone selectivity declines with conversion, typical behavior in intermediates products (76); additionally, it could be observed that, similar to limonene

reaction, carvone yield in carveol dehydrogenation increased only until 75 % conversion was reached, then it tends to decrease. This is consistent with behavior previously explained for carvone produced from limonene with the same catalytic system. The higher yield obtained toward carvone from carveol, respect to limonene reaction agrees with the less amount of byproducts detected in carveol reaction.

Considering the effect of time on both, substrate conversion and carvone selectivity the optimum reaction time for the reactions will be 3 hours for limonene and 1 hour for carveol; both carried out at 875 rpm, 313 K, substrate concentration of 0.03 M, TBHP concentration of 0.31 M and active sites (Fe) concentration of  $3 \times 10^{-4}$  M.

### ***2.3.5 Initial elucidation of mechanisms***

The results from the literature review indicate that radicals are involved in cycloterpenes oxidation with immobilized FePc (54), and the hydrogen abstraction from the allylic position and the substrate hydroperoxide formation are typical in allylic oxidation reactions, especially by the free radical mechanism (65,77). Therefore, these hypotheses were studied for concerning reactions.

#### ***2.3.5.1 Involvement of free radicals in reactions***

In previous studies about anchored FePc behavior, it has been suggested that the first step in the oxidation over immobilized FePc catalysts and TBHP is the formation of the tert-butyl iron phthalocyanine peroxide complexes (*Figure 2.3.8*) (5). Then high-valent oxo-metal species are formed through the possible pathways proposed for monomeric and dimeric phthalocyanine platforms, shown in *Figure 2.3.9*, which consider homolytic and heterolytic cleavage of O-O peroxide bonds. The homolytic cleavage is usually favored by monomeric species leading to a radical process, while dimeric species frequently favors heterolytic cleavage due to delocalization of the charge at two Fe and two macrocyclic ligands (6).

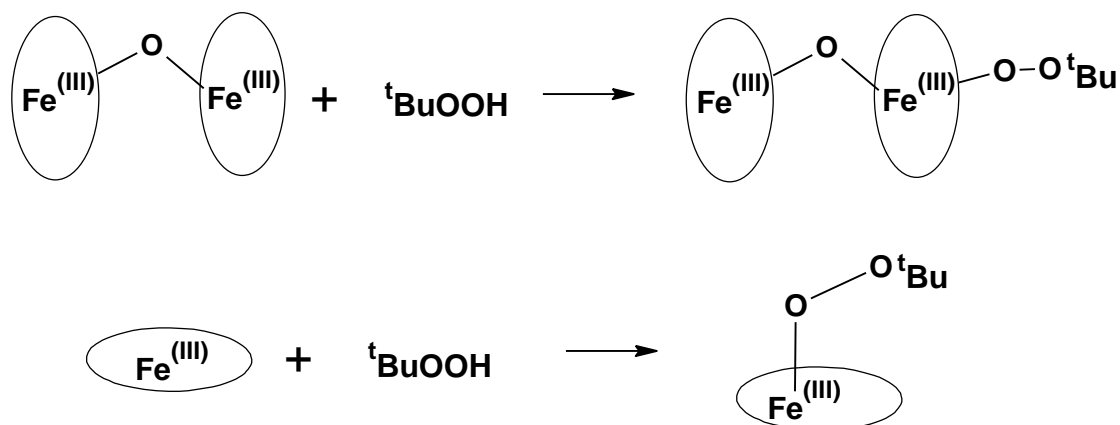


**Figure 2.3.8: Iron phthalocyanine peroxide complexes formation.** Taken from (5).  
 Note: In this work, the iron enclosed in the circle represents the iron phthalocyanine complex ( $\text{FePcCl}_{16}$ )

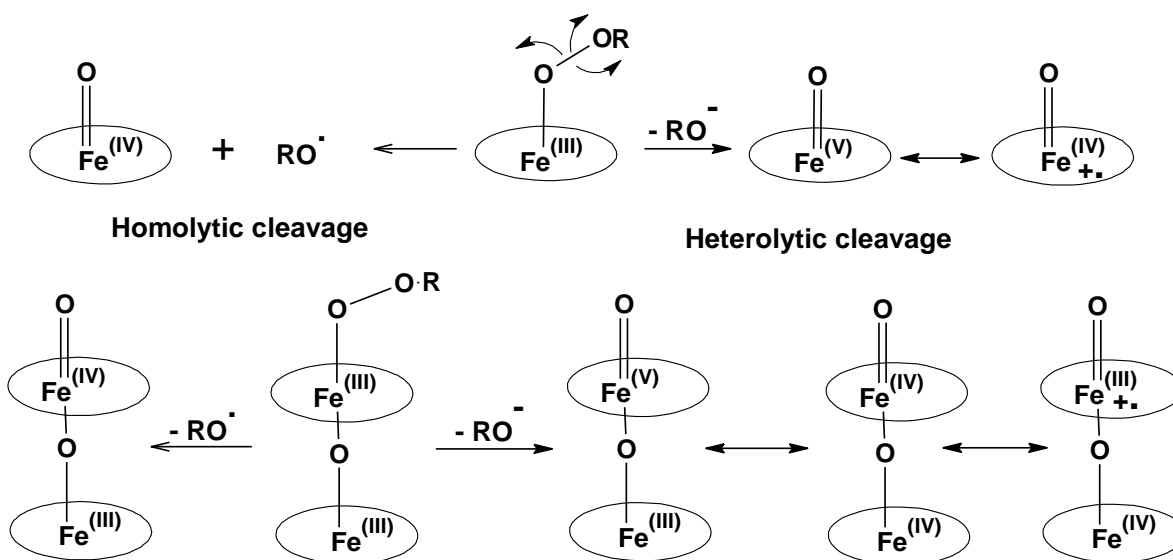


**Figure 2.3.9: Homolytic and heterolytic cleavage.** Taken from (2)  
 Note: In this work, the iron enclosed in the circle represents the iron phthalocyanine complex ( $\text{FePcCl}_{16}$ ) and the peroxide adsorbed on active sites ( $\text{ROOH}$ ) is the TBHP ( $t\text{BuOOH}$ ).

It has been also reported that alkoxy radicals ( $t\text{BuO}^\cdot$  for this work) and iron-oxo species ( $\text{Fe}^{\text{IV}}=\text{O}$ ) formed from monomeric complex can abstract the allylic hydrogen for allylic oxidation. In the case of dimeric complex, although the formation of radical is not favored, the  $\text{Fe}^{\text{IV}}-\text{O}-\text{Fe}^{\text{IV}}=\text{O}$  species can also accomplish this task (2,10). Respect to the oxidation of allylic alcohol to allylic ketone, it has been also reported that Oxo metal species ( $\text{Fe}^{\text{IV}}=\text{O}$ ) are the responsible of this reaction (10). Given these possibilities reported for the first step

in the oxidation over immobilized FePc catalysts and TBHP, it is important to prove the involvement of radicals in the reactions studied in this work.

According to **Figure 2.3.10**, free radicals are involved in limonene oxidation reaction, since both, the conversion of limonene and TBHP decreased in the presence of the radical scavenger 2, and 4-DPB. It is also observed that the conversion of TBHP is higher than limonene conversion, denoting an ineffective decomposition TBHP, phenomenon characteristic in oxidation reactions (11), which can also explain the necessity of a high excess of oxidant in this reaction.

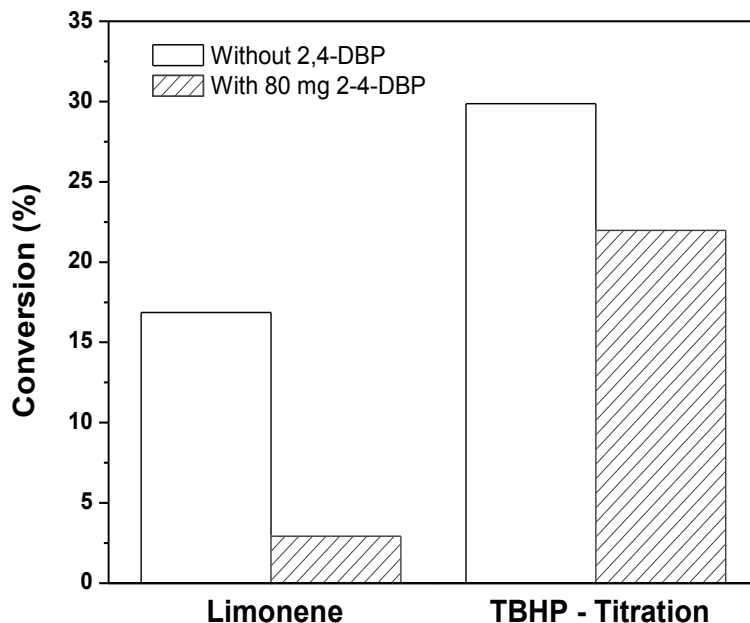


**Figure 2.3.10: Effect of the scavenger (2,4-DBP) in the conversion of limonene and TBHP.** Reaction conditions: 1.5 mL of 0.13 M limonene in acetone, active sites (Fe) concentration of  $3 \times 10^{-4}$  M, 80 mg of 2,4-DBP, 0.35 mmol of commercial TBHP, 875 rpm 313 K, 30 min.

**Figure 2.3.11** shows that thermal decomposition of TBHP (in acetone at 313 K) is very low, while the presence of catalyst (thermal and catalytic decomposition), increase notably this decomposition, which in combination with the previous **Figure 2.3.10**, confirm the role of the catalyst in the decomposition of TBHP into free radicals (5). From **Figure 2.3.11**, can also be observed that the thermal and catalytic decomposition in presence of acetone, is higher than the decomposition when limonene is included in the mixture (thermal and catalytic decomposition (Limonene)). This might indicate that limonene could be adsorbed

on catalyst active sites, competing with TBHP and explaining in this way the decrease in the oxidant conversion.

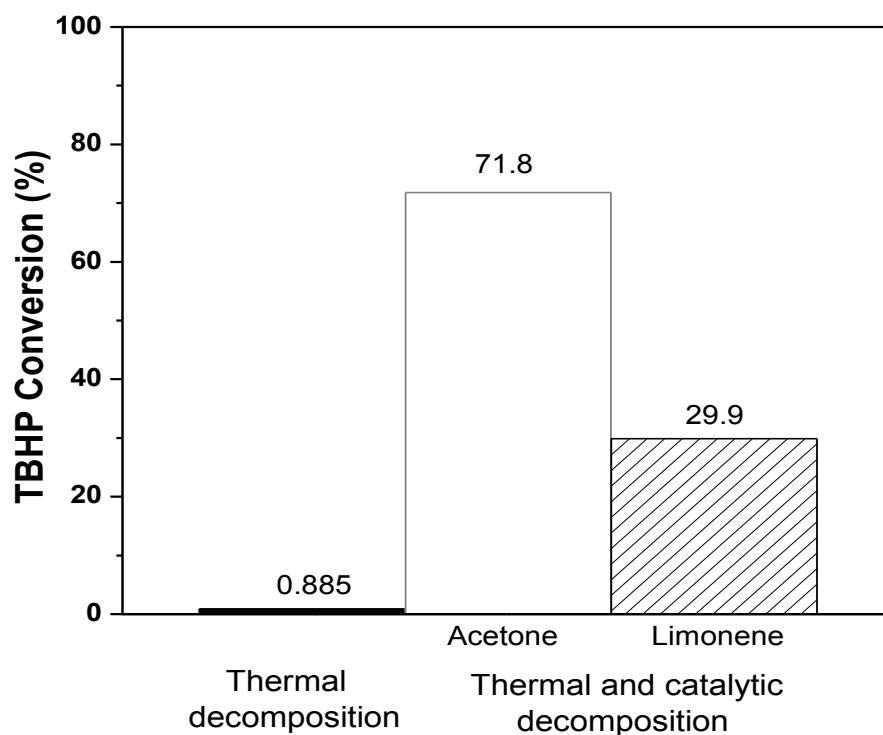


**Figure 2.3.11: Effect of the catalyst in the TBHP decomposition.**

Reaction conditions: 1.5 mL of 0.13 M limonene in acetone, active sites (Fe) concentration of  $3 \times 10^{-4}$  M, 80 mg of 2,4-DBP, 0.35 mmol of commercial TBHP, 875 rpm 313 K, 30 min.

The results obtained so far, can confirm for limonene reaction, the high presence of homolytic cleavage of O-O TBHP bond, but they also indicate the existence of alternative pathways for both TBHP decomposition and limonene oxidation; since the reactions were not totally suppressed with the presence of free radicals scavenger. The alternative pathways could be related to the presence of dimeric species on the catalyst, and the production of limonene epoxide which is usually directly related to the metal oxo complex and not necessarily to free radicals formation.

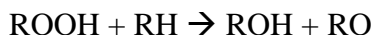
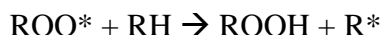
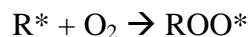
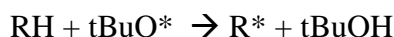
In the case of carveol, the reaction was carried out during 30 minutes in the presences of 80mg of free radicals scavenger (2,4-DPB) and at 875 rpm, 313 K, substrate concentration of 0.03 M, TBHP concentration of 0.31 M and active sites (Fe) concentration of  $3 \times 10^{-4}$  M. The conversion obtained in this reaction was almost null (0.8%), which could indicate that

the formation of oxo metal species ( $\text{Fe}^{\text{IV}}=\text{O}$ ) involved in carveol oxidation is mainly homolytic. The apparent lack of participation of dimeric oxo species ( $\text{Fe}^{\text{IV}}-\text{O}-\text{Fe}^{\text{IV}}=\text{O}$ ), could be due to steric constraints related to the anchoring of the high dimeric complex inside the SBA-15 pores.

Titrations of TBHP before and after reactions were not performed, since a small concentration of hydroperoxide (around 0.5M) was detected in carveol solution, maybe due to traces of limonene hydroperoxide. With this situation, it would be difficult to determine to which hydroperoxide corresponds the conversion detected by titration.

### *2.3.5.2 O<sub>2</sub> participation in reaction*

Some proposed mechanism for cycloterpenes in literature (10,70), mention the following reaction steps:



Where **R** represents the cycloterpene. This set of reactions describes the cycloterpene alcohol (ROH) and cycloterpene epoxide (RO), through the cycloterpene hydroperoxide formation (ROOH) with O<sub>2</sub>, which usually occurs in the CH allylic carbon, because it is preferentially activated for this purpose. In our reaction it was not possible to detect the formation of limonene hydroperoxide with PPh<sub>3</sub> treatment at any of the conditions described in the experimental procedure. This could be due to the small concentration used in this work which could difficult the detection of change in carveol concentration. However, oxygen participation in the reaction did be established, as explained bellow.



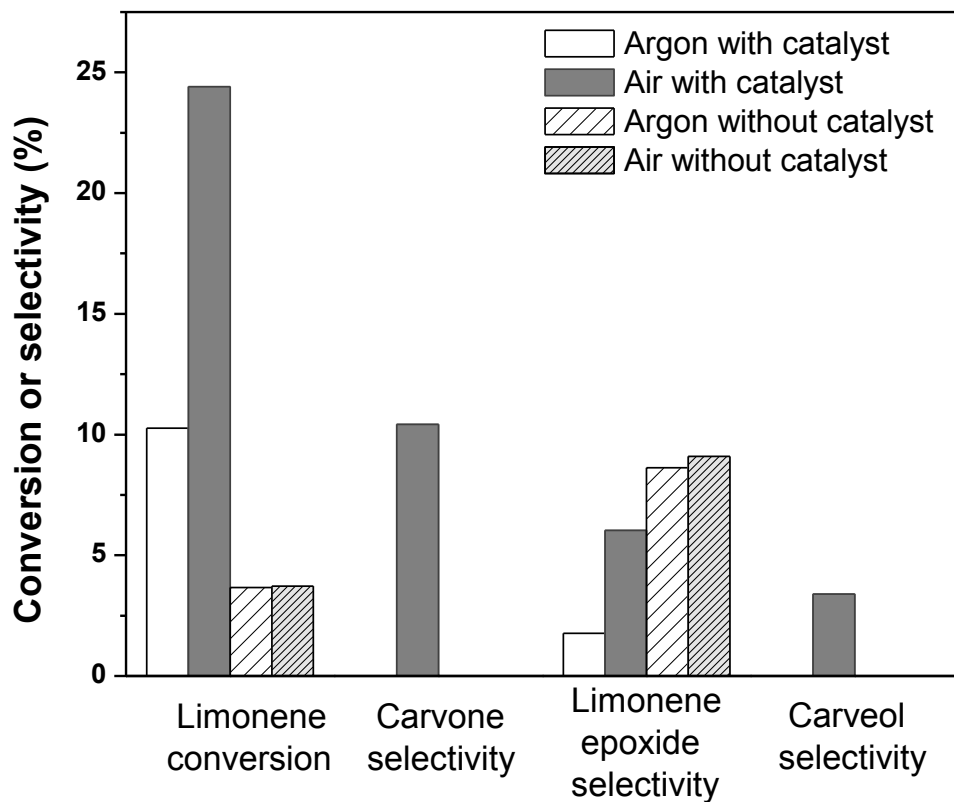


**Figure 2.3.12: Limonene allylic oxidation under air and inert atmosphere.**  
 Reaction conditions: 4 mL of 0.13 M limonene in acetone, 0.21 mol of Fe per 100 mol of substrate, 1.3 mmol of commercial TBHP, 313 K, 30 min.

The **Figure 2.3.12** shows the results obtained for 30 minutes reactions under air and argon atmosphere, this figure indicates that the presence of the catalyst effectively favors limonene conversion and it promotes the production of carvone over limonene epoxide for air atmosphere. Due to the better conversion and selectivities achieved under air atmosphere with catalyst, it could be inferred that the air oxygen does favored limonene conversion as well as carvone, carveol and epoxide production in the catalytic system, being this more evident for carveol and carvone than for limonene epoxide. These results agree with the reactions steps previously mentioned and the alternative non radical pathway already addressed in this work. No limonene conversion was detected without TBHP neither for inert nor for air atmospheres, which support the conclusion that this is the responsible of limonene oxidation and that probably oxygen from air only participate in intermediates steps, like those suggested for other cycloterpenes (10,70).

### 2.3.6 Mechanisms and kinetics models

In *Figure 2.3.13* it is observed that both substrate consumption rates increase in an almost linear trend with the iron concentration; that could mean that change in substrates concentration in time unit, has a first order proportionality to iron (active sites) concentration.

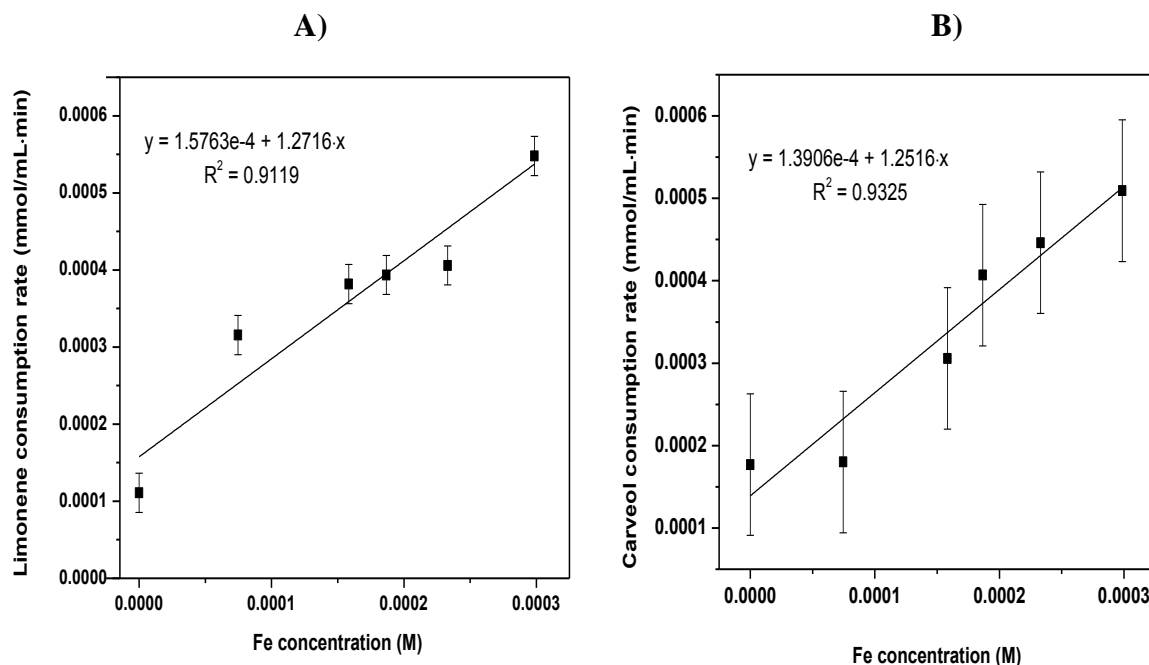


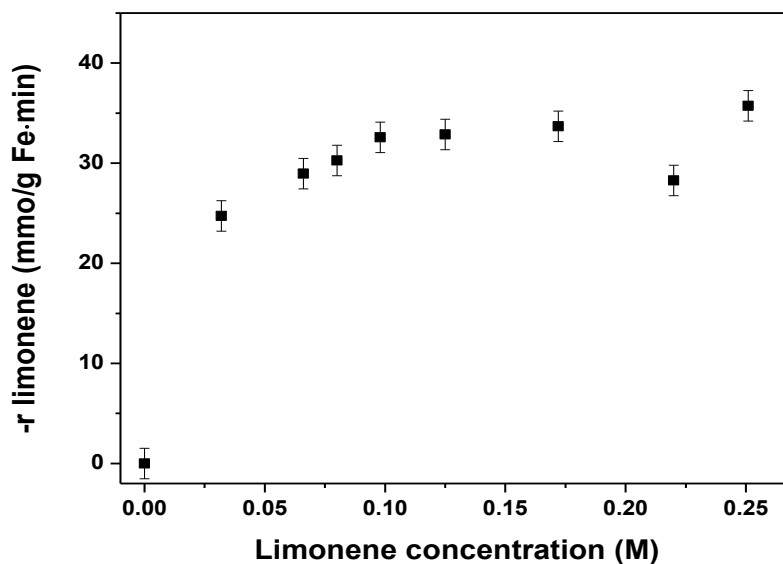
**Figure 2.3.13:** Effect of active sites (*Fe*) concentration (*L*) on limonene (*Figure A*) and carveol (*Figure B*) consumption initial rates (change of substrate concentration in the time unit).

Reaction conditions: 1.5 mL, 875 rpm, 313 K, substrate concentration of 0.03 Molar, TBHP concentration of 0.31 Molar, up to 30 minutes

*Figure 2.3.14* shows that reaction rate increase with substrate concentration; however, they do not have linear trend, which could indicate a possible adsorption of substrates in active sites, and maybe a competitive interaction with TBHP (76). On the other hand, the behavior of initial reactions rates observed in *Figure 2.3.15*, presents an almost linear trend for variation of TBHP concentration; which is not consistent with literature reports, since it is well known that the first step in this kind of catalytic systems is very likely, the adsorption of TBHP on FePc active sites, as it was previously explained in this work (section 2.3.5.1). This inconsistency could be due to the availability of two kinds of active sites (monomeric and dimeric) and the potential side reactions or alternative pathways, which would be occurring in parallel to allylic oxidation of limonene and carveol dehydrogenation. For

example, alternative TBHP decomposition, carvone overoxidation, carvone hydrogenation and substrates isomerization or polymerization (22,62).

A)



B)

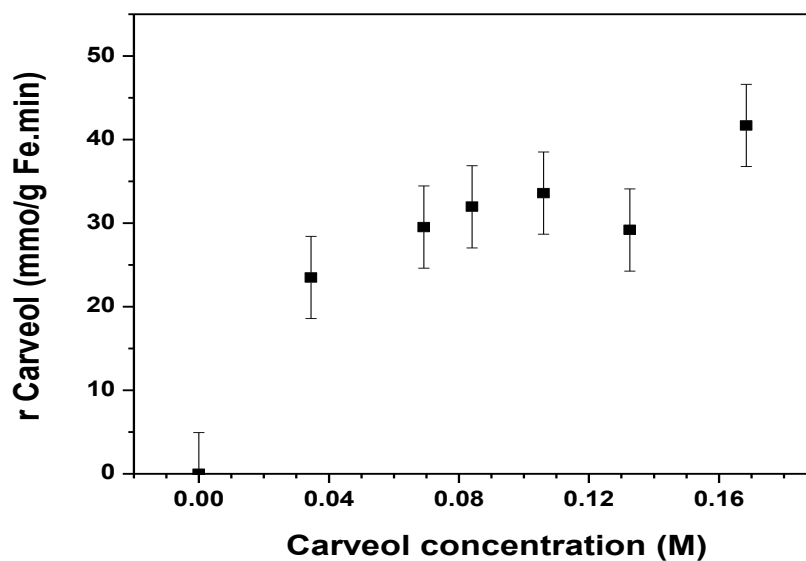
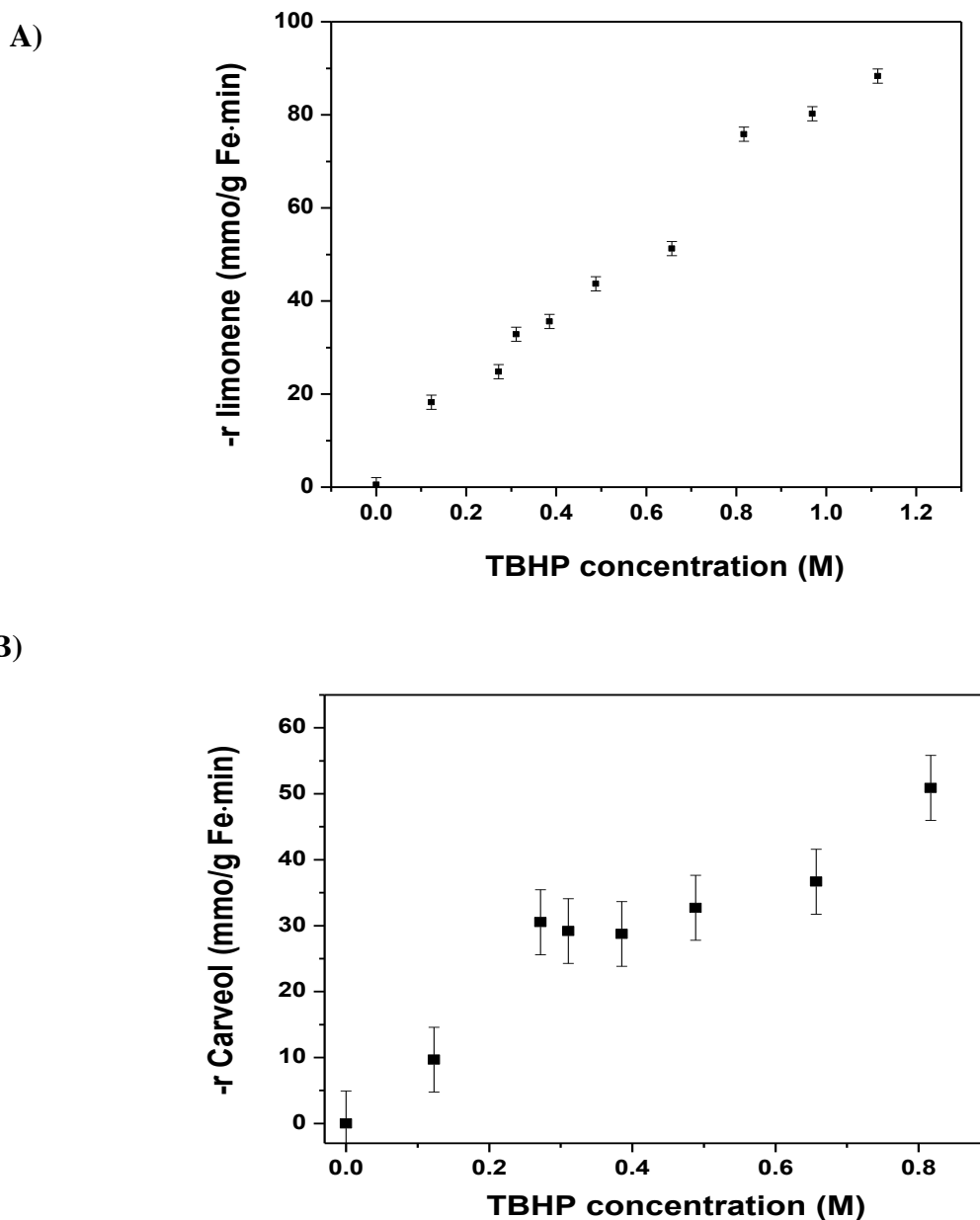


Figure 2.3.14: Effect of substrates concentration on limonene (Figure A) and Carveol (Figure B) initial reaction rate.

Reaction conditions: 1.5 mL, 875 rpm, 313 K, TBHP concentration of 0.31 Molar, active sites (Fe) concentration of  $3 \times 10^{-4}$  Molar, up to 30 minutes



**Figure 2.3.15: Effect of TBHP concentration ( $C_B$ ) on limonene (Figure A) and carveol (Figure B) initial reaction rate.**

Reaction conditions: 1.5 mL, 875 rpm, 313 K, substrate concentration of 0.03 Molar, active sites (Fe) concentration of  $3 \times 10^{-4}$  Molar, up to 30 minutes.

Due to the similarities between these two reactions, and the fact that carveol production is an intermediate step in limonene allylic oxidation; it was decided to perform a more detailed analysis of carveol kinetics and use its conclusions to have a better idea about limonene kinetics. To do this, several rate expressions were proposed for the catalytic

dehydrogenation of carveol with  $\text{FePcCl}_{16}$  complex immobilized on SBA-15 and TBHP at 313 K and 875 rpm. The expressions were derived from the pseudo homogeneous (PH), Langmuir –Hinshelwood (L-H), Hougan-Watson (H-W) and Eley-Rideal (R-E) models, using Quasi-equilibrium (QEA) and Hybrid steady state (HSSA) approximations (78,79).

### **General assumptions for all models**

- Uniform ideal surface is considered
- Adsorption/desorption steps are quasi-equilibrated and Langmuir isotherms can be used, with its assumptions (79)
- Only the main products were considered in these expressions.
- The initial reaction rate method was used to calculate the substrate reaction rate, therefore the products initial concentration is taken as 0.
- The following nomenclature is used for all mechanisms proposed:

A: Limonene,  $\text{C}_{10}\text{H}_{16}$

B: TBHP or tBuOOH,  $\text{C}_4\text{H}_{10}\text{O}_2$

C: Limonene Hydroperoxide,  $\text{C}_{10}\text{H}_{15}\text{OOH}$

D: Carveol,  $\text{C}_{10}\text{H}_{15}\text{OH}$

E: Limonene epoxide,  $\text{C}_{10}\text{H}_{16}\text{O}$

F: Carvone,  $\text{C}_{10}\text{H}_{14}\text{O}$

G: tert-butanol,  $\text{C}_4\text{H}_{10}\text{O}$

S: Catalyst active site,  $\text{Fe}^{\text{III}}$

OS: iron oxo species:  $\text{Fe}^{\text{IV}}=\text{O}$

L: active sites (Fe) concentration.

$k_i$ : forward reaction constant for reaction i

$k_{-i}$ : backward reaction constant for reaction i.

$K_i$ : equilibrium constant for reaction i ( $K_i = k_i / k_{-i}$ )

\*: indicate that the substance is a free radical

### **Pseudo homogeneous model**

For this model, no reactant adsorption on the catalyst was assumed; the derived expression is shown in **Table 2.3.9** and labeled as J. This model could be represented by the following reaction:



The adsorption phenomenon must be considered when a solid material is used in a catalytic reaction, with the reactants in liquid or gaseous phase (64), then adsorption of one (R-E) and two reactants (L-H and H-W) were considered.

### Eley-Rideal model

This type considers the reaction between adsorbed species (TBHP) and a liquid phase species (Carveol) (79). In this work, two different sequences of reactions steps were considered:

#### **R-E 1**

- 1)  $S + B \rightleftharpoons BS$
- 2)  $BS \rightleftharpoons OS + G^*$
- 3)  $D + OS \rightleftharpoons FS$
- 4)  $FS \rightleftharpoons F+S$

The second sequence combines the two first reactions in one:

#### **R-E 2**

- 1)  $S + B \rightleftharpoons OS + G^*$
- 2)  $D + OS \rightleftharpoons FS$
- 3)  $FS \rightleftharpoons F+S$

To derive the reaction rate expressions the QEA was used considering each reaction as rate-determining step (RDS), like it could be observed in **Table 2.3.9**, mechanisms A, B, F and G for model **R-E-1** and mechanisms C-E for model **R-E-2**.

Other combinations of reactions were considered, but they are not presented here, because the expressions obtained for  $C_F = 0$  were identical to other already shown.

Table 2.3.9. Rate expressions for carveol proposed mechanism

| Model | Label | Controlling step                                 | Equation  | R-Square | Adj. R-Square | SSE    | MSE   | RMSE  |
|-------|-------|--|---|----------|---------------|--------|-------|-------|
| R-E 1 | A     | 3) Surface reaction of D and OS                  | $\frac{L * k_3 * K_1 * K_2 * C_B * C_D}{1 + K_1 * C_B + K_1 * K_2 * C_B}$                                     | 0.71     | 0.66          | 796.2  | 72.4  | 8.51  |
| R-E 1 | B     | 2) Decomposition of B on surface                 | $\frac{L * k_2 * K_1 * C_B}{1 + K_1 * C_B}$   | 0.59     | 0.55          | 1149.7 | 95.8  | 9.79  |
| R-E 2 | C     | 2) Surface reaction of D and OS                  | $\frac{L * k_2 * K_1 * C_B * C_D}{1 + K_1 * C_B}$   | 0.71     | 0.69          | 796.2  | 66.3  | 8.15  |
| R-E 2 | D     | 3) Desorption of F                               | $\frac{L * k_3 * K_2 * K_1 * C_B * C_D}{1 + K_1 * C_B + K_2 * K_1 * C_B * C_D}$                               | 0.84     | 0.81          | 454.5  | 41.3  | 6.43  |
| R-E 2 | E     | 1) Adsorption and decomposition of B             | $L * k_1 * C_B$   | 0.50     | 0.50          | 1376.5 | 105.9 | 10.29 |
| R-E 1 | G     | 4) Desorption of F                               | $\frac{L * k_4 * K_1 * K_2 * K_3 * C_B * C_D}{1 + K_1 * C_B + K_1 * K_2 * C_B + K_1 * K_2 * K_3 * C_B * C_D}$ | 0.76     | 0.69          | 669.7  | 67.0  | 8.18  |
| PH    | J     | Dos not apply                                    | $k * C_B^\alpha * C_D^\beta$  | 0.88     | 0.86          | 339.3  | 30.8  | 5.55  |
| L-H 1 | K     | 4)Surface reaction of adsorbed B with adsorbed D | $\frac{L * k_4 * K_1 * K_2 * K_3 * C_B * C_D}{(1 + K_1 * C_B + K_1 * K_2 * C_B + K_3 * C_D)^2}$               | 0.81     | 0.76          | 515.0  | 51.5  | 7.18  |
| L-H 1 | L     | 2) Decomposition of B on surface                 | $\frac{L * k_2 * K_1 * C_B}{1 + K_1 * C_B + K_3 * C_D}$   | 0.77     | 0.72          | 648.6  | 59.0  | 7.68  |
| H-W 1 | M     | 1) Adsorption of B                               | $\frac{L * k_1 * C_B}{1 + K_3 * C_D}$   | 0.46     | 0.36          | 1501.9 | 136.5 | 11.68 |

| Model        | Label | Controlling step   | Equation  | R-Square | Adj. R-Square | SSE     | MSE    | RMSE  |
|--------------|-------|--|---|----------|---------------|---------|--------|-------|
| <i>H-W 1</i> | N     | 3) Adsorption of D   | $\frac{L * k_3 * C_D}{1 + K_1 * C_B + K_1 * K_2 * C_B}$   | 0.21     | 0.07          | 2197.0  | 199.7  | 14.13 |
| <i>H-W 1</i> | O     | 5) Desorption of F   | $\frac{L * k_5 * K_1 * K_2 * K_3 * K_4 * C_B * C_D}{1 + K_1 * C_B + K_1 * K_2 * C_B + K_3 * C_D + K_1 * K_2 * K_3 * K_4 * C_B * C_D}$                   | 0.86     | 0.80          | 394.0   | 43.8   | 6.62  |
| <i>H-W 2</i> | T     | 5) Desorption of F   | $\frac{L * k_5 * K_1 * K_2 * K_3 * K_4 * C_B * C_D}{1 + K_1 * C_B + K_1 * K_2 * C_B + K_1 * K_2 * K_3 * C_B * C_D + K_1 * K_2 * K_3 * K_4 * C_B * C_D}$ | 0.74     | 0.62          | 725.1   | 80.6   | 8.98  |
| <i>L-H 1</i> | U     | 2) Decomposition of B on surface and 4) Surface reaction of adsorbed B with adsorbed D | $\frac{L * k_2 * K_1 * C_B - \frac{k_2^2 * K_1^2 * C_B^2}{k_4 * K_3 * C_D}}{(1 + K_1 * C_B + K_3 * C_D)}$   | -5.54    | -8.80         | 13007.0 | 1625.9 | 40.32 |
| <i>R-E 1</i> | V     | 2) Decomposition of B on surface and 3) Surface reaction of D and OS                   | $\frac{L * k_2 * K_1 * C_B}{1 + K_1 * C_B + \frac{k_2 * K_1 * C_B}{k_8 * C_D}}$   | 0.84     | 0.81          | 309.45  | 30.94  | 5.56  |

Note: Due to product concentration is considered zero, some of the mechanisms proposed here results in identical rate expressions for this consideration; however, it would be different in the case that initial concentration of products could be evaluated.



### Langmuir –Hinshelwood and Hougen-Watson

These models consider a bimolecular surface reaction between the two adsorbed reactants (79). In this work, two different sequences of reactions steps were considered:

First sequence considers the adsorption of each reactant in an active site:

#### *L-H 1 or H-W 1*

- 1)  $S + B \rightleftharpoons BS$
- 2)  $BS \rightleftharpoons OS + G^*$
- 3)  $D + S \rightleftharpoons DS$
- 4)  $DS + OS \rightleftharpoons FS + S$
- 5)  $FS \rightleftharpoons F+S$

In contrast, this second sequence considers that B is adsorbed on an active site, then D is adsorbed over the metal oxo species:

#### *L-H 2 or H-W 2*

- 1)  $S + B \rightleftharpoons BS$
- 2)  $BS \rightleftharpoons OS + G^*$
- 3)  $OS + D + S \rightleftharpoons OSD$
- 4)  $OSD \rightleftharpoons FS$
- 5)  $FS \rightleftharpoons F+S$

To derive the reaction rate expressions the QEA was used considering a reaction on the surface as RDS (L-H) and adsorption or desorption as RDS (H-W). Resulting rate expressions could be observed in *Table 2.3.9*.

The expressions derived from L-H 2 with steps 1 (P) and 4 (Q) as RDS, are not presented since the expressions are the same to mechanism B and G, respectively. When H-W 2 is considered, only the expression derived using reaction 5 as RDS results in a different expression for the worked conditions.

Finally, two rate expressions were determined using the HSSA for the sequence of reactions L-H 1 (U) and R-E-1 (V).

**Table 2.3.10. Parameter estimated for rate expressions with the best fitting**

| <i>Model</i>        | <b>Label</b> | <b>Controlling step</b>  | <b>Parameters</b>                         | <b>Value</b>                                 | <b>Confidence interval</b>   |
|---------------------|--------------|--------------------------|---|--|--|
| <b><i>R-E 2</i></b> | <b>D</b>     | 3)<br>Desorption<br>of F | $k_3$<br>$K_2$<br>$K_1$                   | 186928.04<br>475371.77<br>7.7456E-05         | $\pm 1.40$<br>$\pm 275809.43$<br>$\pm 4.55E-05$                            |
| <b><i>PH</i></b>    | <b>J</b>     | Dos not<br>apply         | $k$<br>$\alpha$<br>$\beta$                | 71.90<br>0.46<br>0.16                        | $\pm 5.27E-04$<br>$\pm 2.71E-06$<br>$\pm 3.56E-06$                         |
| <b><i>H-W 1</i></b> | <b>O</b>     | 5)<br>Desorption<br>of F | $k_5$<br>$K_1$<br>$K_2$<br>$K_3$<br>$K_4$ | 913698.67<br>0.77<br>25.33<br>118.70<br>0.03 | $\pm 656.63$<br>$\pm 806.86$<br>$\pm 27607.71$<br>$\pm 0.28$<br>$\pm 1.28$ |

From the mechanisms proposed, the rate expression with the best fitting to the experimental data, were those labelled as D, J and O. The parameter estimated for these mechanisms are shown in **Table 2.3.10** with their confidence intervals (determined with the Matlab function *nlparci*) and their fitting are graphically presented in **Appendix D, E and F**. In those appendices, it can be observed that there is similarity between experimental reaction rate ( $r$ ) and calculated reaction rate ( $r_{cal}$ ) (**Figures D**), that residuals ( $r - r_{cal}$ ) are randomly distributed around the line of error zero (**Figures C**), and the trend of rate expressions are similar to the data trend (**Figures A and B**).

From **Appendix D: Matlab results for mechanism J**, and **Table 2.3.10**, it could be concluded that between the expressions analyzed, the carveol rate expression derived from pseudo homogeneous mechanism (J) represents better the experimental results, since it has, not only the best fitting, but also the best confidence intervals. Despite this fitting is not very high, and the pseudo homogeneous assumption does not chemically represent the

heterogeneous nature of the catalytic system studied, the mechanism J mathematically represents the carveol reaction with the catalytic system FePcCl<sub>16</sub>-NH<sub>2</sub>-SBA-15/TBHP and will be used for the scope of this work, furthermore the pseudo homogeneous behavior could be caused by the free radicals generated in the first steps of reactions, which may be promptly propagated to the homogeneous liquid solution causing some side reactions and a not entirely heterogeneous nature.

Analyzing mechanism D and O, which does take into account the heterogeneous nature of the catalytic system, seems to be clear that the product desorption is probably the rate determining step and that a mechanism including the adsorption of both reactants could represent better this reaction (mechanism O). The low mathematical fitting of these two mechanisms could be associated with the no analysis of the effect of carvone concentration on the reaction rate, and the fact that other products from side reactions or carvone overoxidation were not considered. Those products, despite their low selectivity, could influence the reaction behavior, shifting it from the proposed mechanisms.

Given the drawbacks found in Carveol mechanism fitting and the higher complexity of the reaction with limonene, clearly mentioned in the first part of this chapter; it was decided to present in this work, only a pseudo homogeneous model for limonene reaction on the base that the high fitting obtained (**Table 2.3.11**), would allow its use as a good approximation for the ultimate goal of this work, the economic feasibility.

The fact that the fitting of pseudo homogeneous mechanism for limonene is better than all fittings obtained for carveol mechanisms, agrees with the idea that the free radicals participation is causing the pseudo homogeneous behavior, since limonene reaction has a higher involvement of free radicals during the reaction, due to their participation in allylic hydrogen abstraction and limonene hydroperoxide formation (see section 2.3.5.2).

Table 2.3.11. Pseudohomogeneous mechanism for limonene and estimated parameter

| Pseudo homogeneous reaction rate expression: $r = k * C_B^\alpha * C_A^\beta$ |                   |        |       |      |            |        |                     |
|---|-------------------|--------|-------|------|------------|--------|---------------------|
| R-Square  | Adjusted R-Square | SSE    | MSE   | RMSE | Parameters | Value  | Confidence interval |
| 0.98  | 0.98              | 155.71 | 10.38 | 3.22 | k          | 105.52 | $\pm 5.72E-04$      |
|   |                   |        |       |      | $\alpha$   | 0.83   | $\pm 1.41E-06$      |
|   |                   |        |       |      | $\beta$    | 0.12   | $\pm 2.57E-06$      |

#### 2.4 Partial conclusions

- TBHP and FePcCl<sub>16</sub> complex favor the conversion and carvone selectivity in the limonene and carveol reactions, being TBHP essential for carvone production and carveol conversion.
- Immobilization of FePcCl<sub>16</sub> on SBA-15 causes a decrease in limonene conversion and limonene epoxide formation, but the carvone selectivity increases. Immobilization also generates a slight reduction in carvone production from carveol respect to unsupported catalyst. The activity of this catalyst could be limited due to the possible immobilization of complex inside the channels, which may affect access of the reactants to the active sites of the catalyst.
- The main reaction products obtained with the catalytic system FePcCl<sub>16</sub>-NH<sub>2</sub>-SBA-15/TBHP were: tert-butanol and carvone for carveol substrate and limonene epoxide, carveol, tert-butanol and carvone for limonene substrate. Others byproducts were detected in small amounts.
- Between the reaction conditions evaluated in this work, the conditions under which carvone production is favored are: 875 rpm, 313 K, substrate (carveol or limonene) concentration of 0.03 M, TBHP concentration of 0.31 M, active sites (Fe) concentration of  $3 \times 10^{-4}$  M, 3 hours reaction for limonene and 1 hour reaction for carveol.
- The maximum substrates conversion, obtained at the experimental conditions mentioned in the previous conclusion, were around 97% (24 h reaction). Furthermore, in the catalytic

system for both substrates, carvone behaves as an intermediate product, maybe due to its possible overoxidation.

- Experimental results and the mechanism analyzed, indicate that there could be a competition between substrate and TBHP to be adsorbed on active sites during the reactions.
- The behavior of the catalytic system with carveol as substrate is better than with limonene as substrate; and the mechanism for limonene is considerably more complex than for carveol mechanism., While for carveol, results seems to indicate that the formation of oxo metal species ( $\text{Fe}^{\text{IV}} = \text{O}$ ) involved in carveol oxidation, is mainly through homolytic cleavage, for limonene it seems to exist alternative pathways for both, TBHP decomposition and limonene oxidation. Hence, results suggest the existence of two different limonene oxidation pathways. One of these pathways, the allylic oxidation of limonene to carvone may be favored by the presence of heterogeneous catalyst (radical pathway), while the other, epoxidation of limonene is disadvantaged by heterogeneous catalyst, perhaps due to its extensively heterogeneous nature, and the restricted access of the reactants to the active sites due to support characteristics.
- Between the expressions analyzed in his work, the carveol rate expression derived from pseudo homogeneous mechanism, better represents the experimental results. However, the goodness-of-fit obtained for the carveol reaction in the catalytic system studied is not very high, maybe due to a possible hybrid behavior (homogeneous-heterogeneous) or the influence of products concentration that could shift the reaction behavior from the proposed mechanisms.
- The better goodness-of-fit of pseudo homogeneous mechanism for limeonene and carveol, could be because the free radicals involvement in reactions, being higher for limonene, due to the free radical participation in allylic hydrogen abstraction and limonene hydroperoxide formation.

## **3 Chapter 3: Catalyst stability and recyclability**

### **3.1 Introduction**

One of the major advantages of heterogeneous catalysts is their easier and cheaper reutilization (80); hence not only the catalytic activity but also the stability and recyclability of the catalyst are of high importance.

Deep investigations about MPc stability and reuse in oxidation reactions are scarce published; despite the catalyst stability in oxidation reactions is much more challenging compared with other reactions. Phthalocyanine complexes have been stated as stable compound, but they can undergo degradation under strong oxidative conditions; covalent anchoring of MPc on a support usually makes the catalyst more stable; however, some deactivation of the catalyst by complex lixiviation or blocking of active sites with reactants or products adsorbed could also happens (2)

Previous works reported that the N-oxidation of the phthalocyanine ring and the complex lixiviation are the main causes of deactivation of the catalysts FePcS-NH<sub>2</sub>-S, CoPcS-NH<sub>2</sub>-S and MnPcS-NH<sub>2</sub>-S (10,81) and suggest than FePcCl<sub>16</sub>-NH<sub>2</sub>-S catalyst is stable for oxidation reactions (10).

This chapter aims to evaluate the stability and recyclability of FePcCl<sub>16</sub>-NH<sub>2</sub>-SBA-15 in the carvone production from limonene and carveol using TBHP, additionally the possible adsorption of reactants on active sites, suggested in previous chapter, is also considered as a cause for catalyst deactivation

### **3.2 Experimental procedure**

With the objective to determine possible variations occurred in the catalyst during the reactions and the catalyst reusability; the following procedures were performed:

### 3.2.1 Leaching tests

In order to prove whether the catalyst behaves as heterogeneous one, a leaching test was performed. Reaction was carried out at the best initial conditions determined in previous chapter, after certain time (1 hour for limonene and 30 minutes for carveol) the catalyst was removed to continue the reaction up to 3 hours and the products were analyzed to find if conversion increase after catalyst removal, comparing that observed when the catalyst was not filtered. The initial reactions time were selected in order to ensure detectable amounts of carvone without reaching maximum substrate conversion. In order to verify the results from the leaching test, UV-Vis liquid analysis was also performed to the filtered reaction mixtures in order to determine the presence or not of the catalyst complex in them. This analysis was completed in a UV-visible spectrophotometer Thermo Spectronic Helios  $\alpha$  (200 – 800 nm).

### 3.2.2 Recycling experiments

To study the stability and recycling ability of FePcCl<sub>16</sub>-NH<sub>2</sub>-SBA-15 under the best reaction conditions determined previously, recycling experiments were carried out. After the initial reaction, the catalyst was separated by centrifugation, washed 3 times with acetone and then dried at 358 K. The recovered catalyst was used again under the same reaction conditions in order to evaluate the possibility of using the same catalyst more than once.

### 3.2.3 Used catalyst characterization

Some of the samples of used catalyst were characterized through SEM, TEM, BET, UV-vis, Raman and TGA. These analyses helped to compare the structure and characteristic of fresh and used catalyst and were carried out as explained in *Table 1.2.1*.

## 3.3 Results and discussion

### 3.3.1 Leaching tests

*Figure 3.3.1* and *Figure 3.3.2* show that after catalyst removal by filtration, the filtrate reacted little further (gray triangle) comparing that observed when the catalyst was not filtered (black circle). Although both reactions continue after catalyst removal, it could be

due to the already generated free radicals. To support this assumption an experiment was carried out adding free radical scavenger (2, 4-DPB) when the catalyst was filtrated, obtaining no significant conversion after this (*Figure 3.3.3*).

Note: the reaction conditions for those reactions were: 1.5 mL, 875 rpm, and 313 K, substrate concentration of 0.03 M, TBHP concentration of 0.31 M and active sites (Fe) concentration of  $3 \times 10^{-4}$  M

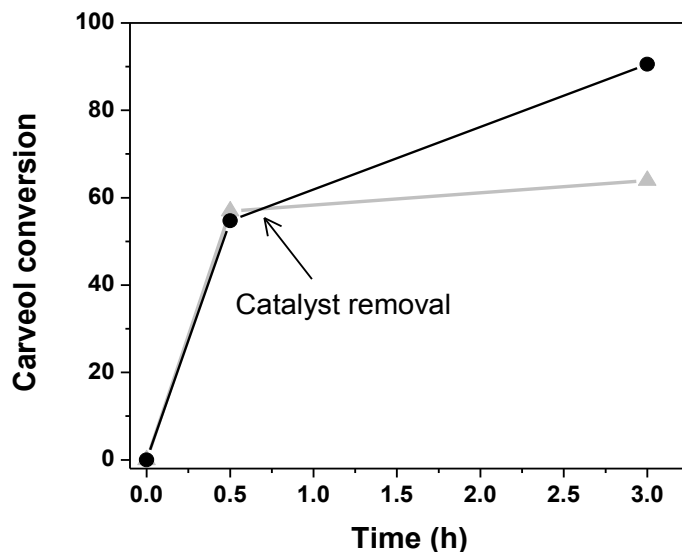


**Figure 3.3.1:** *FePcCl<sub>16</sub>-NH<sub>2</sub>-SBA-15* leaching test in carveol reaction.

Comparison of carveol conversion under typical conditions (black circle) with that obtained when catalyst was removed after 0.5 hour reaction (gray triangle).

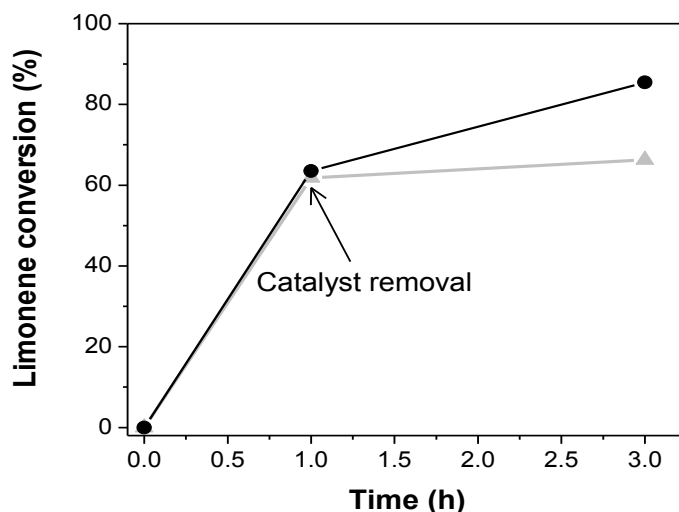


**Figure 3.3.2:** *FePcCl<sub>16</sub>-NH<sub>2</sub>-SBA-15* leaching test in limonene reaction.

Comparison of limonene conversion under typical conditions (black circle) with that obtained when catalyst was removed after 1 hour reaction (gray triangle).



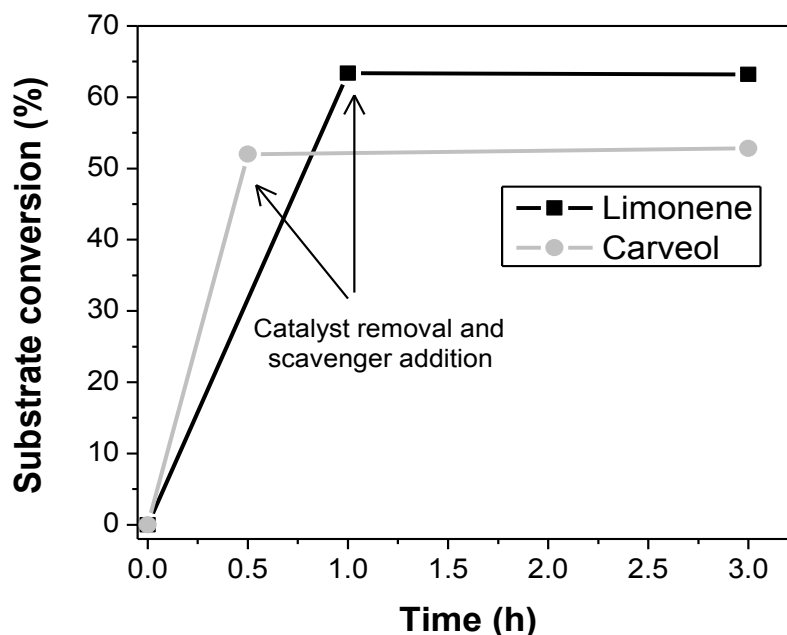


**Figure 3.3.3:** Conversion of carveol and limonene after catalyst removal and addition of free radical scavenger (2, 4-DPB) at 0.5 and 1 hours respectively.

The aforementioned results could indicate that catalyst behaves as heterogeneous one in both reactions (54); however, they are not entirely conclusive. Therefore the following a Uv-Vis liquid analysis was performed.

The UV-vis analysis of  $\text{FePcCl}_{16}$  complex (**Figure 3.3.4 black line**), shows a typical UV-vis spectra of Pc complex, with a Soret (B) Band in the UV region (300-400nm) and a Q-band in the visible region between 550 and 750 nm (43). Experimentally, we verified that the UV-vis spectrums of reactants and products have their characteristic bands in the visible region (wavelength lower than 400nm) (82–84), which could partially overlaps the phthalocyanine Soret (B) Band; thus, the presence of Pc complex in the filtrate should be determined with the presence of phthalocyanine characteristic Q-band. The resulting mixture after 0.08, 3 and 24 hour reaction for both substrates at best conditions were filtrated and analyzed, the UV-vis spectra obtained for all samples were similar to gray line depicted in **Figure 3.3.4**, no bands between 450 and 800 nm were detected, which could indicate that there is no complex in the liquid mixture, hence there is no complex lixiviation during the reactions.

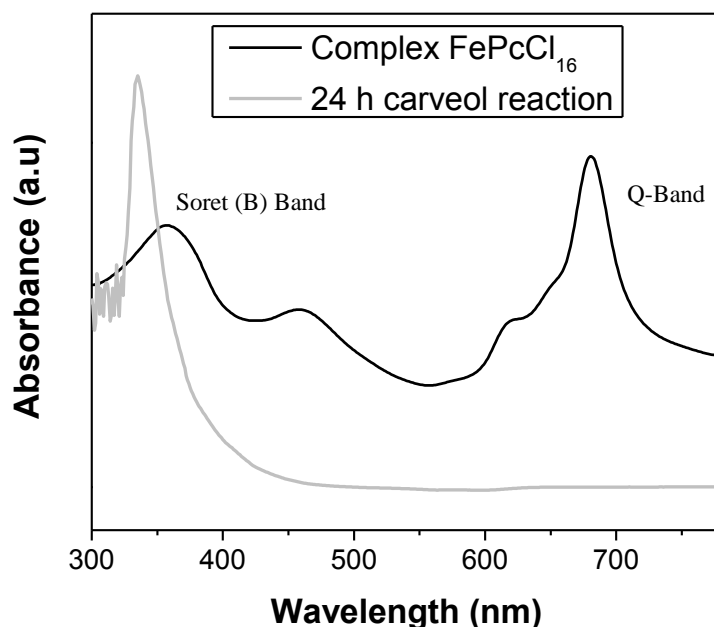


Figure 3.3.4: Uv-vis analysis for  $\text{FePcCl}_{16}$  (black line) and liquid reaction mixture after 24 hour carveol reaction at best conditions.

### 3.3.2 Recycling experiments

Table 3.3.1 and Table 3.3.2 show the recycling experiments results for limonene and carveol, respectively.  $\text{FePcCl}_{16}\text{-NH}_2\text{-SBA-15}$  showed good reusability in the reactions up to 3 times, since substrate conversion and selectivity vary between the ranges of experimental error. However when catalyst was used the fourth time a significant change in conversion and selectivities was observed. These results and the changes in color and weight of the catalyst observed after reactions, suggest that catalyst undergoes transformation, but the products of this transformation can also show catalytic activity (2) and that one of the transformations occurring in this process could be the blocking of active sites by adsorbed reactants or products (2), further analysis were performed (section 3.3.3).

Table 3.3.1: Recycling experiments for limonene reaction.

| Use                 | Limonene conversion | Limonene Epoxide selectivity | Carvone Selectivity |
|---------------------|---------------------|------------------------------|---------------------|
| 1 <sup>o</sup> time | 66.2                | 7.0                          | 7.1                 |
| 2 <sup>o</sup> time | 65.4                | 9.2                          | 8.0                 |
| 3 <sup>o</sup> time | 60.3                | 9.2                          | 8.5                 |
| 4 <sup>o</sup> time | 47.4                | 9.6                          | 4.0                 |
| SD ( $\pm$ )        | 1.2                 | 0.9                          | 1.9                 |

Reaction condition: 1 hour reaction, 875 rpm, 313 K, substrate concentration of 0.03 M, TBHP concentration of 0.31 M and active sites concentration of  $3 \times 10^{-4}$  M

**Table 3.3.2: Recycling experiments for carveol reaction.**

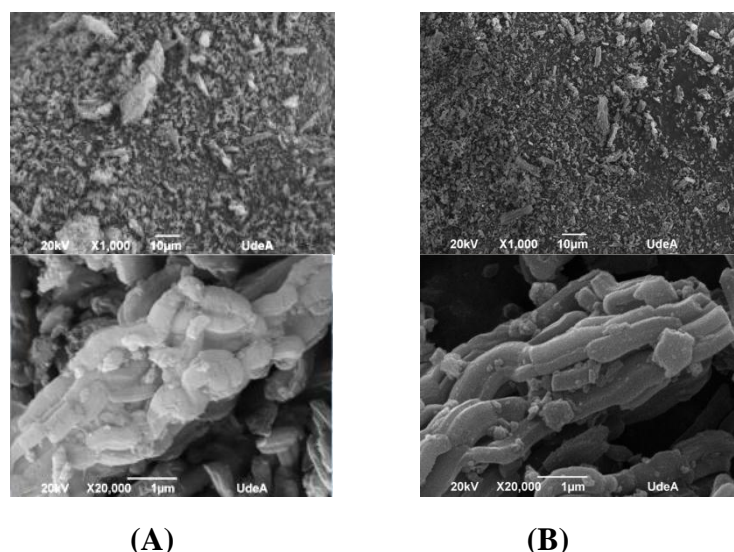
| Use          | Carveol conversion | Carvone selectivity |
|--------------|--------------------|---------------------|
| 1° time      | 90.5               | 24.8                |
| 2° time      | 90.6               | 28.3                |
| 3° time      | 82.0               | 41.8                |
| 4° time      | 71.8               | 45.4                |
| SD ( $\pm$ ) | 3.0                | 10.2                |

Reaction condition: 3 hour reaction, 875 rpm, 313 K, substrate concentration of 0.03 M, TBHP concentration of 0.31 M and active sites concentration of  $3 \times 10^{-4}$  M

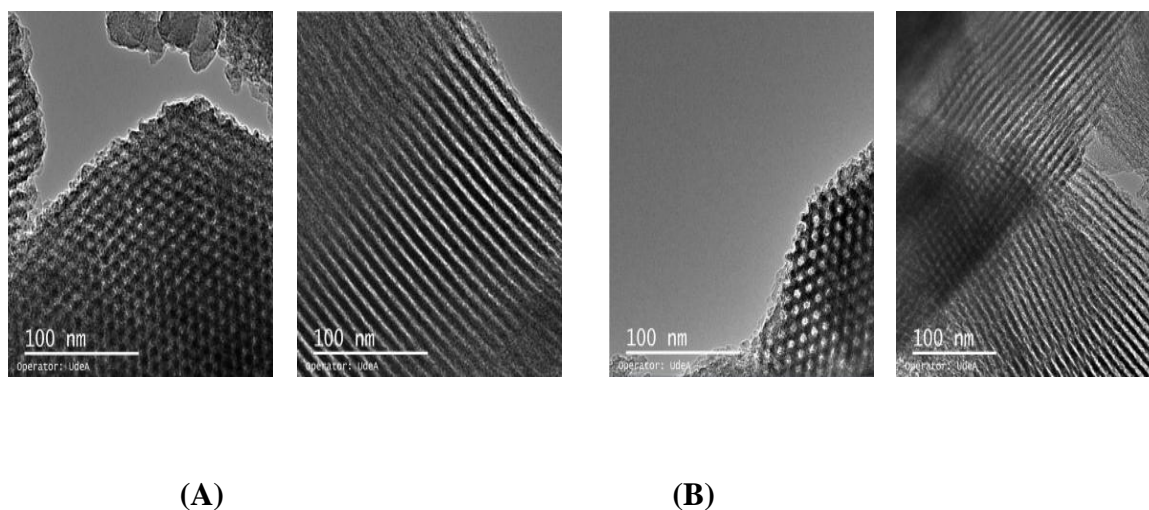
### 3.3.3 Used catalyst characterization

Catalyst used 3 times after 24 hours of reaction showed similar catalytic results to that mentioned in the previous section (3.3.2) and they were characterized in order to identify transformations undergone in the catalyst.

*SEM* and *TEM* analysis confirm that the external morphology and structure of FePcCl<sub>16</sub>-NH<sub>2</sub>-SBA-15 catalyst remained unchanged after reactions, since the recovered used catalyst shows also many rope-like domains that aggregate into a wheat-like microstructure (35) (*Figure 1.3.1* and *Figure 3.3.5*) and well-ordered hexagonal mesopores in a 2D array with long 1D channels (*Figure 1.3.2* and *Figure 3.3.6*). The only significant difference observed between the fresh (*Figure 1.3.1*) and used catalyst (*Figure 3.3.5*), is the apparent decrease of the wheat-like aggregates size that occur after catalyst use. This size reduction could be due to friction between the catalyst, the stir bar and the reaction vessel that occurs during the reaction; however the typical morphology of this kind of materials is not affected.



(A) (B)  
**Figure 3.3.5: SEM images (x1,000 and x20,000) of recovered catalysts used 3 times in 24 hours Limonene (Figure A) and carveol (Figure B) reactions.**



(A) (B)  
**Figure 3.3.6: TEM images of recovered catalysts used 3 times in 24 hours Limonene (Figure A) and carveol (Figure B) reactions.**

**BET** analysis of catalyst used 3 times in limonene reactions shows a surface area ( $S_{\text{total}}$ ) of 53.04 m<sup>2</sup>/g and a pore volume ( $V_p$ ) of 0.13 cm<sup>3</sup>/g. These results are approximately 7 times less than fresh catalyst values (**Table 1.3.2**), which agrees with the hypothesis that reactants and products could be adsorbed inside the pores, blocking them without damaging the SBA15 mesoporous structure.

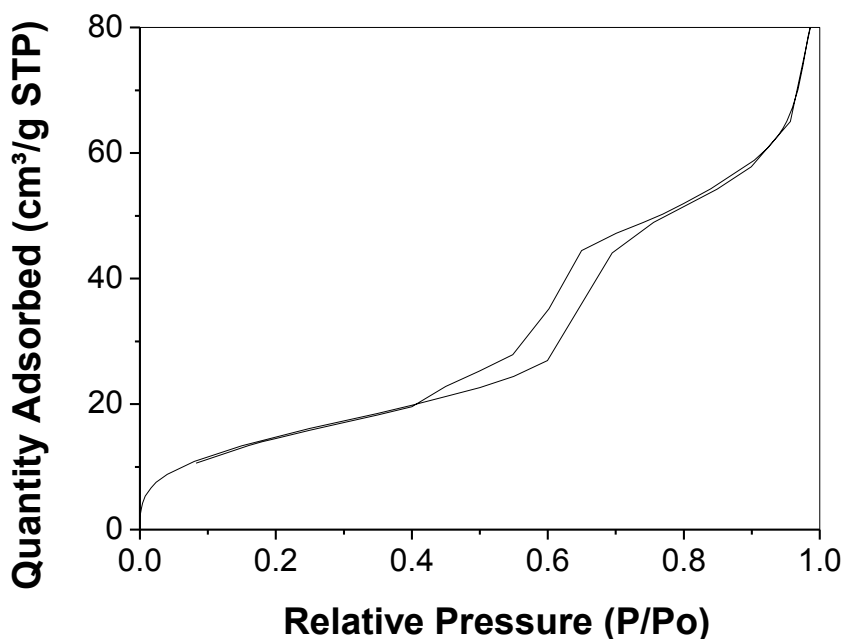


*Figure 3.3.7: N<sub>2</sub> adsorption/desorption isotherms of the catalyst used 3 times in 24 h limonene reactions.*

*Figure 3.3.7* presents N<sub>2</sub> adsorption/desorption isotherm for the catalyst used 3 times in limonene reactions, showing a typical irreversible-type IV adsorption isotherm with H1 hysteresis loop, similar to fresh catalyst (*Figure 1.3.3*). However, besides the huge reduction of porous volume observed in this figure, it could be seen that the isotherm inflection was altered, because the position of adsorption branches shifted toward lower pressure and it is sharper. These observations agree with the lower primary mesopore ( $w_{DFT}$ ) of 58.8 Å shown in *Figure 3.3.8*, since capillary condensation pressure is directly proportional to pore diameter and the sharpness of the adsorption branches is indicative of narrow mesopore size distribution (25,85). These results support the idea that SBA-15 structure was not damaged during reactions and they could indicate that not only the micropores are plugged, but also the mesopores.

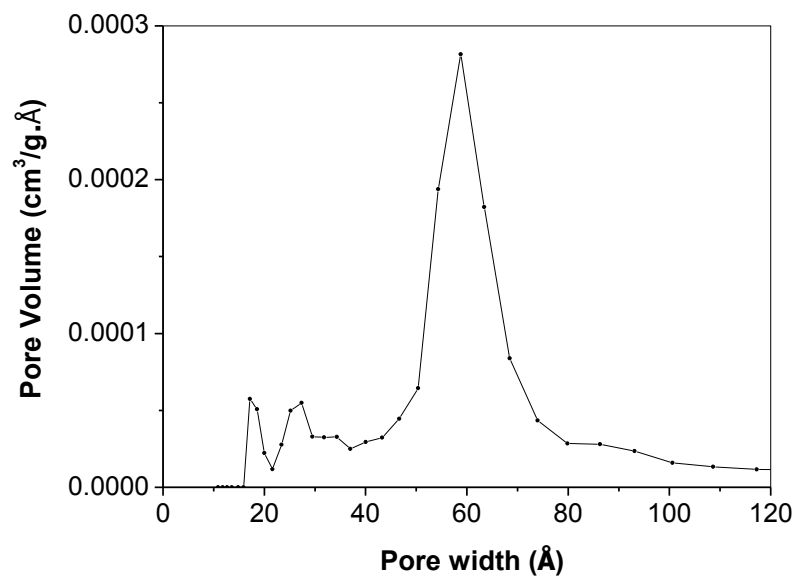


Figure 3.3.8: Pore size distribution of the catalyst used 3 times in 24 h limonene reactions.

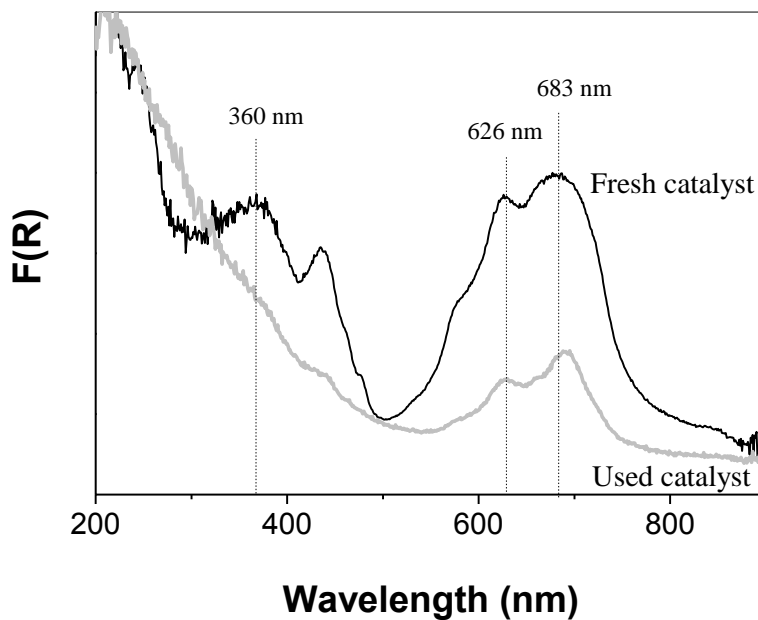
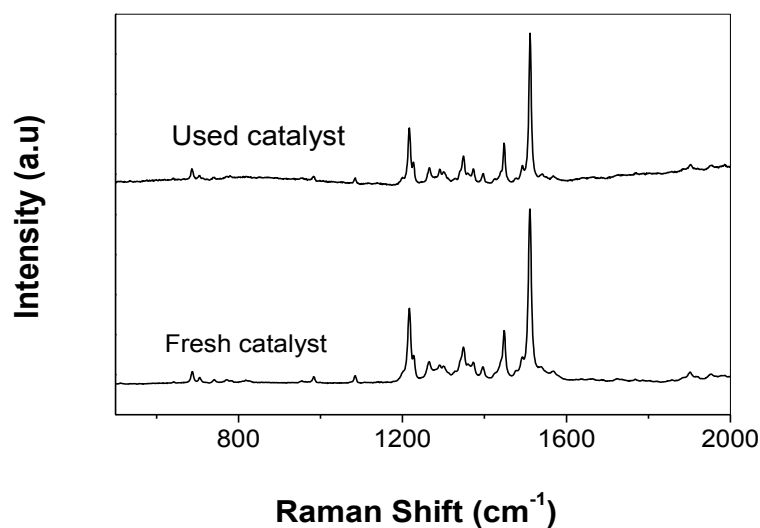


Figure 3.3.9: UV-vis analysis of fresh catalyst (black line) and catalyst used 3 times in 24 h limonene reactions (gray line).

Figure 3.3.9 shows the comparison between UV-vis analysis of fresh and used catalyst, there, it could be observed that both catalysts present the monomeric band around 683 nm and the dimeric band around 626 nm; in contrast, the other monomeric band (around

423nm) and the band associated to  $\pi - \pi^*$  transitions of the C = C double bonds of the phthalocyanine complex (around 360 nm) could not be observed in the Uv-vis analysis of used catalyst (gray line). These results could indicate some damage in the complex structure, however it was dismissed by *Raman* analysis results (*Figure 3.3.10*) since used catalyst does not present differences in the phthalocyanine characteristic bands that were observed in fresh catalyst, which could indicate that the catalyst was not deactivated or damaged. The differences found in the low wavelengths UV-vis spectra of used catalyst (*Figure 3.3.9*) can probably be explained by the presence of reactants and products on the catalyst, because their characteristic Uv-vis bands are around this range (82–84).



*Figure 3.3.10: Raman analysis of fresh catalyst and catalyst used 3 times in 24 h limonene reactions.*

Thermogravimetric analysis between 100 °C and 800 °C showed 38.62 % weight loss in the catalyst used 3 times (24 hours/reaction) in limonene reactions. This value is much higher than in the fresh catalyst (18.39 % *Table 1.3.4*), which suggest poor organic species removal from the catalyst using acetone during the washing.

### **3.4 Partial conclusions**

- FePcCl<sub>16</sub>-NH<sub>2</sub>-SBA-15 catalyst behaves as a heterogeneous catalyst in both reactions, with limonene or carveol.
- FePcCl<sub>16</sub>-NH<sub>2</sub>-SBA-15 catalyst can be re-used at the selected conditions for both substrates at least three times without significant changes in its activity.
- The slight decrease in catalyst activity observed in the fourth use of the catalyst seems to be due to active sites blocking caused by the reactants and product adsorption on them.



## 4 Chapter 4: Technical feasibility of the process

### 4.1 Introduction

Carvone is part of a sector termed *fine chemicals*, with specific features (86,87), as shown in **Figure 4.1.1**. This sector, is growing fast, hence much attention has been paid to selectivity engineering and catalysis, in order to reduce the consumption of raw materials and wastes production.

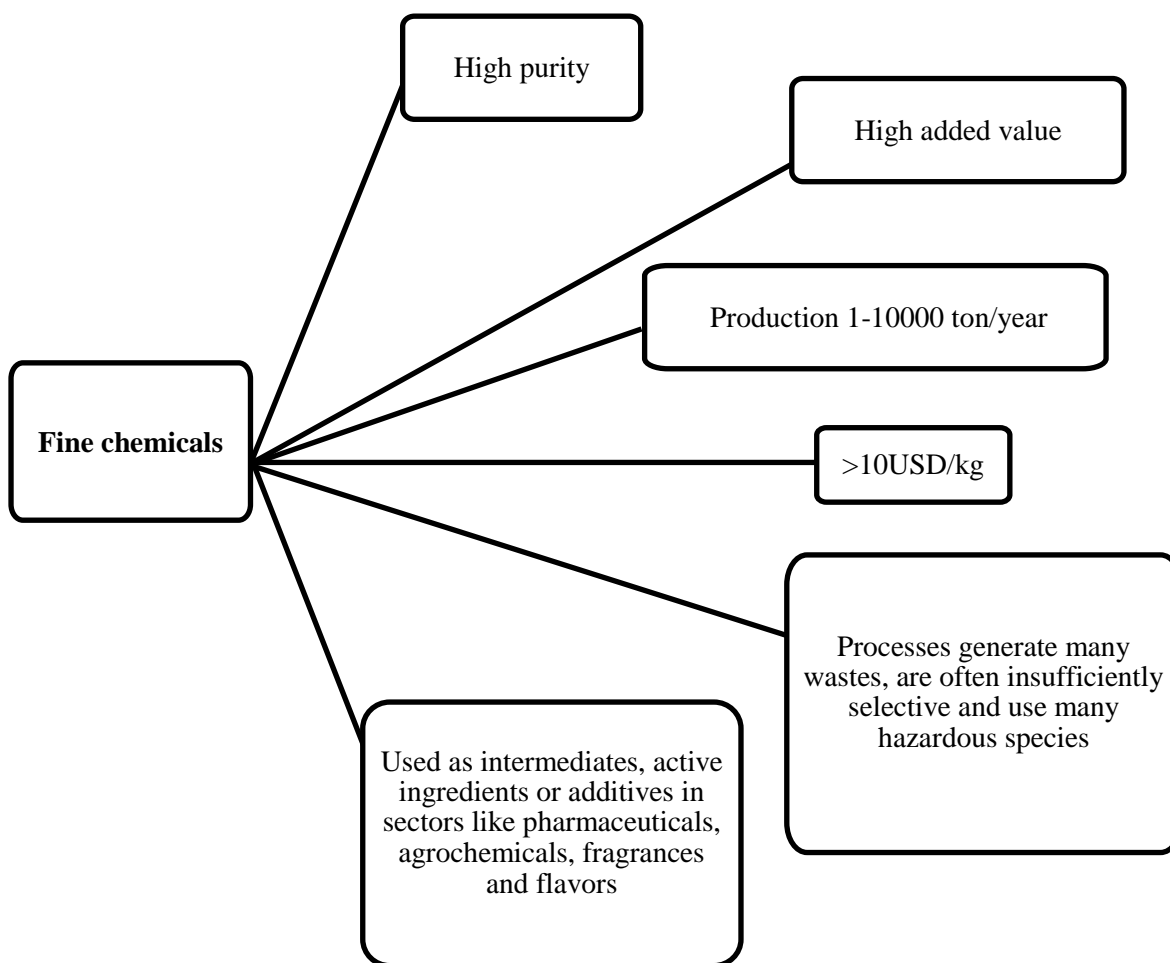


**Figure 4.1.1:** specific features of fine chemicals

Carvone is frequently used in flavor and fragrance industry and has been produced by over 70 different plants (51). In the market, it could be found as two enantiomers:

- S (+) Carvone: it could be extracted from its essential oil, usually from caraway seeds (*Carum carvi*) and dill leaves (*Anethum graveolens*). It is considerably expensive and has a limited use in synthetic essential oils (e.g. caraway) and spice flavors.
- R (-) carvone: it could be extracted from its essential oil, usually produced by spearmint (*Mentha spicata*) plants. It is extensively used in the formulation of nature identical essential oils besides in spearmint and mint flavors; thus it finds extensive use in Toothpaste, Mouth washes and Gum flavors. The racemate of carvone is totally unsuited for use in spearmint flavors (88).

The extraction process of the natural oil has several drawbacks related to harvesting date, large required crop time, weather conditions, soils and fertilizer composition, among others (73). Thence, some chemical and microbial biotransformation of limonene and carveol to produce carvone have being researched and used by big companies (54,57,73,75).

R (-) carvone biggest buyers are Colgate-Palmolive and Procter & Gamble. Its market is estimated in around 2,000 tonnes per year, and it is mainly covered by Paramount Aromachem Pvt Ltd., Symrise AG and Shanghai Wanxiang Flavors & Fragrances Co. Ltd (75). Paramount Aromachem Pvt Ltd. has set up a plant to produce Carvone (99% purity) and derivatives as carvacrol from limonene using a solvent free route, without any chlorine compound. This plant maximal capacity is 2,000 tonnes per year and in this way they can offer a cleaner greener product with no additional costs (89).

Analyzing the information reported by several suppliers (75,90–92), it was found that R(-) carvone price is around 119 USD/kg (average value), but it depends on R(+) Limonene prices.

A study of essential oils in the Colombian market made in 2003, showed a business opportunity due to the high amount of money in importation of mixtures flavors and fragrances; which are used by national and multinationals industries (93).

However, specific information about importation of carvone in Colombia could not be found, since it enters the country under the code 2914299000 which corresponds to “Other cyclical and cycloterpenic ketones, without other oxygen function”. Importations under this code in 2015 were worth around of 143 ton and around 10 ton in the first month of 2016, but this data do not include only carvone (94).

Since the main buyers of carvone are toothpaste manufacturers, a broad approximation for carvone demand in Colombia could be made from toothpaste consumption. Information found states that toothpaste demand in Colombia is around 1,000 ton/month (95,96) (average value considering annual growth (97)). Taking into account the composition of carvone in toothpaste (around 0.89%) (98), it could be said that the required amount of Carvone to meet the toothpaste demand in Colombia would be around 9 ton/month. It is important to keep in mind that this approach is not by any means, a detailed market study; it was only performed as a general approach that allows sizing roughly the quantities of Carvone that could be handled in Colombia.

The aim in this chapter is to develop a preliminary analysis about the feasibility of carvone production using the catalytic system here studied, limonene/TBHP/FePcCl<sub>16</sub>-NH<sub>2</sub>-SBA-15 and carveol/TBHP/FePcCl<sub>16</sub>-NH<sub>2</sub>-SBA-15. To this end, some Aspen simulations were performed to analyze some technical and economic aspects of these processes.

## **4.2 Aspen simulation**

Aspen Plus ® V8.6 is a simulation software commonly used by the bulk, fine, specialty, and biochemical industries, as well as the polymer industry for the design, operation, optimization of safe, and profitable manufacturing facilities. It has an extensive array of unit operations, several specialized work environments, and a robust solver (99). For that reason it can be used to simulate the reactor and the basic separation equipment, in order to develop a preliminary analysis of process feasibility.

To model the reactor, Aspen has different types of reactors, among them two of our interest RBatch and RYield (100).

- RBatch: It is a rigorous model for batch reactor, a perfectly mixed vessel in which reactants (previously charged) are converted to products during the course of a batch cycle. This kind of reactors is commonly used in fine chemicals industries, and is selected in Aspen when the kinetics and stoichiometry of reaction are well known (100,101).

- RYield: It is a model widely recommended when kinetics and/or stoichiometry are not well understood, or the inlets to the reactor are not completely known, since Ryield requires a mass balance only, not an atom balance, neither a complete rate expression with stoichiometry (100,102).

Regarding the distillation column Aspen provides an approximate model, DSTWU that uses the Winn-Underwood-Gilliland methods and a rigorous model, RADFRAC that uses the Newton-Raphson modified algorithm, in which can be performed a simulation, sizing, and rating of tray and packed columns. The DSTWU model can be easily used to calculate the initial value of some parameters used later in the rigorous model (103,104), as it was performed in this work.

#### **General considerations for Aspen simulation**

- Decane was not considered in the simulation, because it was only used as internal standard for calculations of composition during the chromatographic analysis.

- The substances considered in simulation Limonene (D-LIM-01), TBHP (T-BUT-01), tert-butanol (TERT- -01), Acetone (ACETO-01) and water (WATER) are part of the Aspen databases; while Carvone (CARVONE), carveol (CARVEOL) and Limonene epoxide (L-EPOXID), which are not available in Aspen databases, were entered as “User Defined” substances, using their molecular formula and structure. The other subproducts were not considered in simulation due to the lack of real data of their concentration and their participation in mechanism.

- The thermodynamic method used to determine the physico-chemical properties required in the simulation was UNIFAC-DM, since it is a predictive method based on group contribution, thence it becomes a valuable alternative when the experimental data are limited as is the case in this work. Furthermore, NRTL was used for the simulation, since it

is recommended for unique liquid organic phase with presence of water and the binary interaction coefficients could be estimated by UNIFAC-DM (105,106).

- Heat transfer and mixing problems, as well as other scale up problems were not considered in this preliminary analysis.
- The separation of the catalyst was not considered, since Aspen has not a simplified model to simulate the filter and obtaining its design parameter (107) was not between the scopes of this work.
- With the idea of covering around the 7% of the required amount of Carvone demand of toothpaste industry in Colombia (9 ton/month), the production capacity was defined as explained in the following table:

**Table 4.2.1. Definition of reactor capacity.**

| Entry | Parameter   | System with<br>limonene | System with<br>carveol |
|-------|---|-------------------------|------------------------|
| 1     | Monthly carvone production, ton/month                     | 0.66                    | 0.66                   |
| 2     | Workdays per month  | 28                      | 28                     |
| 3     | Work hours per day  | 24                      | 24                     |
| 4     | Hourly carvone production, kg/h                           | 0.99                    | 0.99                   |
| 5     | Reactor load time, h                                      | 1                       | 0.25                   |
| 6     | Reactor unload time,                                      | 1                       | 0.25                   |
| 7     | Reaction time, h  | 3                       | 1                      |
| 8     | Total batch time, h                                       | 5                       | 1.5                    |
| 9     | Carvone produced in one batch, kg*                        | 5                       | 1.5                    |
| 10    | Experimental carvone mass fraction at the end of reaction | 0.0004                  | 0.0018                 |
| 11    | Reactor capacity, kg**:                                   | 12500                   | 825                    |
| 12    | Reactor volume considering (75% filling), m <sup>3</sup>  | 20                      | 1.5                    |

*\*Estimated with entry 4 and 5, taking into account 1% of loss in separation process.*

*\*\*Estimated with entry 9 and 10, assuming ideal scale-up.*

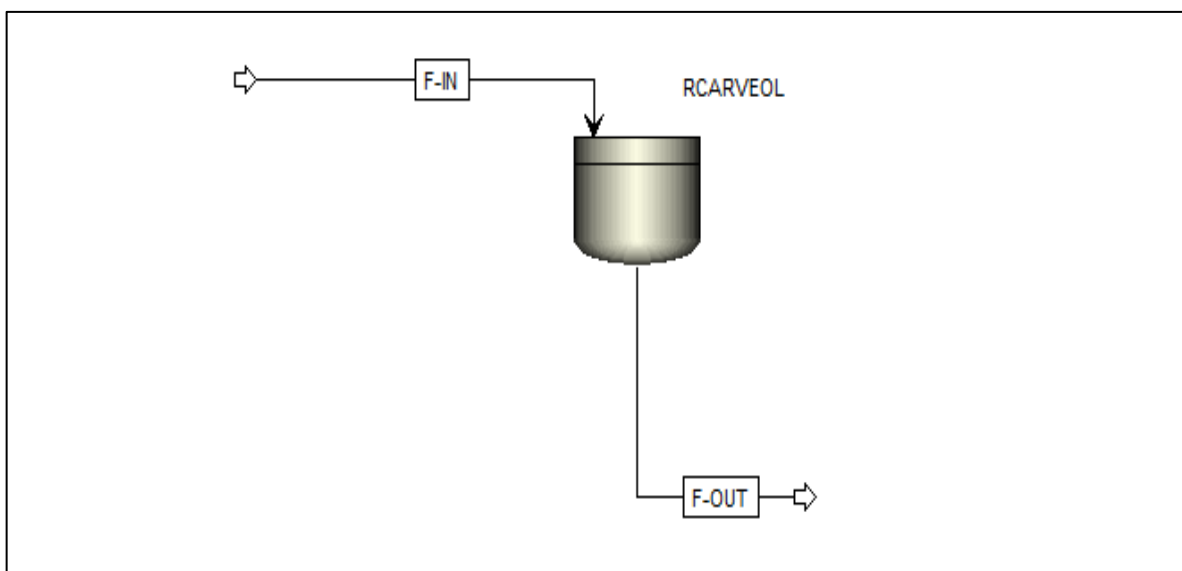
- Reactions were simulated at constant temperature (313 K) and atmospheric pressure (0.84 bar).
- The composition (mass fraction) of input streams for reactor were calculated from experimental data:

Table 4.2.2. Composition of reactors input stream.

|                             | Limonene reaction | Carveol reaction |
|-----------------------------|-------------------|------------------|
| CARVONE                     | 0.00000           | 0.00004          |
| CARVEOL                     | 0.00000           | 0.00600          |
| L-EPOXID (limonene epoxide) | 0.00000           | 0.00000          |
| TERT—01 (tert-butanol)      | 0.00000           | 0.00000          |
| D-LIM-01 (Limonene)         | 0.00518           | 0.00000          |
| ACETO-01 (Acetone)          | 0.94462           | 0.94380          |
| T-BUT-01 (TBHP)             | 0.03514           | 0.03511          |
| WATER                       | 0.01506           | 0.01505          |

### 4.3 Results and discussion

Initially, the best model was used for running a process simulation in an RBatch reactor using Aspen Plus (*Figure 4.3.1*) and the experimental conditions already mentioned (*Table 4.2.2*).



*Figure 4.3.1: RBatch reactor.*

*Figure 4.3.2* shows all specifications for reaction (stoichiometry and reaction rate) in RCARVEOL block. The apparent activation energy and apparent pre-exponential factor used for this reactor, were determined from experimental data by an Arrhenius plot as reported in literature (78).

1) CARVEOL(MIXED) + T-BUT-01(MIXED) --> CARVONE(MIXED) + TI

Reacting phase: **Liquid** Rate basis: **Cat (wt)**

Power Law kinetic expression

If To is specified: Kinetic factor =  $k(T/T_0)^n e^{-(E/R)[1/T-1/T_0]}$

If To is not specified: Kinetic factor =  $kT^n e^{-E/RT}$

k: **0.0157408**

n: **0**

E: **14007.4** **kJ/kmol**

To: **C**

[C] basis: **Molarity**

**Edit Reaction**

Reaction No.: **1** Reaction type: **Kinetic**

| Reactants |             |          | Products  |             |          |
|-----------|-------------|----------|-----------|-------------|----------|
| Component | Coefficient | Exponent | Component | Coefficient | Exponent |
| CARVEOL   | -1          | 0.159587 | CARVONE   | 1           |          |
| T-BUT-01  | -1          | 0.464314 | TERT--01  | 1           |          |
|           |             |          | WATER     | 1           |          |

Close

**Figure 4.3.2: Specification for carveol reaction in RBatch.**

The reactor (RBatch) simulation in Aspen predicted a complete carveol conversion and 100% carvone selectivity before 1 hour (0.66 hours), while experimental data shows only 75 % conversion and 38% selectivity at 1 hour reaction. High differences through time could be easily observed in **Figure 4.3.3** and **Figure 4.3.4**, indicating that pseudo-homogeneous mechanism does not represent completely the carveol reaction. These differences could be due to the slow desorption of formed carvone or because probably the assumed stoichiometry (1 o 1) does not fully represent the real reaction, given the inefficient TBHP decomposition and side reactions that can exist.

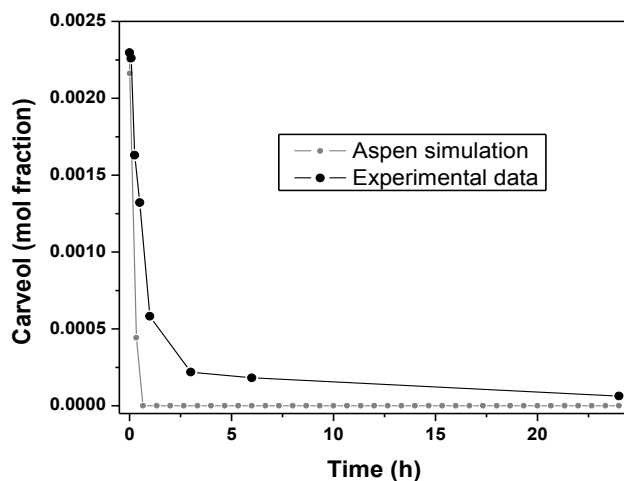


**Figure 4.3.3: Comparison between carveol mole fractions predicted with ASPEN and the experimental data.**

Reaction conditions: 1.5 mL, 875 rpm, 313 K, substrate concentration of 0.03 M, TBHP concentration of 0.31 M and active sites (Fe) concentration of  $3 \times 10^{-4}$  M.

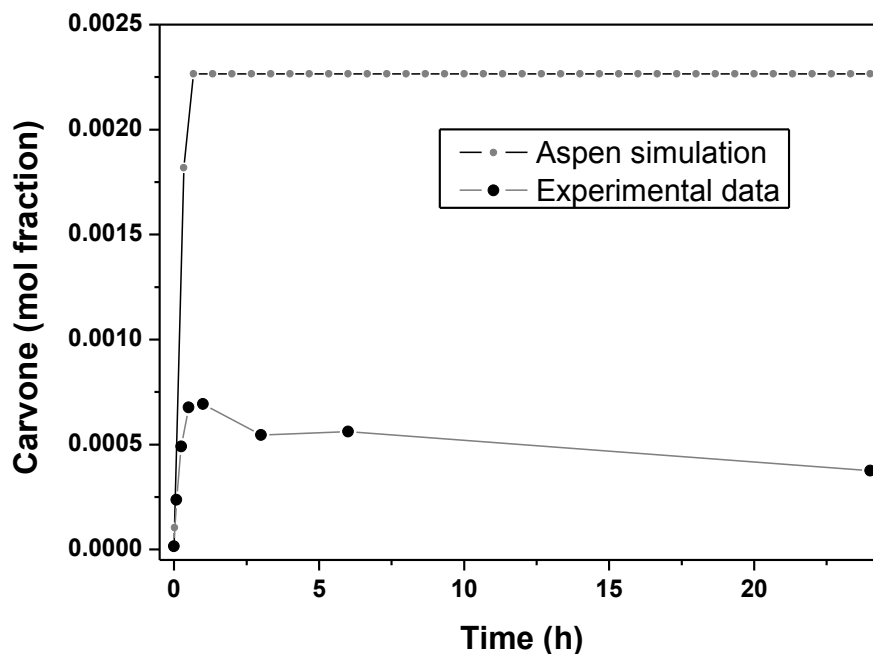


**Figure 4.3.4:** Comparison between carvone mole fractions predicted with ASPEN and the experimental data.

Reaction conditions: 1.5 mL, 875 rpm, 313 K, substrate concentration of 0.03 M, TBHP concentration of 0.31 M and active sites (Fe) concentration of  $3 \times 10^{-4}$  M.

The inaccuracy obtained in the results is not so overwhelming, due to the low correlation of the model with the experimental data, and the complexity of reactions widely explained in the previous chapter. Similar results could be anticipated for limonene reaction, because although its model has better correlation with experimental data, its stoichiometry could not be determined due to the  $O_2$  participation in reactions and the higher amount of byproducts.

Given these results it was decided to simulate both reactors using a RYield model, defining the yield as the mol of each component per total mass input to the block and determining acetone as inert component (**Figure 4.3.5 A and B**). Since byproducts were not considered, the substrate conversion was redefined in order to maintain the overall material balance, assuming as actual conversion, only the substrate which converts to main products; thus simulating the byproducts as non-reacted substrate. This assumption is supported by the high similarity of subproducts and substrates structures.



(A)

(B)

| Yield specification   |       |             |
|---|-------|-------------|
| Yield options: <span style="border: 1px solid black; padding: 2px;">Component yields</span> |       |             |
| Component yields  |       |             |
| Component   | Basis | Basis Yield |
| > CARVONE   | Mass  | 0.007232    |
| > CARVEOL   | Mass  | 0           |
| > L-EPOXID  | Mass  | 0.005425    |
| > TERT--01  | Mass  | 0.003726    |
| > D-LIM-01  | Mass  | 0.08207     |
| > T-BUT-01  | Mass  | 0.629724    |
| > WATER   | Mass  | 0.271823    |

| Yield specification   |       |             |
|---|-------|-------------|
| Yield options: <span style="border: 1px solid black; padding: 2px;">Component yields</span> |       |             |
| Component yields  |       |             |
| Component   | Basis | Basis Yield |
| > CARVONE   | Mass  | 0.03245     |
| > CARVEOL   | Mass  | 0.07459     |
| > L-EPOXID  | Mass  | 0           |
| > TERT--01  | Mass  | 0.01566     |
| > D-LIM-01  | Mass  | 0           |
| > T-BUT-01  | Mass  | 0.60573     |
| > WATER   | Mass  | 0.27157     |

| Inert Components |  |
|------------------|--|
| ACETO-01         |  |

Figure 4.3.5: Definition of yield for Limonene (Figure A) and Carveol (Figure B) RYield reactors.

For the simulation of RYield reactor, pseudo-flow rate must be defined since this reactor simulates continuous reactions and not batch. To this end, the reactor capacity (entry 11 of Table 4.2.1) was divided into the total batch time (Entry 8 of Table 4.2.1), resulting in a flow rate of 2500 kg/h for limonene reactor and 550kg/h for carveol reactor. The reactor (RYield) simulation under these assumptions reproduces properly the results (mass fractions).

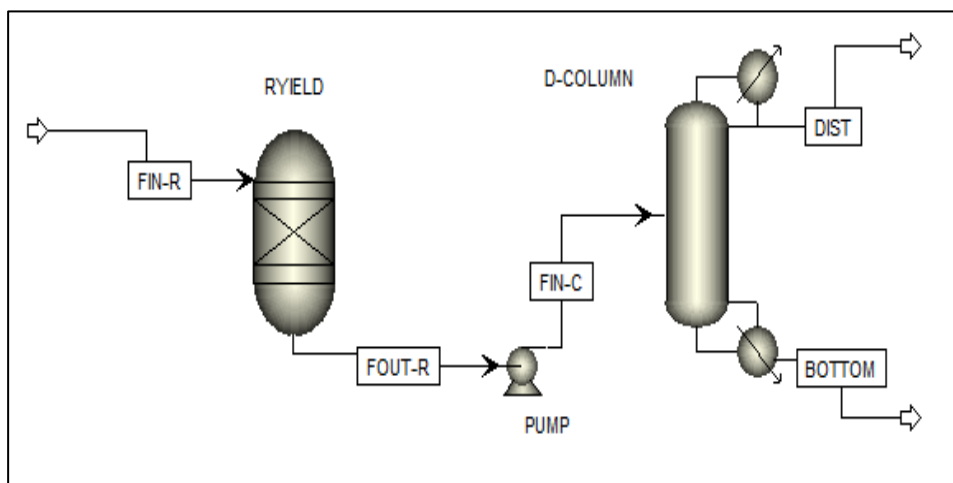


Figure 4.3.6: General flowsheet for both processes.

With the output streams from RYield reactors, it was obtained with a DSTWU model, the first estimate of some parameters (number of stages, reflux ratio, pressure drop, feed stage and feed temperature). Then, this parameter were used to simulate the distillation column with the rigorous model (RADFRAC) linked to the Ryield reactor. **Figure 4.3.6** presents the general flowsheet of complete processes and **Table 4.3.1 A and B** display the operating conditions of distillation columns for limonene and carveol, respectively.

**Table 4.3.1. Operating conditions for RADFRAC model in limonene (A) and Carveol process (B)**

| (A)  |          | (B)  |          |
|--|----------|--|----------|
| Limonene process                                   |          | Carveol process                                |          |
| Parameter  | Value    | Parameter                                      | Value    |
| Feed total Flow kmol/h                             | 43.81864 | Feed total Flow kmol/h                         | 9.63955  |
| Feed total Flow kg/h                               | 2500     | Feed total Flow kg/h                           | 550      |
| Feed temperature                                   | 40.05451 | Feed temperature                               | 40.03495 |
| Top stage pressure [bar]                           | 0.74968  | Top stage pressure [bar]                       | 0.757    |
| Reboiler pressure [bar]                            | 1.09468  | Reboiler pressure [bar]                        | 1.447    |
| Number stage                                       | 12       | Number stage                                   | 6        |
| Feed stage   | 11       | Feed stage                                     | 3        |
| Reflux ratio                                       | 1.5      | Reflux ratio                                   | 0.88     |
| Molar bottoms to feed ratio<br>(Based on carveone) | 0.99     | Molar bottoms to feed ratio<br>(Based on TBHP) | 0.9      |
| Condenser (stage 1)                                | TOTAL    | Condenser (stage 1)                            | TOTAL    |

The Aspen simulation results, obtained with the conditions previously defined, and the flowsheet depicted in **Figure 4.3.6**, are presented in **Table 4.3.2** and **Table 4.3.3**. From limonene process results (**Table 4.3.2**), it could be observed that, despite its low yield, the desired amount and purity of carveone could be obtained in BOTTOM flowstream (Entry 8 and 10) with one distillation column at defined conditions. On the other hand, the carveol process presents some problems in separation process. The required amount of carveone is produced and leaves the distillation columns in BOTTOM flowstream (**Table 4.3.3, entry 1**), but the carveone purity in this stream is very low (BOTTOM entry 10). This is not surprising, given the similarities between the reactants and products boiling points. Therefore, with the assumed conditions for carveol process, carveone could only recovery

from the bottoms (BOTTOM) with significant fractions of carveol and TBHP, which would need further separation.

Table 4.3.2. Aspen simulation results for limonene process

| Entry | Estimated parameter      | Flowstreams ( <i>Figure 4.3.6</i> ) |            |            |            |            |
|-------|--------------------------|-------------------------------------|------------|------------|------------|------------|
|       |                          | FIN-R                               | FIN-C      | DIST       | BOTTOM     |            |
| 1     | CARVONE                  | 0                                   | 1.00127    | 0.0112885  | 0.9899818  |            |
| 2     | CARVEOL                  | 0                                   | 0          | 0          | 0          |            |
| 3     | Mass Flow<br>kg/hr       | L-EPOXID                            | 0          | 0.7510912  | 0.7504435  | 0.00064775 |
| 4     |                          | TERT--01                            | 0          | 0.5158647  | 0.5158647  | 1.1922E-08 |
| 5     |                          | D-LIM-01                            | 12.95      | 11.36259   | 11.36242   | 0.00017075 |
| 6     |                          | ACETO-01                            | 2361.55    | 2361.55    | 2361.55    | 0.00014292 |
| 7     |                          | T-BUT-01                            | 87.85      | 87.18529   | 87.18524   | 4.6573E-05 |
| 8     |                          | WATER                               | 37.65      | 37.63389   | 37.63389   | 1.3807E-07 |
| 9     |                          | Total                               | 2500       | 2500       | 2499.009   | 0.99099    |
| 10    | Mass fraction            | CARVONE                             | 0          | 0.00040051 | 4.5172E-06 | 0.99898263 |
| 11    |                          | CARVEOL                             | 0          | 0          | 0          | 0          |
| 12    |                          | L-EPOXID                            | 0          | 0.00030044 | 0.0003003  | 0.00065364 |
| 13    |                          | TERT--01                            | 0          | 0.00020635 | 0.00020643 | 1.203E-08  |
| 14    |                          | D-LIM-01                            | 0.00518    | 0.00454504 | 0.00454677 | 0.0001723  |
| 15    |                          | ACETO-01                            | 0.94462    | 0.94462    | 0.9449946  | 0.00014421 |
| 16    |                          | T-BUT-01                            | 0.03514    | 0.03487412 | 0.03488793 | 4.6996E-05 |
| 17    | WATER                    | 0.01506                             | 0.01505356 | 0.01505953 | 1.3933E-07 |            |
| 18    | Temperature, °C          | 23                                  | 40.0248    | 48.53315   | 228.5363   |            |
| 19    | Pressure, bar            | 0.84                                | 0.978      | 0.74968    | 1.00068    |            |
| 20    | Vapor Frac               | 0                                   | 0          | 0          | 0          |            |
| 21    | Density, g/cc            | 0.7977675                           | 0.7776172  | 0.7672025  | 0.7580286  |            |
| 22    | Average molecular weight | 57.05157                            | 57.05335   | 57.03932   | 150.1794   |            |

Table 4.3.3. Aspen simulation results for carveol process.

| Entry | Estimated parameter      | Flowstream (Figure 4.3.6) |            |            |            |
|-------|--------------------------|---------------------------|------------|------------|------------|
|       |                          | FIN-R                     | FIN-C      | DIST       | BOTTOM     |
| 1     | CARVONE                  | 0.022                     | 1.00303    | 2.142E-05  | 1.003008   |
| 2     | CARVEOL                  | 3.3                       | 2.305577   | 9.4744E-06 | 2.305567   |
| 3     | L-EPOXID                 | 0                         | 0          | 0          | 0          |
| 4     | TERT--01                 | 0                         | 0.4840506  | 0.4823104  | 0.00174022 |
| 5     | D-LIM-01                 | 0                         | 0          | 0          | 0          |
| 6     | ACETO-01                 | 519.09                    | 519.09     | 519.0008   | 0.0892366  |
| 7     | T-BUT-01                 | 19.3105                   | 18.72311   | 4.398956   | 14.32416   |
| 8     | WATER                    | 8.2775                    | 8.394229   | 8.310374   | 0.0838543  |
| 9     | Total                    | 550                       | 550        | 532.1924   | 17.80756   |
| 10    | CARVONE                  | 0.00004                   | 0.00182369 | 4.0249E-08 | 0.05632484 |
| 11    | CARVEOL                  | 0.006                     | 0.00419196 | 1.7803E-08 | 0.12947125 |
| 12    | L-EPOXID                 | 0                         | 0          | 0          | 0          |
| 13    | TERT--01                 | 0                         | 0.00088009 | 0.00090627 | 9.7724E-05 |
| 14    | D-LIM-01                 | 0                         | 0          | 0          | 0          |
| 15    | ACETO-01                 | 0.9438                    | 0.9438     | 0.97521272 | 0.00501116 |
| 16    | T-BUT-01                 | 0.03511                   | 0.03404202 | 0.00826572 | 0.80438645 |
| 17    | WATER                    | 0.01505                   | 0.01526223 | 0.01561536 | 0.00470892 |
| 18    | Temperature, °C          | 23                        | 40.03495   | 48.33181   | 127.7523   |
| 19    | Pressure, bar            | 0.84                      | 1.03       | 0.757      | 1.447      |
| 20    | Vapor Frac               | 0                         | 0          | 0          | 0          |
| 21    | Density, gm/cc           | 0.7988749                 | 0.7783866  | 0.7638314  | 0.8009544  |
| 22    | Average molecular weight | 57.09506                  | 57.05661   | 56.30134   | 95.23919   |

Finally, a preliminary economic analysis was carried out. The total cost of raw material streams for each process was calculated with commercial average prices (75,90–92) and the required amounts estimated with Aspen simulation (first columns *Table 4.3.4*), similarly the total income from carvone sales were calculated taking into account the hourly carvone production established in this work (last column *Table 4.3.4*). According to these results, neither limonene process nor carveol process, with the assumptions and conditions used in

this work, are economically feasible, since the cost of each raw material required, is higher than the total income from carvone sales at the price of carvone in the market.

**Table 4.3.4. Cost of raw material and product for each process.**

| <b>Process</b>  | <b>Cost of raw materials (USD/h)</b> |           |                | <b>Total income from carvone sale (USD/h)</b> |
|-----------------|--------------------------------------|-----------|----------------|---|
|                 | Acetone                              | Substrate | TBHP (aqueous) |   |
| <b>Limonene</b> | 33061.7                              | 569.8     | 2259           | 117.9256                                      |
| <b>Carveol</b>  | 7267.26                              | 798.6     | 496.584        | 117.9256*                                     |

*\*Despite obtained product does not meet the purity required, the commercial price was used for this analysis, assuming further purification is possible.*

#### **4.4 Partial conclusions**

- The inaccuracy obtained in RBatch simulation with Aspen, could be due to the low correlation between the model and the experimental data; as well some difficulties for determining the fully reactions stoichiometry due to their complexity.
- In spite of limonene cheapness, the low yield and high excess of oxidant for the production of carvone from limonene using TBHP/FePcCl<sub>16</sub>-NH<sub>2</sub>-SBA-15 influence negatively the feasibility of the process, since it requires high amounts of raw materials and high reactor capacity.
- The performance of the catalytic system (TBHP/FePcCl<sub>16</sub>-NH<sub>2</sub>-SBA-15) is better for carveol than for limonene; notwithstanding the high excess of oxidant required, the high price of carveol (275 USD/kg more expensive than carvone) and the problems found for its purification impact highly its feasibility

Given the assumptions made for this analysis and the restrictions found to simulate accurately the mechanisms, the results in this work are the base for improvements needed to complete design and technical analysis. Results also suggest that improvements in the catalytic systems should be made, before the application of the process at larger scale.

## *General conclusions*

The performance of the hexadecachlorinated iron phthalocyanine catalyst immobilized on mesostructured silica (SBA15), was evaluated in the production of carvone from limonene and carveol using Tert-butyl hydroperoxide, concluding that:

- The presence of FePcCl<sub>16</sub> complex favors the conversion and carvone selectivity in the reaction of TBHP with limonene and with carveol. Immobilization of this complex on SBA-15 causes a decrease in limonene conversion, but the carvone selectivity increases, restricting slightly the limonene epoxide formation. Immobilization also generates a slight reduction in carvone production from carveol respect to unsupported catalyst. The activity of this catalyst could be limited due to the possible immobilization of complex inside the channels, which may affect access of the reactants to the active sites of the catalyst.
- Among the reaction conditions evaluated in this work, the conditions under which carvone production is favored are: 875 rpm, 313 K, substrate (carveol or limonene) concentration of 0.03 M, TBHP concentration of 0.31 M and active sites (Fe) concentration of  $3 \times 10^{-4}$  M and the optimum reaction time is 3 hours for limonene and 1 hour for carveol.
- FePcCl<sub>16</sub>-NH<sub>2</sub>-SBA catalyst is stable under the reaction conditions worked in this research, and it can be used up to three times without significant decrease in its catalytic activity.
- The behavior of the catalytic system with carveol as substrate is much higher than with limonene as substrate

The results also give an approach to the mechanisms of carvone production from limonene and carveol with FePcCl<sub>16</sub>-NH<sub>2</sub>-SBA catalyst:

- For both catalytic systems there is a high presence of O-O TBHP bond homolytic cleavage. However, while for carveol results seems to indicate that the formation of oxo metal species ( $\text{Fe}^{\text{IV}} = \text{O}$ ) involved in carveol oxidation is mainly homolytic breakage, for

limonene it seems to exist alternative pathways for both, TBHP decomposition and limonene oxidation.

- Probably there is competition between substrate and TBHP to be adsorbed on active sites during the reactions and the carveol behaves as an intermediate product, maybe due to its possible overoxidation.
- The mechanism for limonene is considerably more complex than for carveol, since results suggest the existence of two different limonene oxidation pathways. One of these pathways, the allylic oxidation of limonene to carveol may be favored by the presence of heterogeneous catalyst (radical pathway), while the other, epoxidation of limonene is disadvantaged by heterogeneous catalyst, perhaps due to its extensively heterogeneous nature and the, restricted access of the reactants to the active sites due to support characteristics.
- According with the rate expressions analyzed in this work, the carveol rate derived from pseudo-homogeneous mechanism better represents the experimental results. However, this expression does not represent completely the reaction mechanism, since it does not consider parallel heterogeneous behavior due to reactants adsorption and the possible effect of carveol concentration, byproducts and side reactions on the reaction rate.
- The high goodness-of-fit of pseudo homogeneous mechanism for limonene and carveol, could be because the free radicals involvement in reactions, being higher for limonene, due to the free radical participation in allylic hydrogen abstraction and limonene hydroperoxide formation.

Finally, the results allowed providing a preliminary analysis of process feasibility:

- For limonene process: despite its affordable raw material, the low yield and high excess of oxidant required, influence negatively the feasibility of the process, since it requires high amounts of raw materials and high reactor capacity.
- For carveol process: despite the better performance of the catalytic system, the high excess of oxidant required, the high price of carveol and the problems found for its purification impact highly its feasibility

- Neither limonene process nor carveol process, with the assumptions and conditions used in this work, are economically feasible, since the cost of each raw material required, is higher than the total income from carvone sales at the price of this in the market.

Summarizing, the results in this work are the base for improvements needed to complete design and technical analysis for a possible scaling up of the process.



## *Recommendations*

According to the results of this work the recommendations for future works in the carvone production from limonene and carveol with the catalytic system FePcCl<sub>16</sub>-NH<sub>2</sub>-SBA-15/TBHP are:

- Performe adsorption analysis of reactants and products on the catalyst, to confirm the possible competitions of these with TBHP during the reaction.
- Evaluate other supports for the FePcCl<sub>16</sub> that could improve the carvone yield for limonene reaction, maybe narrows pores that could restrict more the substrate adsorption, favoring the homolytic pathway of reaction.
- Performe a feasibility analysis using cheaper raw as orange oil, which has high concentration of limonene.
- Evaluate the possible coupling of the process of carvone production from carveol to an existing process with carveol as byproduct, thus avoiding the problem of its high cost.

## *References*

1. Pérollier C, Pergrale-mejean C, Sorokin AB. Mechanistic diversity of the selective oxidations mediated by supported iron phthalocyanine complexes. *New J Chem.* 2005;29(11):1400–3.
2. Sorokin AB. Phthalocyanine Metal Complexes in Catalysis. *Chem Rev.* 2013;113(10):8152–91.
3. Martin-Luengo MA, Yates M, Diaz M, Rojo ES, Gil LG. Renewable fine chemicals from rice and citric subproducts: Ecomaterials. *Appl Catal B Environ.* Elsevier B.V.; 2011;106(3-4):488–93.
4. Gökçe S, Saka ETT, Bıyıklıoğlu Z, Kantekin H, Biyiklioğlu Z, Kantekin H. Synthesis, characterization of metal-free, metallophthalocyanines and catalytic activity of cobalt phthalocyanine in cyclohexene oxidation. *Synth Met.* 2013;176:108–15.
5. Sorokin AB, Tuel A. Metallophthalocyanine functionalized silicas: catalysts for the selective oxidation of aromatic compounds. *Catal Today.* 2000;57(1-2):45–59.
6. Sorokin ABB, Kudrik EV V. Phthalocyanine metal complexes: Versatile catalysts for selective oxidation and bleaching. *Catal Today.* Elsevier B.V.; 2011;159(1):37–46.
7. Alvarez L, Fall F, Belhboub A, Le Parc R, Almadori Y, Arenal R, et al. One-Dimensional Molecular Crystal of Phthalocyanine Confined into Single-Walled Carbon Nanotubes. *J Phys Chem C.* American Chemical Society; 2015;119(9):150223124023006.
8. Fukuda T, Kobayashi N. UV-Visible Absorption Spectroscopic Properties of Phthalocyanines and Related Macrocycles. *Handbook of Porphyrin Science.* New Jersey: World Scientific; 2010. p. 1–644.

9. Restrepo V, González Rodríguez LM. Actividad del sistema catalítico FePcCl16-SiO<sub>2</sub>/TBHP en la oxidación alílica de limoneno. VIII Simposio Colombiano de Catálisis, VI Simposio de Química Aplicada. 2013. p. 1–2.
10. Rodríguez G. Monoterpenes Oxyfunctionalization. Doctoral research work. Universidad de Antioquia; 2008.
11. Wróblewska A. The epoxidation of limonene over the TS-1 and Ti-SBA-15 catalysts. *Molecules*. 2014;19(12):19907–22.
12. Joseph T, Halligudi SB. Oxyfunctionalization of limonene using vanadium complex anchored on functionalized SBA-15. *J Mol Catal A Chem*. 2005;229(1-2):241–7.
13. Saraiva MS, Fernandes CI, Nunes TG, Nunes CD, Calhorda MJ. New Mo(II) complexes in MCM-41 and silica: Synthesis and catalysis. *J Organomet Chem*. 2014;751:443–52.
14. Balula SS, Santos ICMS, Cunha-Silva L, Carvalho AP, Pires J, Freire C, et al. Phosphotungstates as catalysts for monoterpenes oxidation: Homo- and heterogeneous performance. *Catal Today*. 2013;203:95–102.
15. Fenelonov VB, Mel MS. Surface and nanomolecular catalysis. *Materials Today*. Boca Raton: Taylor and Francis; 2006. 8-135 p.
16. Grün M, Unger KK, Matsumoto A, Tsutsumi K. Novel pathways for the preparation of mesoporous MCM-41 materials: control of porosity and morphology. *Microporous Mesoporous Mater*. 1999;27(2-3):207–16.
17. Thielemann JP, Girgsdies F, Schlögl R, Hess C. Pore structure and surface area of silica SBA-15: influence of washing and scale-up. *Beilstein J Nanotechnol*. 2011;2:110–8.
18. Sirotin S V., Tolbin AY, Moskovskaya IF, Abramchuk SS, Tomilova LG, Romanovsky B V. Heterogenized Fe(III) phthalocyanine: Synthesis, characterization and application in liquid-phase oxidation of phenol. *J Mol Catal A Chem*.

- 2010;319(1-2):39–45.
19. Álvarez, González Rodríguez LM, Villa Holguín AL.  $\alpha$ -Pinene allylic oxidation over FePcCl<sub>16</sub> immobilized on functionalized SiO<sub>2</sub> and SBA-15. 24th Biennial ORCS Conference. 2012. p. 83–4.
  20. Shah P, Ramaswamy A V., Lazar K, Ramaswamy V. Synthesis and characterization of tin oxide-modified mesoporous SBA-15 molecular sieves and catalytic activity in trans-esterification reaction. *Appl Catal A Gen.* 2004;273(1-2):239–48.
  21. Maria Chong a. ., Zhao X., Kustedjo AT, Qiao S. Functionalization of large-pore mesoporous silicas with organosilanes by direct synthesis. *Microporous Mesoporous Mater.* 2004;72(1-3):33–42.
  22. Oliveira P, Machado A, Ramos AM, Fonseca IM, Braz Fernandes FM, Botelho do Rego AM, et al. Anchoring manganese acetylacetonate complex on MCM-41: Catalytic testing on limonene oxidation. *Catal Commun.* 2007;8(9):1366–72.
  23. Levinson R, Royal Society of Chemistry (Great Britain) R. More modern chemical techniques. Royal Society of Chemistry; 2001. 184 p.
  24. Welz B, Sperling M. Atomic absorption spectrometry. 3rd ed. Weinheim: Wiley-VCH; 2008. 1-4 p.
  25. Kruk M, Jaroniec M, Ko CH, Ryoo R. Characterization of the porous structure of SBA-15. *Chem Mater.* 2000;12(7):1961–8.
  26. Ferretti CCAC. Valoración catalítica de Glicerol: Síntesis de Monoglicéridos. Tesis de doctorado, Universidad Nacional del Litoral; 2010.
  27. Swapp S. Scanning Electron Microscopy (SEM) [Internet]. [cited 2015 Jan 12]. Available \_\_\_\_\_ from: [http://serc.carleton.edu/research\\_education/geochemsheets/techniques/SEM.html](http://serc.carleton.edu/research_education/geochemsheets/techniques/SEM.html)
  28. Zhou W, Wang ZL. Scanning Microscopy for Nanotechnology: Techniques and

- Applications. Springer Science & Business Media; 2007. 536 p.
29. Oku T. Structure Analysis of Advanced Nanomaterials. *Journal of Chemical Information and Modeling*. Berlin /Boston: Walter de Gruyter GmbH; 2014. 1-170 p.
  30. Zielinski JM, Kettle L. *Physical Characterization : Surface Area and Porosity*. London: Intertek; 2013.
  31. Nanocomposix. Uv/VIS/IR specyrosopy analysis of Nanoparticles. Nanocomposix. San Diego: Nanocomposix; 2012. p. 1–6.
  32. Lyon LA, Keating CD, Fox AP, Baker BE, He L, Nicewarner SR, et al. Raman Spectroscopy. *Anal Chem*. 1998;70(12):341–61.
  33. Sweeney R. Thermal Analysis [Internet]. [cited 2015 Jun 10]. Available from: <http://www.bradford.ac.uk/business/ccsa/analytical-techniques/thermal-analysis/>
  34. Gabbott P. *Principles and Applications of Thermal Analysis. A Practical Introduction To Differential Scanning Calorimetry*. Blackwell Publishing Ltda; 2008. 49 p.
  35. Popa A, Sasca V, Holclajtner-Antunović I. The influence of surface coverage on textural, structural and catalytic properties of cesium salts of 12-molybdophosphoric acid supported on SBA-15 mesoporous silica. *Microporous Mesoporous Mater*. 2012;156:127–37.
  36. Huang H, Ji Y, Qiao Z, Zhao C, He J, Zhang H. Preparation, Characterization, and Application of Magnetic Fe-SBA-15 Mesoporous Silica Molecular Sieves. *J Autom Methods Manag Chem*. 2010;2010:1–7.
  37. Huirache-Acuña R, Nava R, Peza-Ledesma C, Lara-Romero J, Alonso-Núez G, Pawelec B, et al. SBA-15 Mesoporous Silica as Catalytic Support for Hydrodesulfurization Catalysts. *Materials (Basel)*. 2013;6(9):4139–67.
  38. Li X, Ji W, Zhao J, Zhang Z, Au C. n-Butane oxidation over VPO catalysts

- supported on SBA-15. *J Catal.* 2006;238(1):232–41.
39. K. J, Balkus, A.G. Gabrielov, S.L. Bell, F. Bedioui, L. Roue JD, Balkus KJ, Gabrielov JAG, Bell SL, Bedioui F, Roue L, et al. Zeolite Encapsulated Cobalt ( II ) and Copper ( II ) Perfluorophthalocyanines . Synthesis and Characterization. *Inorg Chem.* 1994;33(7):67–72.
  40. Flacau R. Diffraction. 12th International Neutron Scattering Summer School. Chalk River, Ontario, Canada: Canadian Neutron Beam Centre; 2013. p. 1–35.
  41. Li M, Bo X, Zhang Y, Han C, Guo L. Comparative study on the oxygen reduction reaction electrocatalytic activities of iron phthalocyanines supported on reduced graphene oxide, mesoporous carbon vesicle, and ordered mesoporous carbon. *J Power Sources.* Elsevier B.V; 2014;264:114–22.
  42. Kouachi K, Lafaye G, Pronier S, Bennini L, Menad S. Mo/ $\gamma$ -Al<sub>2</sub>O<sub>3</sub> catalysts for the Biginelli reaction. Effect of Mo loading. *J Mol Catal A Chem.* 2014;395:210–6.
  43. El-Nahass MMM, Abd-El-Rahman KFF, Darwish A. Fourier-transform infrared and UV-vis spectroscopies of nickel phthalocyanine thin films. *Mater Chem Phys.* 2005;92(1):185–9.
  44. Lambert JB, Shurvell HF, Cooks RG. *Introduction to Organic Spectroscopy.* Macmillan; 1987. 174-177 p.
  45. Jiang J, Cornelissen U, Arnold DP, Sun X, Homborg H. Raman spectroscopic characteristics of phthalocyanine and naphthalocyanine in sandwich-type (na)phthalocyaninato and porphyrinato rare earth complexes part 2. The effects of different excitation wavelengths. *Polyhedron.* 2001;20(6):557–69.
  46. Lu F, Wang W, Bao G, Cui J. Raman spectroscopic characteristics of octa-substituted bis(phthalocyaninato) rare earth complexes peripherally substituted with (4-methoxy)phenoxy derivatives. *Vib Spectrosc.* 2011;56(2):228–34.
  47. Jiang J, Bao M, Rintoul L, Arnold DP. Vibrational spectroscopy of phthalocyanine

- and naphthalocyanine in sandwich-type (na)phthalocyaninato and porphyrinato rare earth complexes. *Coord Chem Rev.* 2006;250(3-4):424–48.
48. Bao G, Wang W, Mao Y, Lu F. Raman spectroscopic characteristics of phthalocyanine in mixed [5-(4-hydroxyphenyl)-10,15,20-tris(4-octyloxyphenyl)porphyrinato]-(phthalocyaninato) rare earth triple-deckers. *Spectrochim Acta A Mol Biomol Spectrosc.* Elsevier B.V.; 2013;102:275–80.
49. Tatar B, Demiroglu D. Electrical properties of FePc organic semiconductor thin films obtained by CSP technique for photovoltaic applications. *Mater Sci Semicond Process.* 2015;31:644–50.
50. Liu Z, Zhang X, Zhang Y, Jiang J. Theoretical investigation of the molecular, electronic structures and vibrational spectra of a series of first transition metal phthalocyanines. *Spectrochim Acta - Part A Mol Biomol Spectrosc.* 2007;67(5):1232–46.
51. C.C.R. de Carvalho C, da Fonseca MMR. Carvone: Why and how should one bother to produce this terpene". *Food Chem.* 2006;95(3):413–22.
52. Prieto S. GA, Perea V. JA, Ortiz L. CC. Microbial biotransformation of (R)-(+)-limonene by *Penicillium digitatum* DSM 62840 for producing (R)-(+)-terpineol. *Vitae.* 2011;18(2):163–72.
53. Synthetic spearmint-supplier scales up production to offer purer alternative [Internet]. [cited 2013 Oct 29]. Available from: <http://www.confectionerynews.com/Ingredients/Synthetic-spearmint-supplier-scales-up-production-to-offer-purer-alternative>
54. Li J, Li Z, Zi G, Yao Z, Luo Z, Wang Y, et al. Synthesis, characterizations and catalytic allylic oxidation of limonene to carvone of cobalt doped mesoporous silica templated by reed leaves. *Catal Commun.* 2015;59:233–7.
55. Moll HC, Schoot Uiterkamp AJMS. Comparative evaluation by lifecycle and risk assessment of agrobiological and technological routes of production. 1997;6:333–41.

56. Barrera RDJ, Alarcón EA, González LM, Villa AL, Montes De Correa C. Síntesis de carveol, carvona, verbenol y verbenona. *Ing y Compet.* 2008;10(1):43–63.
57. Leffingwell D. Chiral chemistry in flavours & fragrances. *Spec Chem Mag.* 2011;31(3):30–3.
58. Beyer H, Walter W. *Manual de química orgánica.* Reverté, S.A; 1987. 716 p.
59. Guenther E. *The Essential Oils Vol II. History-origin in plants production-analysis.* D. Van Nostrand Company,INC; 1948. p. 46 – .
60. Surburg H, Panten J. *Common Fragrance and Flavor Materials: Preparation, Properties and Uses.* Organic Process Research & Development. Wiley-VCH Verlag GmbH & Co. KGaA; 2007. 924-924 p.
61. Galvan Galeano MJ, Tapias Lidueñas DC. Evaluación de la actividad de catalizadores de paladio en hidrotalcitas en la transformación de limoneno a carvona. Degree work for Chemical Engineering Bachelor, Universidad de Antioquia; 2011.
62. Kolomeyer, G. G.; Oylo JS. Method for preparation of alpha, beta-unsaturated cyclic ketones by dehydrogenation of secondary allylic cyclic alcohols. US; U.S. Patent 6884913 B2, 2005.
63. Shulpin GB, Attanasio D, Suber L. Efficient H<sub>2</sub>O<sub>2</sub> Oxidation of Alkanes and Arenes to Alkyl Peroxides and Phenols Catalyzed by the System Vanadate-Pyrazine-2-Carboxylic Acid. *J Catal.* 1993;142(1):147–52.
64. H.S. Fogler. *Elements of Chemical Reaction Engineering.* Fourth. Prentice Hall; 2006. 200-800 p.
65. González LM, Moreno CD, Villa A, Correa L. 2-cyclohexen-1-one synthesis using a bio-inspired heterogeneous catalyst. 23rd North American Catalysis Society Meeting. 2013.
66. Mathworks. Evaluating Goodness of Fit [Internet]. [cited 2015 Dec 2]. Available



from: [http://www.mathworks.com/help/curvefit/evaluating-goodness-of-fit.html?s\\_tid=gn\\_loc\\_drop](http://www.mathworks.com/help/curvefit/evaluating-goodness-of-fit.html?s_tid=gn_loc_drop)

67. El-Korso S, Khaldi I, Bedrane S, Choukchou-Braham A, Thibault-Starzyk F, Bachir R. Liquid phase cyclohexene oxidation over vanadia based catalysts with tert-butyl hydroperoxide: Epoxidation versus allylic oxidation. *J Mol Catal A Chem.* 2014;394:89–96.
68. Sheldon R a., Arends IWCE, Lempers HEB. Liquid phase oxidation at metal ions and complexes in constrained environments. *Catal Today.* 1998 Jun;41(4):387–407.
69. Skobelev IY, Sorokin AB, Kovalenko K a., Fedin VP, Kholdeeva O a. Solvent-free allylic oxidation of alkenes with O<sub>2</sub> mediated by Fe- and Cr-MIL-101. *J Catal. Elsevier Inc.;* 2013;298:61–9.
70. Bussi J, López A, Peña F, Timbal P, Paz D, Lorenzo D, et al. Liquid phase oxidation of limonene catalyzed by palladium supported on hydrotalcites. *Appl Catal A Gen.* 2003;253(1):177–89.
71. Pena A, Veiga S, Sapelli M, Martínez N, Márquez V, Dellacassa E, et al. Limonene oxidation by molecular oxygen under solvent-free conditions: the influence of peroxides and catalysts on the reaction rate. *React Kinet Mech Catal.* 2012;107(2):263–75.
72. Simón E, Pardo F, Lorenzo D, Santos A, Romero A. Kinetic model of 2-cyclohexenone formation from cyclohexanol and 2-cyclohexenol dehydrogenation. *Chem Eng J.* 2012;192:129–37.
73. Morrish JLE, Daugulis AJ. Improved reactor performance and operability in the biotransformation of carveol to carvone using a solid-liquid two-phase partitioning bioreactor. *Biotechnol Bioeng.* 2008;101(5):946–56.
74. Committee ES. Scientific Opinion on the safety assessment of carvone , considering all sources of exposure. *Eur Food Saf Auth.* 2014;12(7):1–74.

75. Currie J. Information provided by Currie Marketing through the e-mail jim.currie@curriemarketing.co.uk. 2016.
76. Murzin DD, Salmi T. Catalytic Kinetics. Elsevier Science; 2005. 130-280 p.
77. Chang Y, Lv Y, Lu F, Zha F, Lei Z. Efficient allylic oxidation of cyclohexene with oxygen catalyzed by chloromethylated polystyrene supported tridentate Schiff-base complexes. *J Mol Catal A Chem.* 2010;320(1-2):56–61.
78. Lynggaard H, Andreasen a., Stegelmann C, Stoltze P. Analysis of simple kinetic models in heterogeneous catalysis. *Prog Surf Sci.* 2004;77(3-4):71–137.
79. Vannice MA. Kinetics of catalytic reactions. Springer Science & Business Media; 2005. 106-137 p.
80. Farnetti E, Monte R Di, Kašpar J. Homogeneous and Heterogeneous Catalysis. *Life Support Syst.* 1999;II:10.
81. d'Alessandro N, Tonucci L, Bressan M, Dragani LK, Morvillo A. Rapid and Selective Oxidation of Metallosulfophthalocyanines Prior to Their Usefulness as Precatalysts in Oxidation Reactions. *Eur J Inorg Chem.* WILEY-VCH Verlag; 2003 May;2003(9):1807–14.
82. Frydrych E, Foltynowicz Z, Kowalak S, Janiszewska E. Oxygen scavengers for packing system based on zeolite adsorbed organic compounds. *Stud Surf Sci Catal.* 2007;170(B):1597–604.
83. JASCO INC. Purification of Carvone in Spearmint Oil using SFC with PDA and FTIR Dual-Monitoring [Internet]. [cited 2016 Jan 10]. p. 2–5. Available from: <http://www.jascoinc.com/sfc/purification-of-carvone-in-spearmint-oil-using-sfc-with-pda-and-ftir-dual-monitoring>
84. Breitmaier E. Terpenes: Flavors, Fragrances, Pharmaca, Pheromones. Weinheim, Germany: Wiley-VCH Verlag GmbH & Co. KGaA; 2006. 1-200 p.

85. Sing KSW. Reporting physisorption data for gas/solid systems with special reference to the determination of surface area and porosity. *Pure Appl Chem.* 1985;57(4):603–19.
86. A. Cybulski, M.M. Sharma, R.A. Sheldon *JAM. Fine Chemicals Manufacture: Technology and Engineering.* ELSEVIER SCIENCE B.V; 2001. p. 1–13.
87. Blaser HU. Heterogeneous catalysis for fine chemicals production. *Catal Today.* 2000;60(3):161–5.
88. Leffingwell & Associates [Internet]. [cited 2016 Apr 20]. Available from: <http://www.leffingwell.com/chirality/carvone.htm>
89. Paramount [Internet]. 2012 [cited 2016 May 29]. Available from: <http://agoraprofessional.com/blog/carvone/>
90. MOLBASE [Internet]. [cited 2016 Apr 20]. Available from: [http://www.molbase.com/en/search.html?search\\_keyword=1197-06-4](http://www.molbase.com/en/search.html?search_keyword=1197-06-4)
91. Sigma Aldrich [Internet]. [cited 2016 Apr 20]. Available from: <http://www.sigmaaldrich.com/us-export.html>
92. VIGON [Internet]. [cited 2016 Apr 20]. Available from: <https://www.vigon.com/>
93. Biocomercio\_sostenible. Estudio del mercado colombiano de aceites esenciales. Instituto de investigación de recursos biológicos ALEXANDER VON HUMBOLDT, Bogotá, Colombia; 2003.
94. Mincomercio. Industria y turismo [Internet]. [cited 2016 Mar 30]. Available from: <http://bacex.mincit.gov.co/>
95. Montoya C, Martínez P, Celedon M, Khaddaj R, Berbesi A. Eco empaque de la crema dental Toothpaste Eco packaging. *Rev Tecnol.* 2014;13:61–72.
96. Fenalco [Internet]. [cited 2016 Feb 4]. Available from: [http://www.fenalco.com.co/contenido/3134\\_400g/\(anuales.perosna\)\\_2012](http://www.fenalco.com.co/contenido/3134_400g/(anuales.perosna)_2012)

97. Euromonitor International [Internet]. [cited 2016 Feb 4]. Available from: <http://aplicacionesbiblioteca.udea.edu.co:2395/portal/analysis/tab>
98. Mitchell RL y, K, Durga GA. Un método para preparar una crema dental envasada. España; Patent: 8803056, 1989.
99. Dymont J, Mantrala V. Jump Start: Getting Started with Aspen Plus® V8. AspenTech; 2015. p. 1–22.
100. Fogler HS, Gurmen NM, Arbor A. Aspen Plus™ Workshop for Reaction Engineering and Design Department of Chemical Engineering, [Internet]. 2002 [cited 2016 Jan 10]. p. 8–20. Available from: <http://www.umich.edu/~elements/course/lectures/eight/aspenv10.2/resources/aspen.pdf>
101. Luyben WL. Chemical reactor design and control. Wiley-Interscience; 2007. 419 p.
102. Bollas PG. Aspen tutorial # 7 Reactors II [Internet]. [cited 2015 Dec 1]. Available from: <http://pdsol.engr.uconn.edu/material/lecture07.swf>
103. Aspen Plus. Problema diseño de una columna dedestilación propano-isobutano. [Internet]. 2013 [cited 2016 Jan 10]. Available from: [http://www.diquima.upm.es/old\\_diquima/docencia/modysim2000/docs/columna\\_propano.pdf](http://www.diquima.upm.es/old_diquima/docencia/modysim2000/docs/columna_propano.pdf)
104. Barrera Zapata R. Modelo, simulación y diseño del reactor y el proceso de separación para la producción de epóxido de limoneno. Doctoral Thesis, Universidad de Antioquia; 2010.
105. Lohmann J, Joh R, Gmehling J. From UNIFAC to Modified UNIFAC (Dortmund). *Ind Eng Chem Res.* 2001;40(3):957–64.
106. Carlson EC. Don't Gamble With Physical Properties. *Chem Eng Process.* 1996;35–46.

107. Tarleton S, Wakeman R. Solid / Liquid Separation : Equipment selection and process Design. London: Elsevier,; 2007. 2-465 p.

**Appendix A:  
calculation models**

$$X_i = \frac{C_{reactant,0} - C_{reactant,f}}{C_{reactant,0}} * 100$$

$$S_i = \frac{C_{product,f} - C_{product,i}}{C_{reactant,0} - C_{reactant,f}} * 100$$

$$Y_i = \frac{X_i * S_i}{100} = \frac{C_{product,f} - C_{product,i}}{C_{reactant,0}} * 100$$

Where:

$X_i$ : Reactant conversion, %.

$S_i$ : Product selectivity respect to substrate, %.

$Y_i$ : Product yield respect to substrate, %.

$C_{reactant,0}$ : Initial concentration of reactant, M. Calculated with chromatograph calibration curve.

$C_{reactant,f}$ : Final concentration of reactant, M. Calculated with chromatograph calibration curve.

$C_{product,0}$ : Initial concentration of product, M. Calculated with chromatograph calibration curve.

$C_{product,f}$ : Final concentration of product, M. Calculated with chromatograph calibration curve.

## *Appendix B: Matlab ® hybrid algorithm*

```
clc
clear all
%%%%%%%%%%%%%%
%% This part is to place the excel cell where the results will be saved
name_ga=char('ga_mechanism_J');
name_hi=char('hi_mechanism_J');
place=('B10:S10');%use even numbers
place2=('G11:S11');% the last one plus 1
```

```
%% Data
nvars = 3; % Number of variables
m=nvars*15;%default population size
```

```
r=[0.0000
0.0000
9.6803
23.4957
28.7436
29.1808
29.5260
30.5337
31.9607
32.7116
33.5896
36.6694
41.6786
50.9008];%r=-rcarveol [mmol/(gFe*min)]
```

```
L=[0.000313
0.000299
0.000307
0.000299
0.000295
0.000299
0.000299
0.000299
0.000300
0.000299
0.000291
0.000299
0.000283
0.000299
0.000276]; %Fe concentration, M[mmol/mL]
```

```
CB=[0.00000
0.31056
0.12280
0.31056
0.38536
```

---

```

0.31056
0.31056
0.27184
0.31056
0.48833
0.31056
0.65688
0.31056
0.81691];%TBHP concentration, M[mmol/mL]

CD=[0.134
0.000
0.121
0.034
0.127
0.133
0.069
0.130
0.084
0.128
0.106
0.141
0.168
0.135];% Real carveol concentration M[mmol/mL]

r=r'; %the geneti algorith needs this data as row vector
CB=CB';
CD=CD';
L=L';

% Next we run the GA solver.
A = []; b = [];
Aeq = []; beq = [];
LB = [0 0 0]; % Lower bound
UB =[1e6 1e6 1e6];

% This initial values are used to decrease the randomness of the algorithm
initialA=[1e6 1e6 1e6 1e6 1e6
1 1 1 1 1
1e6 10 10 10 1
1e6 1 1 1 1
1 1e6 1e6 1e6 1e6
10 10 10 10 10
100 100 100 100 100
1e6 1e6 1 1 1e6
1e6 1e2 10 10 10
1e5 1e5 1e5 1e5 1e5
1e4 1e4 1e4 1e4 1e4
1e3 1e3 1e3 1 1e3
1 5 15 10 5
1e6 1e4 1 1e3 1e5
1e4 1 1e6 1 1];
initialB=[1.0000e+006 1.0000e+000 1.0000e+000 1.0000e+006 998.4400e+003
1.0000e+003 999.0000e+003 1.0000e+000 1.0100e+000 998.3400e+003
2.0000e+003 998.0000e+003 998.0000e+003 200.0100e+000 1.7600e+003

```



```

140007.16  92981.39251  377359.4188  30.395115  1.8600e+000
996.0000e+003  4.0000e+003  4.0000e+003  999.6000e+003  18.6000e+000
5.0000e+003  995.0000e+003  995.0000e+003  5.0001e+000  997.9400e+003
6.0000e+003  994.0000e+003  994.0000e+003  600.0100e+000  2.1600e+003
1.0000e+003  7.0000e+003  7.0000e+003  999.3000e+003  2.2600e+003
1.0000e+000  8.0000e+003  8.0000e+003  99.9200e+003  997.6400e+003
9.0000e+003  991.0000e+003  991.0000e+003  900.0100e+000  997.5400e+003
10.0000e+003  990.0000e+003  990.0000e+003  1.0200e+003  980.0100e+000
989.0000e+003  11.0000e+003  11.0000e+003  998.8800e+003  1.0800e+003
988.0000e+003  12.0000e+003  1.0000e+000  9.9878e+000  998.8200e+003
100.0000e+000  987.0000e+003  1.0000e+000  1.3200e+003  998.7200e+003
14.0000e+003  986.0000e+003  986.0000e+003  1.4200e+003  1.3800e+000
985.0000e+003  15.0000e+003  15.0000e+003  99.8480e+003  1.4800e+003
984.0000e+003  16.0000e+003  16.0000e+003  998.3800e+003  998.4200e+003
17.0000e+003  983.0000e+003  983.0000e+003  1.7200e+003  998.3200e+003
18.0000e+003  1.0000e+000  982.0000e+003  182.0000e+003  1.7800e+000
981.0000e+003  19.0000e+003  19.0000e+003  998.0800e+003  1.8800e+003
980.0000e+003  20.0000e+003  20.0000e+003  997.9600e+003  1.0400e+003
21.0000e+003  979.0000e+003  979.0000e+003  2.1400e+003  998.8600e+003
22.0000e+003  978.0000e+003  978.0000e+003  2.2400e+003  998.7600e+003
977.0000e+003  23.0000e+003  23.0000e+003  99.7660e+000  1.3400e+003
976.0000e+003  24.0000e+003  24.0000e+003  997.5600e+003  1.4400e+003
25.0000e+003  1.0000e+000  975.0000e+003  2.5400e+003  998.4600e+003
26.0000e+003  974.0000e+003  974.0000e+003  2.6400e+003  998.3600e+003
973.0000e+003  27.0000e+003  27.0000e+003  997.2600e+003  1.7400e+003
972.0000e+003  28.0000e+003  28.0000e+003  997.1600e+003  1.8400e+003
29.0000e+003  100.0000e+000  971.0000e+003  294.0000e+003  998.0600e+003];
initialC=[ 1.0000e+006  999.9800e+003  999.9600e+003  999.9400e+003  999.9200e+003
1.0100e+000  120.0100e+000  140.0100e+000  160.0100e+000  180.0100e+000
200.0100e+000  220.0100e+000  240.0100e+000  260.0100e+000  280.0100e+000
999.7000e+003  999.6800e+003  999.6600e+003  9.6400e+003  999.6200e+003
999.6000e+003  999.5800e+003  999.5600e+003  999.5400e+003  999.5200e+003
5.0001e+000  1.0000e+000  540.0100e+000  560.0100e+000  580.0100e+000
600.0100e+000  620.0100e+000  640.0100e+000  660.0100e+000  680.0100e+000
999.3000e+003  999.2800e+003  999.2600e+003  999.2400e+003  999.2200e+003
99.9200e+003  999.1800e+003  999.1600e+003  999.1400e+003  99.7620e+003
900.0100e+000  920.0100e+000  940.0100e+000  960.0100e+000  980.0100e+000
1.0000e+003  1.0200e+003  1.0400e+003  1.0600e+000  1.0800e+003
998.9000e+003  998.8800e+003  998.8600e+003  998.8400e+003  998.8200e+003
998.8000e+003  9.9878e+000  998.7600e+003  998.7400e+003  998.7200e+003
1.3000e+003  1.3200e+003  1.3400e+003  1.3600e+000  1.3800e+000
1.4000e+003  1.4200e+003  1.4400e+003  146.0000e+003  1.4800e+003
8.5000e+000  99.8480e+003  998.4600e+003  998.4400e+003  998.4200e+003
998.4000e+003  998.3800e+003  998.3600e+003  998.3400e+003  998.3200e+003
17.0000e+003  1.7200e+003  1.7400e+003  1.7600e+003  1.7800e+000
1.8000e+003  182.0000e+003  1.8400e+003  1.8600e+000  1.8800e+003
998.1000e+003  998.0800e+003  998.0600e+003  18.6000e+000  998.0200e+000
1.0000e+003  9.9800e+000  997.9600e+003  997.9400e+003  9.9792e+003
2.1000e+003  212.0000e+000  2.1400e+003  2.1600e+003  2.1800e+003
220.0000e+003  2.2200e+000  2.2400e+003  2.2600e+003  2.2800e+003
997.7000e+003  997.6800e+003  99.7660e+000  997.6400e+003  997.6200e+003
997.6000e+003  997.5800e+003  997.5600e+003  997.5400e+003  997.5200e+003
2.5000e+000  2.5200e+003  2.5400e+003  2.5600e+003  2.5800e+003
2.6000e+000  2.6200e+003  2.6400e+003  2.6600e+003  268.0000e+003
997.3000e+000  997.2800e+003  997.2600e+003  997.2400e+003  997.2200e+003
99.7200e+003  99.7180e+003  997.1600e+003  997.1400e+003  997.1200e+003

```

```

290.0000e+000 29.2000e+00 294.0000e+003 2.9600e+003 2.9800e+003];
initial=[initialA
initialB
initialC];%The default population size is 15 times the number of variables n

options = gaoptimset('TolFun',1e-10000,'Generations',9000,'InitialPopulation',initial(1:1:m,1:1:nvars));

%%

[x,fval,population] = gamultiobj(@J_ga_mechanism,nvars,A,b,Aeq,beq,LB,UB,options
[B,d]=min(fval(:,15)); %B= minimum value of column 15 from fval that corresponds to(sum(((r-rcal).^2,2))o
SSE;
%d= minimum value position, which will be used in order to work with the lower SSE

%http://es.mathworks.com/help/curvefit/evaluating-goodness-of-fit.html
%statistic values
residual=fval(d,1:1:14);
%residual2=r-rcal_ga;
%Sum of Squares due to Error or summed square of residuals
SSE=(sum((residual.^2),2));%also called SSR o SCR
N=length(r);
p=nvars;
%Mean square error
MSE=(SSE/(N-p));
%Root Mean Square Error
RMSE=(MSE)^0.5; % also called RMSD
%Total sum of squares or the sum of squares about the mean
SST=sum(((r-mean(r)).^2),2); %also called SCT in spanish
%determination coefficient
R_square=1-(SSE/SST);
%adjusted R-square statistic is generally the best indicator of the fit quality when you compare two models
that are nested — that is, a
%series of models each of which adds additional coefficients to the
%previous model
Adjusted_R_square=1-SSE*(N-1)/(SST*(N-p));
x_ga=x;

resultados_ga=[R_square Adjusted_R_square SSE MSE RMSE x_ga(d,:) ];
xlswrite('Results_hibrid_Da',resultados_ga,name_ga,place);% this is used to export the data to excel file

%lsqnonlin using x_ga from GA as initial guess
r=r'; %lsqnonlin was programed for column vectors
CB=CB';
CD=CD';
L=L';

x0=x_ga(d,:);
i=1;
s=20;
aa=0;
while s>1e-100
%%
fun_carveol= inline('r-(x(1)*(CB.^x(2)).*(CD.^x(3)))','x','r','CB','CD');
```

```

options=optimset('Algorithm','trust-region-reflective');
%%
[x,RESNORM,RESIDUAL,EXITFLAG]=lsqnonlin(fun_carveol,x0,[],[],options,r,CB,CD);% RESNORM is:
(SSE)Sum of Squares due to Error or summed square of residuals
e=1e-100;
y=x0;
aa=aa+1;
%%Change 6
s=sum(feval(fun_carveol,x,r,CB,CD),1);
matrix(aa,:)=s x];
for j=1:nvars
    if abs(x(j)-x0(j))>e
        x0(j)=x(j);
    end
end
if y==x0
    s=1e-101;
end
end
[C,place_s]=min(matrix(:,1));
x=matrix(place_s,2:1:nvars+1);
%%
rcal_lsq=r-feval(fun_carveol,x,r,CB,CD);% r calculated with the best fitting parameters
%Plot of carveol variation
x_ol_variation=[CD(2)
    CD(4)
    CD(7)
    CD(9)
    CD(11)
    CD(6)
    CD(13)]; %carveol concentration vector for the plot of carveol variation
y_ol_variation=[r(2)
    r(4)
    r(7)
    r(9)
    r(11)
    r(6)
    r(13)] ;% experimental r for the plot of carveol variation
ycal_ol_variation=[rcal_lsq(2)
    rcal_lsq(4)
    rcal_lsq(7)
    rcal_lsq(9)
    rcal_lsq(11)
    rcal_lsq(6)
    rcal_lsq(13)] ;% calculated r for the plot of carveol variation
figure(1), plot(x_ol_variation,y_ol_variation,'bd',x_ol_variation,ycal_ol_variation,'r-')
title('Variation of carveol concentration');
xlabel('Carveol concentration, M[mmol/mL]');
ylabel('r=-rcarveol [mmol/(gFe*min)]');
legend('Experimental data','Calculated data','Location','NorthEastOutside');

%Plot of TBHP variation
x_TBHP_variation=[CB(1)
    CB(3)
    CB(8)

```

```

        CB(6)
        CB(5)
        CB(10)
        CB(12)
        CB(14)]; %TBHP concentration vector for the plot of TBHP variation
y_TBHP_variation=[r(1)
    r(3)
    r(8)
    r(6)
    r(5)
    r(10)
    r(12)
    r(14)] ;% experimental r for the plot of TBHP variation
ycal_TBHP_variation=[rcal_lsq(1)
    rcal_lsq(3)
    rcal_lsq(8)
    rcal_lsq(6)
    rcal_lsq(5)
    rcal_lsq(10)
    rcal_lsq(12)
    rcal_lsq(14)] ;% calculated r for the plot of TBHP variation
figure(2), plot(x_TBHP_variation,y_TBHP_variation,'bd',x_TBHP_variation,ycal_TBHP_variation,'r-')
title('Variation of TBHP concentration');
xlabel('TBHP concentration, M[mmol/mL]');
ylabel('r=-rcarveol [mmol/(gFe*min)]');
legend('Experimental data','Calculated data','Location','NorthEastOutside')

%http://es.mathworks.com/help/curvefit/evaluating-goodness-of-fit.html
%statistic values
residual=[r-rcal_lsq];
%Sum of Squares due to Error or summed square of residuals
SSE=(sum((residual.^2),1));%also called SSR or SCR
N=length(r);
p=length(x);
%Mean square error
MSE=(SSE/(N-p));
%Root Mean Square Error
RMSE=(MSE)^0.5; %also called RMSD
%Total sum of squares or the sum of squares about the mean
SST=sum(((r-mean(r)).^2),1); %also called SCT in spanish
%determination coefficient
R_square=1-(SSE/SST);
%adjusted R-square statistic is generally the best indicator of the fit
%quality when you compare two models that are nested — that is, a
%series of models each of which adds additional coefficients to the
%previous model
Adjusted_R_square=1-SSE*(N-1)/(SST*(N-p));

%Plot of residuals
figure(3),plot(r,residual,'*',[0,max(r)+20],[0,0])
title('Plot of residuals');
xlabel('r');
ylabel('residual');

%rcal_lsq vs r

```

```

figure(4),plot(r,rcal_lsq, '*','r,r');
title('Plot of rcal_lsq vs r');
xlabel('r');
ylabel('rcal_lsq');

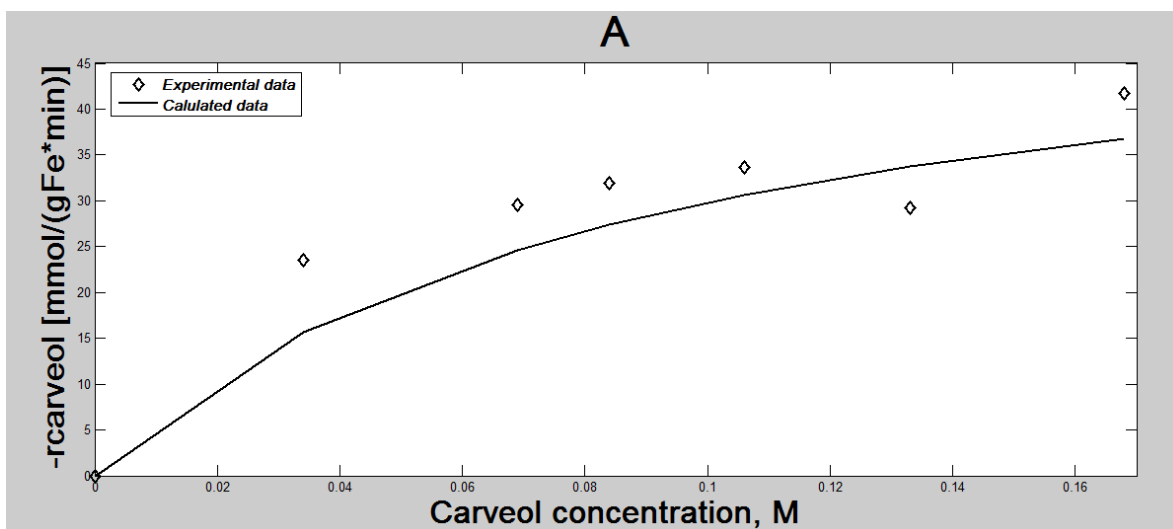
%Nonlinear regression parameter confidence intervals
%http://es.mathworks.com/help/stats/nlparci.html?searchHighlight=nlparci
% Write a function handle that represents the model
data=[L CB CD];%data matrix
%% Change 8
mdl=@(x_ci,data)(x_ci(1)*(data(:,2).^x_ci(2)).*(data(:,3).^x_ci(3)));
%Generate normally distributed noise with standard deviation 0.0001:
x_ci = x;
epsn = abs(normrnd(0,0.0001,14,1));
r_ci = mdl(x_ci,data) + epsn;
%Fit the model to data starting from the guess x_ci =x from lsqnonlin
opts=statset('nlinfit');
opts.RobustWgtFun='bisquare';
%x_ci0= x';

[x_cihat,R,J,cov,mse] = nlinfit(data,r_ci,mdl,x_ci,opts); %Nonlinear least-squares regression. R is residual.
%The estimated covariance matrix COVB for the fitted coefficients, estimate
%MSE of the variance of the error term.
x_cihat;
%Check whether x_ci is in a 95% confidence interval using the Jacobian argument in nlparci:
ci1 = nlparci(x_cihat,R,'covar',cov);
% You can obtain the same result using the covariance argument:
ci=(abs(ci1(:,1))-ci1(:,2))/2);
%Results resum to export
resultados=[R_square Adjusted_R_square SSE MSE RMSE x];
xlswrite('Results_hibrid_Da',resultados,name_hi,place);%used to export the data to an excel file "Resultados"
xlswrite('Results_hibrid_Da',ci,name_hi,place2 used to export the data to an excel file "Resultados")

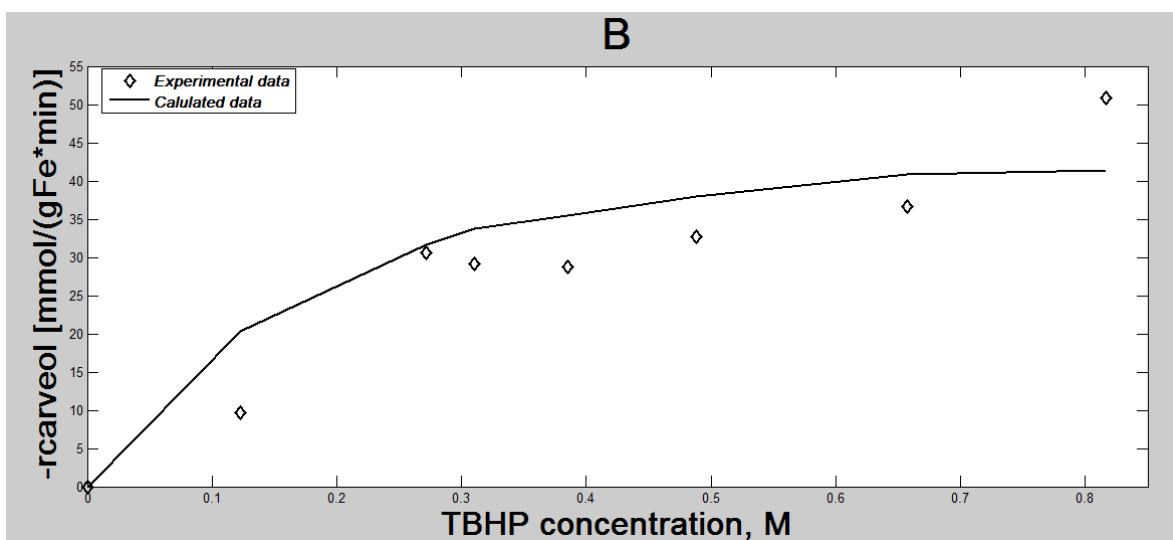
```

*Appendix C: Matlab  
results for mechanism  
D.*

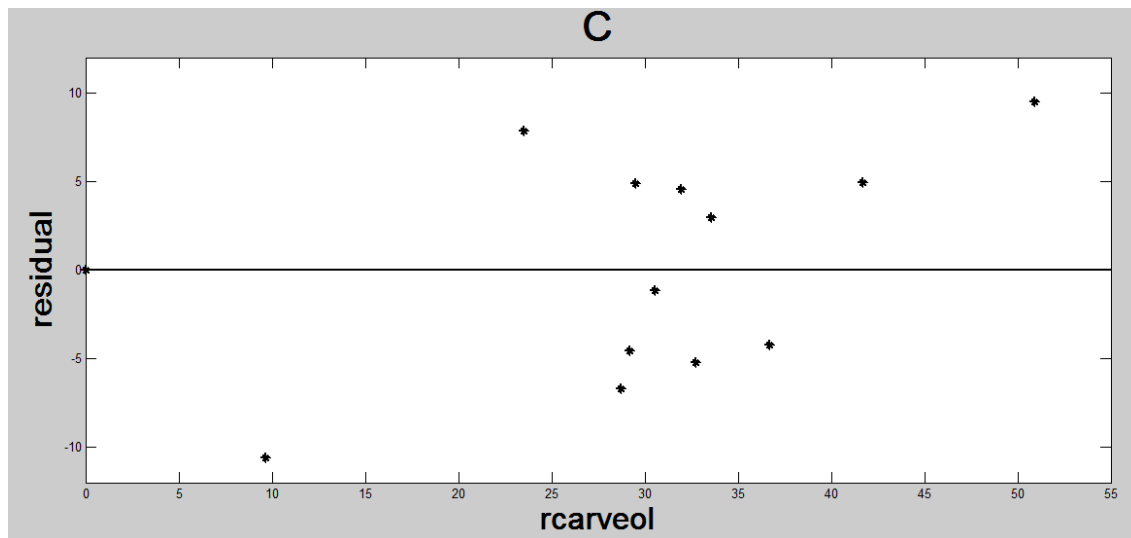
Carveol reaction rate (r) vs Carveol concentration



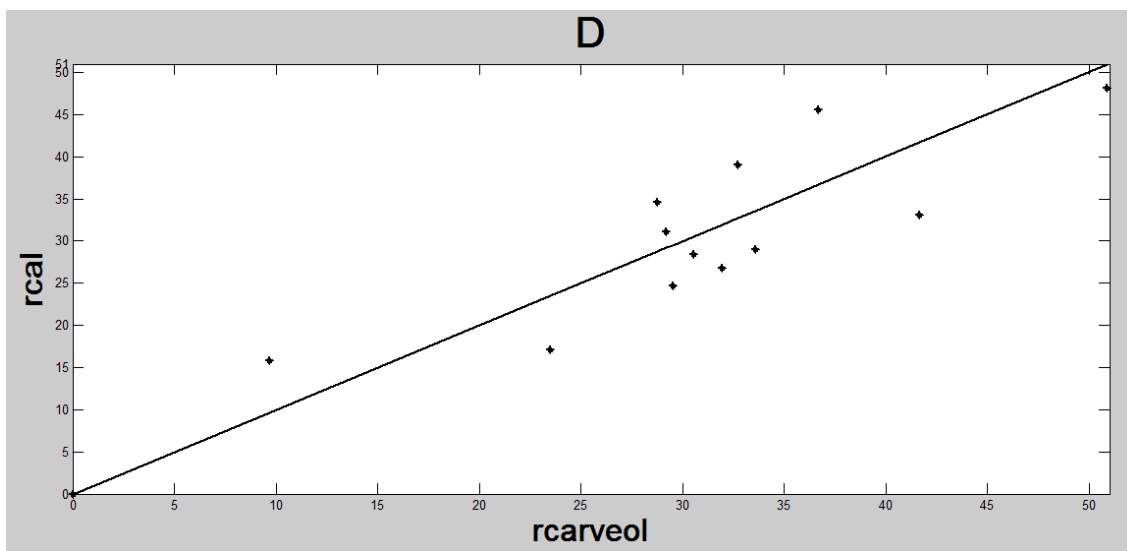
Carveol reaction rate (r) vs TBHP concentration



Rplot of residuals vs r

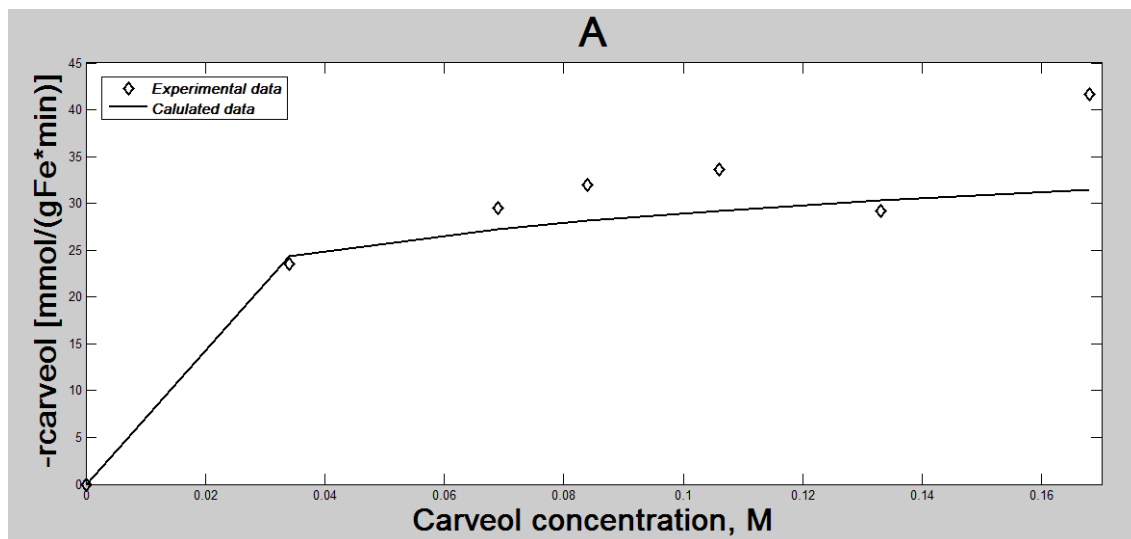


Experimental reaction rate (r) vs calculated reaction rate (rcal)

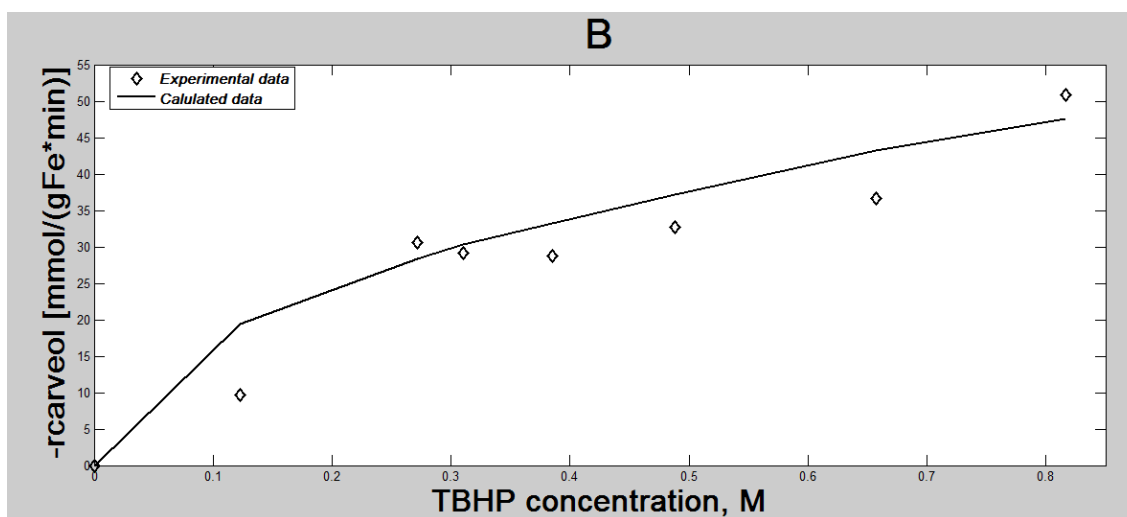


*Appendix D: Matlab  
results for mechanism  
J.*

Carveol reaction rate (r) vs Carveol concentration

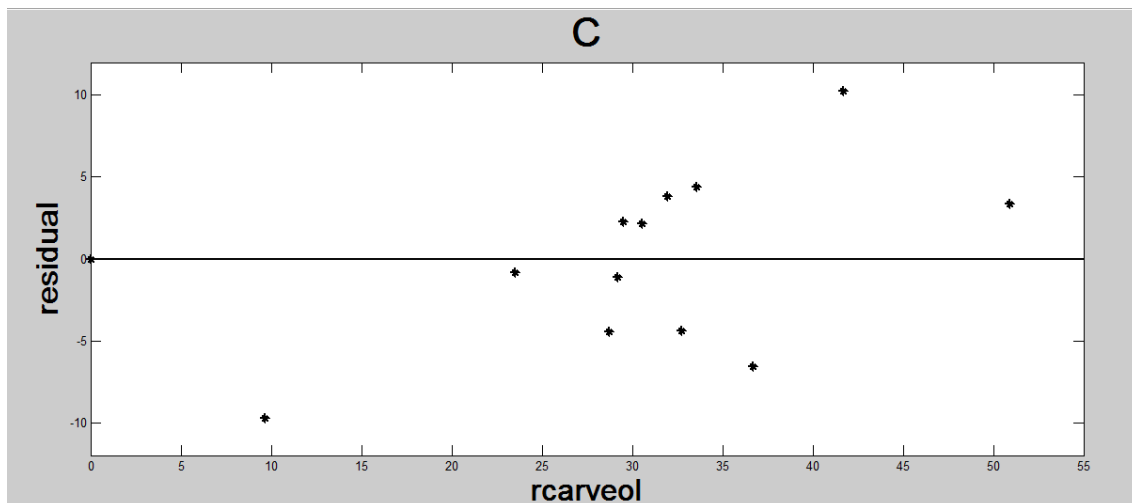


Carveol reaction rate (r) vs TBHP concentration

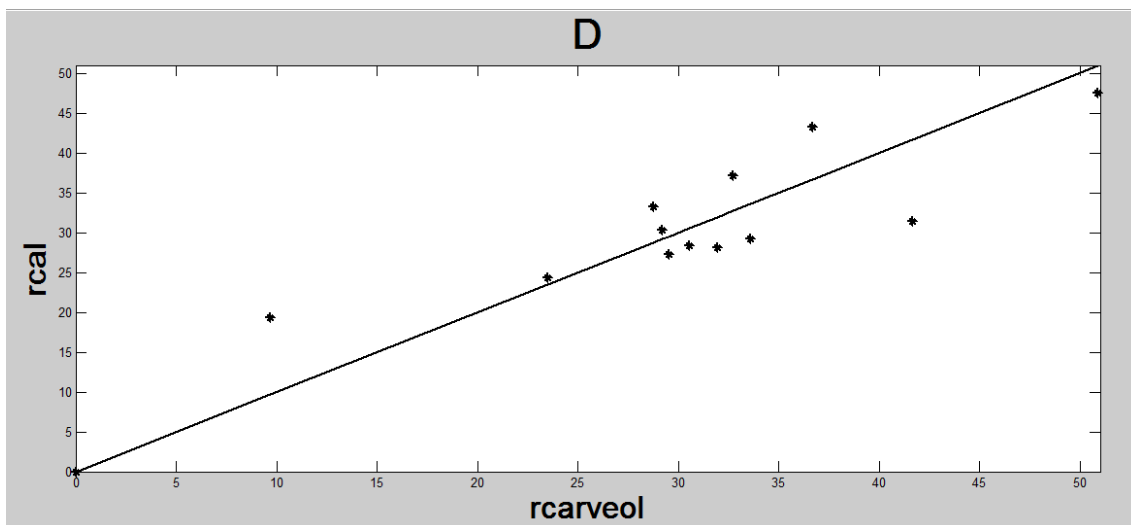




Rplot of residuals vs r

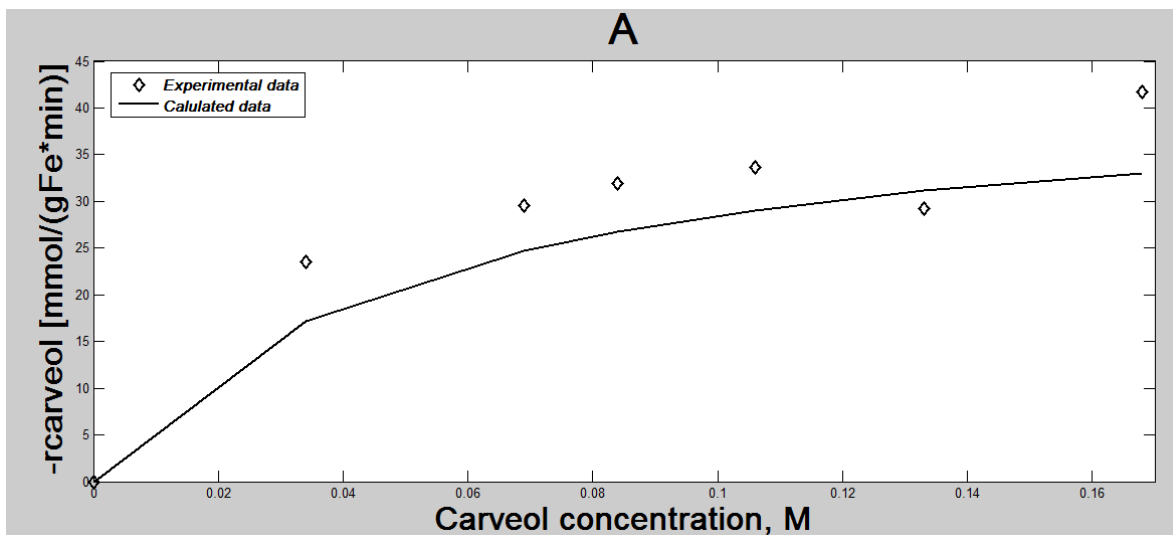


Experimental reaction rate (r) vs calculated reaction rate (rcal)

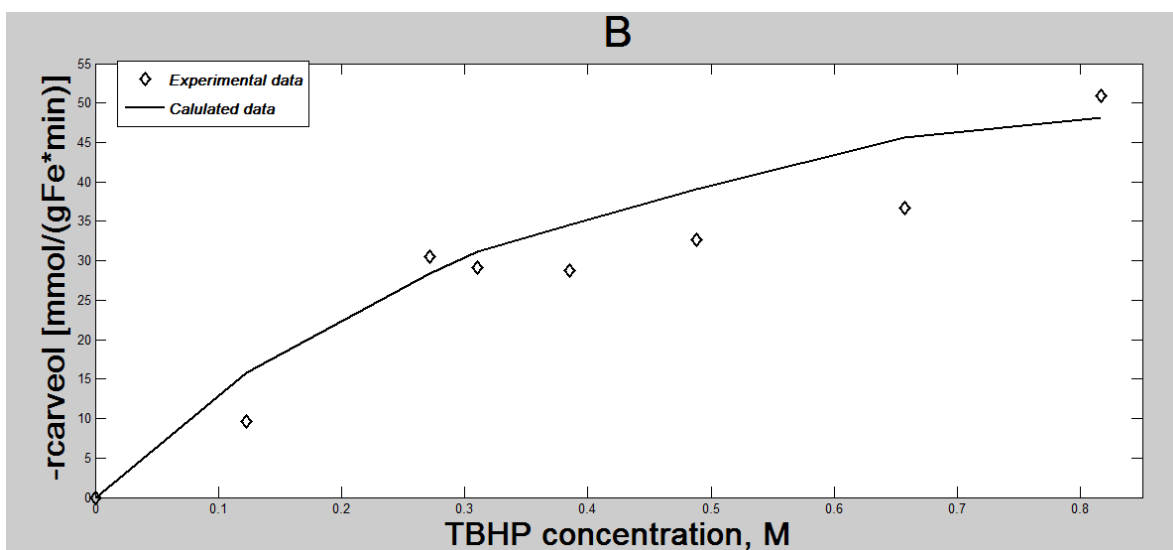


**Appendix E: Matlab  
results for mechanism  
O.**

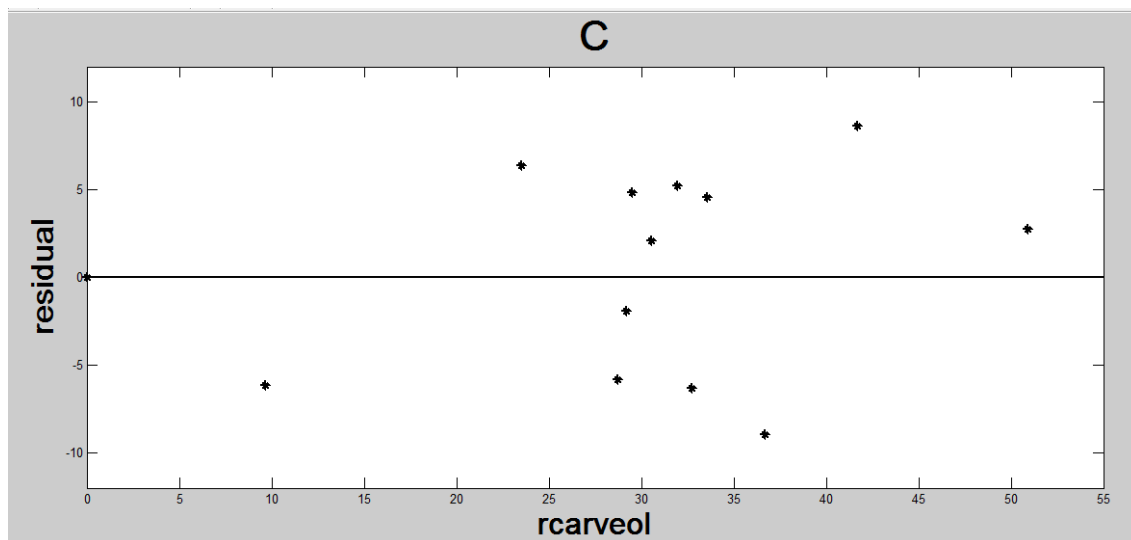
**Carveol reaction rate (r) vs Carveol concentration**



**Carveol reaction rate (r) vs TBHP concentration**



Rplot of residuals vs r



Experimental reaction rate (r) vs calculated reaction rate (rcal)

